Two-Dimensional Inverse Design and Optimisation of Turbomachinery Blades

by

R Firson Joko Raharjo

A thesis submitted for the degree of Master of Philosophy
in the Faculty of Engineering, University of London

Department of Mechanical Engineering
University College London
July 2003

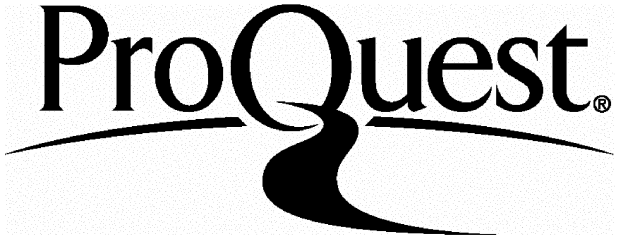

ACKNOWLEDGEMENT

The Author would like to express his gratitude to his supervisor, Dr Mehrdad Zangeneh. I would also like to thanks to Ebara Research company for their financial support for the inverse design project. Additionally, I would like to dedicated my work to my parents and my brother and sister for their financial support and encouraging me to complete this thesis.

R Firson Joko Raharjo
July 2003

ABSTRACT

The two-dimensional multiblock unsteady Euler and Navier-Stokes solver for turbomachinery blades has been developed. These flow solvers were used to analyse and design the turbomachinery blades using inverse and optimisation method. The inverse method employs the Euler solver base on cell-vertex scheme in conjunction with artificial viscosity and Runge-Kutta integrator. Further development of this solver led to the Navier-Stokes solver with the Baldwin-Lomax turbulence model and the Abu-Ghannam and Shaw transition model. The viscous code was applied for designing more complicated design parameter such as heat transfer coefficient distribution using optimisation method. Both flow solvers were first validated by using experimental measurements. Additionally, the result from commercial software Fluent was also used for validation of the viscous flow solver.

In the inverse method, the blade is modified until the obtained mass-averaged tangential velocity is close enough to the specified one. The blade is updated for each iteration using the blade modification algorithm, which derived from the slip condition on the wall and fixed thickness distribution. The inverse method was validated numerically by reproducing a VKI turbine rotor blade in the upper transonic flow. Two examples of inverse method are shown with specific thickness distributions.

While, in the optimisation method the blade is generated for each iteration using the developed subroutine NURBS, which generates camber line and thickness distribution by control points. This subroutine and the viscous flow solver are employed in the framework of iSight to run and analyse the optimisation process. The validation and two examples of optimisation method on the pressure loading and on the heat transfer coefficient are presented.

CONTENTS

LIST OF FIGURES

LIST OF TABLES

NOMENCLATURE

β	flow angle
γ	specific heat ratio
ρ	Density
D	dissipative operator
E	total energy
H	total enthalpy
h	cell area
M	mach number
P	static pressure
Q	an approximation operator to the boundary integral
Q_k	flux velocity
S	blade pitch
T	Temperature
t_θ	blade thickness
u	cartesian velocity components in x direction
v	cartesian velocity components in y direction

Subscript

0	Stagnation
1	Inlet
2	Outlet
bl	the average value of upper and lower surface variable
is	Isentropic

Superscript

+	upper surface
-	lower surface
*	required value
0	initial value
old	current value
new	updated value

COMPUTER PERFORMANCE

Turbo2	AlphaStation 433au System, 433 MHz
Turbo4	AlphaStation 500 System, 400 MHz
Turbo5	AlphaStation 433au System, 433 MHz
Turboserve	AlphaServer DS10 System, 600 MHz
Turbo6	AlphaStation XP1000 System, 667 MHz

Chapter I Introduction and Literature Survey

I.1 Overview

The design of more efficient blades is an important part of turbomachinery development, and hence for the market and environment. For example, the specific fuel consumption of jet engines has been reduced significantly during the last four decades due to the improvement of the blade geometry. The application of Computational Fluid Dynamics (CFD) and new numerical design methods have helped to improve the design of turbomachinery blades with optimum aerodynamic performance.

In the conventional approach, the blade profile is created or modified by the designers based on his knowledge and experience through an iterative process of flow calculations and wind tunnel testing until a desired flow field is achieved. Such a process can be very time consuming, depending on the designer's experience, and may result in high design cost and delays.

Now, with the further development of design strategies, the required blade design profile is obtained by using optimisation and/or inverse method. The inverse design methods allow the designer to have the blade with a desired pressure or loading distribution and even to control the flow field such as secondary flow or exit flow. Therefore, improving the performance and wider stable operating range of the machine. The performance of the obtained blade shape can also be analysed using the same code, which usually can be switched into a conventional flow solver. This important feature is very useful to perform any off design analysis before verification in wind tunnel.

Many designed blades, which were obtained by inverse methodologies have been manufactured and validated experimentally for example Borges (1990), Zangeneh (1996b) and Goto (1996).

Further work has been done by the author in the inverse design and optimisation area. The first work is the extension of Tiow's (1999) inverse methodology. It works by modifying the blade geometry until the mass-averaged tangential velocity similar to the target using the C-type grid topology. This type of topology can model the blunt leading edges accurately. The validation and investigation has been performed numerically.

Moreover, the author has performed optimisation design where the blade was optimised with loading or heat transfer coefficient distribution as designed specifications. The optimisation of turbomachinery blade for heat transfer coefficient distribution is still new in this area and very important in the design and development of aeroengine. The performance of modern aeroengine can be improved by the increased turbine entry temperature. However, this can not easily be done due to the limitation of the metallurgical temperature of the blade. The design of modern turbine blades relies on the use internal cooling or film cooling for the high temperature application. In both cases considerable amount of compressor mass flow rate (i.e. cooling air) is bled into the cooling system, which results in reductions in performance of the gas turbine.

At the moment the design process of a turbine blade for high temperature applications normally starts with the design for an optimum aerodynamic performance. Then, the cooling system is investigated. This design process fails to take account of the strong relationship between the aerodynamics and heat transfer of the blade. In fact, the local heat transfer coefficient is strongly dependent on the state of the boundary layer, which also affects the aerodynamic performance.

Unfortunately, the development of inverse method, which shortens the design process, has not reached to this stage. Most of them are still concentrating on the aerodynamics design.

To the best of the author's knowledge, there are no examples of combine aero-thermal design as well in the optimisation areas. However, during the writing of this thesis Manna and Tuccillo (2002) published their works on the issue of aerodynamic and heat transfer optimisation. The technique is quite basic as it optimised the global parameter of heat load and loss coefficient. The flow condition ruled out some certain conditions, which could help the stability and solution domain of the optimisation.

In the other optimisation techniques, the objective function is to minimise the difference between an actual and specified distribution of blade surface velocity or other types of distribution, such as Fan (1998). Hence, the blade geometry is determined by a specified distribution on the surface of the blade. This type of approach is more preferable as it gives more control on the desirable designed blade. Moreover, this technique is a sort of 'inverse design' approach, which obtained the required blade geometry with the specified design distribution without a direct mathematical relationship between them.

The author's work on this aero-thermal optimisation is to develop a design methodology for design of highly thermally loaded turbine blades in which the blade geometry is designed subject to a specified distribution of heat transfer coefficient. The interesting part of this work is to see whether it is possible to redesign a turbine blade with less heat transfer coefficient in certain part of the blade. This could reduce the aerodynamic and thermal efficiency penalties, which is produced by the cooling system. This optimisation approach will be a great help for the designer to have blade geometry by concentrating more on the aerodynamic and heat transfer performance.

The optimisation was performed on the iSight framework, which is integrated with the blade geometry generator, grid generator, and solver. The blade profile is generated smoothly by two Non-Uniform Rational B-Splines (NURBS) subroutines. The first subroutine produces the camber line and the

other one produces the thickness distribution. Then a set of point or mesh on the flow field is automatically generated and solved by Navier-Stokes solver.

Modern turbomachinery operates under very complex three dimensional flow conditions. This reason with the additional demand of heat transfer calculation forces us to look at viscous model. The Favre-averaged Navier-Stokes solver closed with Baldwin-Lomax turbulent model is the convenient choice for flow and thermal simulation, and of course, for optimisation. The turbulence level in most turbomachinery flow is high, but the boundary layer profile is originally laminar at the leading edge of the blade and then develops into turbulent boundary layer downstream. The Abu-Ghannam and Shaw transition model is incorporated to treat transition, hence improving the prediction of heat transfer.

The main objective of the research described in the following chapters is to develop the inverse method with the C-type grid topology, which can treat better at the leading edge of the blade, especially for large leading edge and thickness such as turbine blades. The research, validation and investigation of the method are performed numerically.

This thesis consists of six chapters and is created concisely. It is suggested to read through this thesis from beginning in order, as some theories that have been previously described are no longer written. For example, in chapter four some numerical methods of the developed Navier-Stokes flow solver can be found in chapter two and the theoretical background of it can be read in chapter one.

In chapter one, we give general view of inverse design and optimisation method. Some relevant matters, such as basic theory, equations, and the progress of inverse design and optimisation to the recent time are presented in the literature survey. This section is very useful to see the comparison between the methods and to understand more clearly the assumptions or conditions that will be defined in the other chapters.

Chapter two presents the development of inverse method. It begins from the theory of grid generator to the blade modification code. The validations of the Euler solver using published experimental result can be seen in chapter three. Two examples of inverse method are given in this chapter.

Chapter four and five are concerned with optimisation method. Firstly, the development of Navier-Stokes flow solver is given in chapter four. The Baldwin-Lomax turbulence model and the Abu-Ghannam and Shaw transition model can be found in this chapter. Then, chapter four is closed by the description of the developed optimisation method. Chapter five completes the optimisation method discussion by presenting the solver validation and two examples of optimisation method.

Finally, chapter six draws some conclusions from the present work and makes some suggestions for future development.

I.2 Literature Survey

Optimisation and inverse method are numerical design method, which employ CFD to analyse turbomachinery blade performance. This section will describe some theoretical background for the development of optimisation and inverse method.

I.1.1 CFD

As implicitly described in the introduction, the rapid evolution of computer and consequently CFD has revolutionised the way of designing the geometry of the blade. CFD play a major role in these numerical approaches and it is important for the researchers of optimisation and inverse method to have knowledge and experience with CFD. It is absolutely impossible for especially the developer of inverse method to develop a mathematical relationship between the governing flow equations, blade geometry and specified design parameters without any knowledge of CFD. This is why the author put CFD in this thesis, meanwhile it is also a big part of the author's works.

Following Chapman, Green, Rubbert, Fletcher (1987), and Versteeg (1996) CFD provides several advantages compared with experimental fluid dynamics and hence, shows the advantages of inverse method and optimisation:

1. Design and development time of turbomachinery blade is significantly reduced.
2. Reduced cost as it "virtually" produced blade geometry and flow calculations in computer.
3. It can provide more detailed and comprehensive information
4. It can easily performed off design analysis and simulate flow conditions not reproducible in experimental model tests.
5. Lower energy consumption.
6. Reduced wind tunnel testing and more cost effective.

The inverse method and optimisation are mainly build by CFD (i.e. grid generation and solver), their methods and performance depends on the computer capability. The development of CFD had a great impact on the inverse design capability as the speed of digital computer, storage capacity and memory size improved. For example, the development of inverse method uses more complicated solver and the possibility of optimisation design in three-dimensional analysis.

I.1.2 Grid Generation

The most desirable characteristics of a method for generating grid are that it be able to treat arbitrary boundary shapes. This is very important in inverse method or optimisation where the blade is always modified for each iteration. The method of generating grid should offer complete freedom in choosing the body shape and outer boundary shape. Another important characteristic is the ability to specify the spacing between points at the boundary. The spacing is required especially between the body and the adjacent mesh line of the same family, which depends on the flow model being used, for example viscous or inviscid.

Orthogonality is another desirable feature to delete some certain terms from the governing flow equations. However, the orthogonality at every mesh point must be guaranteed to ensure that terms can be deleted. For some applications, it is desirable to control the location of the points and the orthogonality of the grid at the boundary. Co-ordinate systems that are orthogonal, or at least nearly orthogonal near the boundary, make the application of boundary conditions more straightforward. Although strict orthogonality is not necessary.

The grid generation techniques can be classified as conformal mapping, partial differential methods, and algebraic methods (Thompson 1984). The

classical technique, conformal mappings is based on complex variables so that it requires a reasonable knowledge in the area of complex variables. The implementation of this technique is quite difficult and the determination of mapping functions is not easy. Furthermore, there is limitation for complicated configurations and the grid that is generated is inherently two-dimensional. The second technique, partial differential equations are more popular than the first one. This method generate grid by solving the partial differential equations such as elliptic, parabolic, or hyperbolic system in a rectangular domain with uniform grid spacing for the location of the grid points in the physical space. The elliptic grid generator is commonly used and extensively developed method than parabolic and hyperbolic grid generators, although they have some interesting features. This technique is commonly used for 2-D configurations, but it can be extended for 3-D problems. Finally, the algebraic method is geometrical construction using algebraic equations to relate grid points in the computational domain to those of the physical domain. This technique is the fastest procedure in many cases. The other advantages of this technique are mathematically unsophisticated and easy direct control of grid points distribution. However, the problems in the regard to the experience using this technique are there is no inherent smoothing mechanism and for some cases it propagates boundary slope discontinuities into the field.

The other area of grid classification is that the grid system can be categorised as fixed or adaptive grid. A fixed grid system is generated prior to the solution of the governing fluid motions and remains fixed independent of the solution. While, an adaptive grid system evolves in response to the developing physical solution being done on the previous grid. The point distribution over the field is thus readjusted dynamically to concentrate points in the regions of larger solution variation. Therefore, several considerations should be made on the adaptive grid in order to retain the smoothness or not become too skew on the developed grid. This could be one of the reasons why the inverse design or optimisation developers avoid this type of mesh. The author prefers the fixed grid for the speed advantages where the grid should be generated several times in inverse method and optimisation.

The shape of the grid can be seen from the structure of mesh around the blade, which is simply related to the letter such as 'O', 'C', or 'H'. For example, Denton (1974), Arnone (1993) and Tiow (1998) used H-type grid, and Furukawa et al. (1991), Leonard et. al. (1991) and Arnone (1993) used C-type grid. There are two requirements that help to decide which is the best basic structure. Firstly, the requirement to calculate the development of the wake from the blade (King et al. 1988). It means that the grid has lines, which approximately follow the path of the physical wake from each blade: this can be catered for by either a "C" or "H" topology. The second requirement is associated with the grid near the leading edge (Thompson 1984). The C-type gives better treatment at this region since it wraps around the leading edge of the blade. Thirdly, concentration of co-ordinate lines near the blade is also more efficient with the C-type grid, especially O-type grid if the wake is out of consideration. It is also possible to use H-type grid, but points are wasted upstream. Finally, the treatment of upstream and downstream region is better for H-type grid. While the C-type grid is very sparse and badly skewed far upstream, especially of highly staggered and cambered blades. For many turbomachinery blades, it is important to wrap the leading edge as this part will give a big effect on the performance of the blade, such as turbine blade or diffuser (Yoshinaga et. al., 1980)

Of the computational point of view, the grid generator can be divided into two main groups namely structured and unstructured. The distinction between structured and unstructured grid resides in the type of data structure. In structured grid, the points have an implicit connectivity relationship. While in unstructured grid, the points can not be represented in such a manner, and additional information is needed (i.e. the connectivity of points is defined explicitly). The combination of structured and unstructured, hybrid grid is used to have the advantages of both approaches. Most of the optimisation and inverse design method applied structured grid. The researchers prefer on the simplicity and the speed that effect on the whole calculations of inverse method. However, unstructured grid could be found on the inverse method (e.g. Ahmadi et. al., 1998) and optimisation (e.g. Elliott et. al., 1996)

The grid can also be seen from the number of grid points as coarse and fined grid. Some researchers prefer to call them as inviscid and viscous grid as shown in many paper or publications. It is true that in order to calculate the viscous effect more grid points are needed near the wall, for example Rhie (1998) employed 200,000 grid points to resolve viscous layers. However, some researches who applied inviscid grid are still considering the viscous effect (e.g. Tiow, 1998) by the used of viscous model proposed by Denton (1992).

I.1.3 Flow Solver

Basically, there are four numerical solution techniques: finite difference, finite element, finite volume, and spectral method. The main differences between them are associated with the way in which the flow variables are approximated and with the dicretisation processes.

The finite volume method was introduced into the field of CFD by McDonald in 1971 and MacCormack and Paullay in 1972 for the solution of two-dimensional. Then, It was extended to three-dimensional flows by Rizzi and Inouye in 1973. This technique as seen on its name is the integral formulation of the conversion laws, which are discretized directly in the physical space. The conservation of a general flow variable $\varnothing$, for example a velocity component or enthalpy, within a finite control volume can be expressed as a balance between the various processes tending to increase or decrease it. In other words:

$$\begin{bmatrix}\text{Rate of change}\\ \text{of } \varnothing \text{ in the control}\\ \text{volume with}\\ \text{respect to time}\end{bmatrix} = \begin{bmatrix}\text{Net flux of}\\ \varnothing \text{ due to}\\ \text{convection into}\\ \text{the control volume}\end{bmatrix} + \begin{bmatrix}\text{Net flux of}\\ \varnothing \text{ due to}\\ \text{diffusion into}\\ \text{the control volume}\end{bmatrix} + \begin{bmatrix}\text{Net rate of}\\ \text{creation of } \varnothing\\ \text{inside}\\ \text{the control volume}\end{bmatrix}$$

There are two basic finite volume techniques for the discretization. The first scheme is cell centre and the other one is cell vertex scheme. In the cell centre scheme, the flow variables are located at the centre of the cell. While, in the case of cell vertex scheme the flow variables are located at the vertices of the cell. The comparison for both schemes is provided by Swanson (1991). His results show that both schemes give almost identical results and an analysis of discretization error indicates that the cell vertex scheme should exhibit smaller discretization errors on stretched mesh.

As indicated by the research of the past few years, the flow solution can be obtained rapidly by solving the potential equation, but it does not allow for vorticity and entropy changes related to shock waves. Many numerical methods have been developed to solve Euler equations (e.g. as Subramanian et. al., 1985). However, inviscid analysis requires some assumption about the circulation to get a unique solution. The problem may become ambiguous when dealing with a rounded trailing edge. Arnone (1993) added that heat transfer and boundary layer thickening, which can lead to separation and hot spots, can not be represented in an inviscid solution.

In recent years, considerable progress has been made in the development of flow solvers for computation of flow in turbomachinery. There are many fully three-dimensional multistage solvers have been published, such as Denton (1992). As computers became powerful, the research is increasingly focused on the viscous solver based on Navier-Stokes equations (e.g. LeJambre et. al., 1998). It includes research on the calculations of turbulence and transition model which are very important for the calculations of heat transfer or cooling design system. For example, Xiao and Amano (2000) performed numerical study of the heat transfer distribution using algebraic turbulence model. Advanced turbulence models have been studied for turbomachinery, although most of them are two-dimensional calculations. Further discussion can be seen on the turbulence and transition model section.

I.1.4 Multiblock

In the beginning, the researchers concentrated on highly efficient flow solvers dealing with a single-block-structured grid. There was a problem when attempted to cover a complex flow domain with a monoblock grid. Then, following the single-block method was the technique of multiblock structured grid, which allowed more complex geometries to be mapped. However, the geometric flexibility offered by multiblock grids was paid for by significant human-interaction times. It is possible to perform flow-solution for a complex geometry in a day or two, but to obtain an adequate grid could take up to six months of human interaction time (Smith, 1996).

Several authors have developed multiblock grid generation schemes. Different constraints are applied at the block boundaries, and details of the methods for generating the grids within blocks may vary. Alternative methods for generating grids suited to complex configuration have been described by many authors. Some of these methods yield grids with a block like structure, but the blocks may not be rectangular, or the grid within each block may be generated independently of the grids in other blocks, leading to a lack continuity at block boundaries. For example, Dannenhoffer and Baron (1986) use solution-adapted grid embedding to produce desired grid point in the region of high flow gradients. In the point of view of grid points, this procedure is efficient, but leads to irregularly shaped blocks. Moreover, a cell-based data structure is necessary for a completely irregular grid. The other researcher, Ni and Bogoian (1989) published a method for calculating multistage turbine flows in which grids adjacent blocks move relative to each other. Obviously, there is no grid line continuity at internal block boundaries in such a case, and so a complicated approach to the calculation of the flow at this boundary must be adopted.

There is another schemes also called multiblock, but differs from those examples. The criteria for dividing the physical space are completely different and blocks are not necessarily associated with particular components of the configuration. However, it essentially provides a means for dividing the physical space into blocks of a size such that the associated data will fit into the available computer memory.

Now, the multiblock strategy begins to be implemented for the inverse method such as proposed by Demeuleaere (1997). He uses a fully inter-block boundary connectivity in order to allow the use of hyperbolic O-grid and C-grid around the blade and also the H-grid at the upstream.

I.1.5 Turbulence Model

As most turbomachinery flows are turbulent with the laminar and transitional regions occurring near the leading edge of the blade, the turbulent flow regime is not just of theoretical interest. The designers need a tool that at least capable to predict the effect of turbulence to the aerodynamic and heat transfer performance.

At the moment in the engineering fields, the effect of turbulence is approximated popularly by turbulence model. The turbulence model is a computational procedure to close the Reynolds-averaged Navier-Stokes equations. According to Menter (1992) and Lakshminarayana (1996) the closure models can be classified as follows:

1. Zero-equation or algebraic eddy viscosity models. These models do not employ any differential equation for the turbulence quantities. Hence, they are the simplest, easiest, and economical to run, for example Cebeci-Smith and Baldwin-Lomax models.
2. Half-equation model, for example Johnson-King (1985) model. In this model, the eddy viscosity of an algebraic model is related to the maximum

Reynolds shear stress, which is derived from the partial differential equation.

3. One-equation models. These models are more expensive than the previous models since It solve a partial differential equation (PDE) over the whole field for a working variable related to the eddy viscosity at each time step, for example Baldwin-Barth and Spalart-Allmaras models.
4. Two-equation models. Two transport equations (partial differential equations) are solved for a turbulence length scale and for a turbulence velocity scale. The examples of two-equation models are k-ω model (Wilcox), and k-ε (including Standard, RNG and Realisable).
5. Reynolds Stress Model. (RSM) This model closes the Reynolds-averaged Navier-Stokes equations by solving the transport equations for the Reynolds stresses, together with an equation for the dissipation rate. This means four PDEs are required in 2D flows or seven for 3D. RMS is also called the second-order or second-moment closure model.

In fact, there is no single turbulence model that globally accepted as being superior for any flow conditions. Every model has different characteristic and weaknesses. The choice of turbulence model are generally depend on consideration such as the physics of flow condition, the level of accuracy, the time of computation, and the computational resources. Therefore, in order to make a right decision of model, it is necessary to understand the capabilities and limitations of the models. Some researches have done some general comparison of turbulence models such as Menter (1992), Rumsey and Vatsa (1993), Noguchi (1994), and Compton (1996). Moreover many researchers investigated, verified, and implemented in another application such as Abid et. al. (1990). Hence, more suggestion and modification had been made to improve the turbulence model such as Johnson (1987).

In the turbomachinery field itself, several turbulence models have been tested and validated such as Larsson (1987), Arnone et. al. (1991), Amano et. al. (1996), Garg et. al. (2001). Moreover, the turbulence models also compared

and investigated in a complex turbomachinery flow such as Turner et. al. (1993), including RSM model such as Gerolymos et. al. (2001)

I.1.6 Transition Model

The turbomachinery flows are mostly turbulent. However, the boundary layer along the blade surface is normally subject to laminar-turbulent transition with the boundary layer profile around the leading edge is originally still laminar. The process of transition has a great effect on the aerodynamics and heat transfer on the blade. Errors in the analysis of the transition location could affect the machine efficiency by several percents and the component life by more than an order of magnitude. Therefore, an understanding and prediction of boundary-layer transition are important to turbomachine design and therefore can not be neglected.

The laminar-turbulent transition can be simulated using several methods such as experiment-based empirical correlation, transport turbulence models, or large-eddy simulation. For many years, engineers employed empirical correlation (e.g. Abu-Ghannam and Shaw, 1980), as the computational cost is relatively small. The correlation approach is generally reliable for attached flow. Birch (1987) published the comparison of transition flow of a turbine cascade using Abu-Ghannam model and his one-equation transport turbulence model. He concluded that his one-equation turbulence model predicts better on the suction side. Another research on transition flow was performed for heat transfer analysis by Sarkar (2001). He showed that the coupled Baldwin-Lomax and Abu-Ghannam model was better than the two-equation model.

The literature on the transition flow from the flat plate and aerofoil is abundant, but the publications of transition flow for turbomachinery blades are still limited. However the development of transition model continues as many

experiments have been done such as Roach et. al. (2000) and Johnson (2002). Furthermore, there has been an effort to simulate three-dimensional turbomachinery flow using transition model (i.e. Abu-Ghannam and Shaw model) as published by Gier et. al. (2000).

I.1.7 Heat Transfer

The research of heat transfer in turbomachinery is an important point for designing turbine blade and continues as the market demand for higher performance of aeroengines increasing. The performance of aeroengines can be improved by the increased of turbine entry temperature and compressor pressure ratio (Boyle, 2001 and Sarkar, 2001). However, increased pressure ratio results in high exit velocities and often accompanied by complex shock-boundary layer interactions. The increased turbine inlet temperature results in hostile environment for the turbine blade, especially for the first-stage turbine blade. According to Heiser (1978) the hostile environment is defined as the nozzle and blade rows are subjected to high temperatures, large variation in temperature along the blade, unsteady thermal field due to rotor-stator interaction, and high inlet turbulence intensity, resulting in random temperature fluctuation.

The major problem is associated with the availability of material that can withstand with such hostile environment and combined stresses (due to temperature, rotation and aerodynamic loading). Therefore, a greater research of predicting and simulation of aerodynamics and heat transfer is important for the designers to increase the performance of aeroengine and to support the life of the blade.

Normally at low to moderate temperatures, such as encountered in turbines, the heat transfer is greatly coming from convection and conduction. The effect of heat transfer by radiation is not significant. The overall heat transfer in a fluid including both conduction and convection is frequently named as

convective heat transfer. On this environment, the temperature and velocity fields are coupled and interacted.

For the convective heat transfer to uncooled blade, the boundary layer is the critical element. The boundary layer acts as a buffer zone between the main stream and the solid and it also acts as a resistor to the heat transfer. The property and environment of the boundary layer determines the rate of heat transfer.

According to Lakshminarayana (1996), the blade heat transfer phenomena can be categorised as follows: stagnation point, laminar boundary layer, transitional boundary layer, turbulent boundary layer, shock-boundary layer interaction, separation with reattachment, and separation without reattachment. At stagnation point and near leading edge where the boundary layer is thin, the velocity and temperature gradients is very high. Hence, the heat transfer rate is very high in this region. The heat transfer is normally higher for a thin boundary layer than for a thick one. Furthermore, the heat transfer in a turbulent boundary layer is higher than in a laminar boundary layer. In separated flows, the velocity and temperature gradients are small, so that the momentum and heat exchange normal to the wall are low. The heat transfer under this region is low. Then if the flow reattach, the heat transfer is high.

Research activity in prediction and simulation of the heat transfer are coupled with turbine aerodynamics due to the strong relations between them. A good prediction of heat transfer strongly depends on the accuracy of the aerodynamics simulations applied. Prediction of the turbine aerodynamics was a difficult problem that has received a great amount of research over the past decades. This could be the reason why the research for the prediction of heat transfer is lagging behind. As the prediction of aerodynamics is getting better for the complex turbine flows, the heat transfer prediction had only had limited success.

A good heat transfer prediction should have a proper model that can cope with complicated turbine flow environment, which comes from combustor, such as turbulent intensity, boundary layer, and transition. If the aerodynamics prediction is not correct, it is unlikely the corresponding heat transfer calculations will be correct. Numerous researches on prediction of the heat transfer to an uncooled blade had been done using some turbulence and transition model, and compared results against experimental data. The accurate prediction of heat transfer to an uncooled blade is an important step in predicting the blade surface temperature distribution and designing an efficient cooling system. Birch (1987) presented the heat transfer of turbine cascade. A two-dimensional explicit Navier-Stokes was adopted and two turbulence-transition models were implemented. The first model was an algebraic model based on Cebeci-Smith turbulence model, coupled with a modified Abu-Ghannam and Shaw transition correlation. The heat transfer result was quite good on the suction surface but unsatisfactory on the pressure side. While, the second model, one equation turbulence model, predicted better on the pressure side, but very poor on the suction surface. Larsson (1997) used a Navier-Stokes solver to simulate two-dimensional heat transfer on turbine blade. The heat transfer results were obtained and investigated using two k-ε (Chien and Launder-Sharma) and two k-ω (Wilcox, standard and transition) turbulence models. All models predicted heat transfer results too high near the leading edge and had the problem with the transition on the suction side. The transition was predicted too early and too short. Smith et. al. (2001) investigated another heat transfer distribution around two uncooled blades, which include repeat measurements made by different instrumentation. A three dimensional Navier-Stokes code was used and the Baldwin-Lomax turbulence model was chosen. The transitional boundary layer was modelled by an algebraic model produced from the research of Mayle, Abu Ghannam, Shaw, Brown, and Martin. The heat transfer result on the pressure surface is at the limit of uncertainty of the experiments, while on the suction surface is unsatisfactory. Furthermore, Smith et. al. Investigated the sensitivity of the solution to the wall spacing. They concluded that the results were better for y^+ below than 5.

Unlike the pressure or Mach Number validation, none of the numerical validations can exactly match to the experiments and mostly gave results very poor near leading edge. Arts in his paper (1998) validated two of his codes with his experimental data. The quasi-3D code gave the best result, but the 3D one which employed k-e turbulence model could catch the separation bubble close to the leading edge. Xiao (2000) showed that his 3D Baldwin-Lomax turbulence model code gave improved results as compared to the 3D predictions of Arts. In his paper, Xiao excerpted Larsson (1997) analysis that k-e or k-w turbulence model could not able to accurately predict the heat transfer on the suction surface, especially in the transition regimes.

I.1.8 Optimisation

In contrast to the direct approach that has been explained in the introduction, the designer prescribes certain conditions for the flow field and then the method provides the resulting blade profile. This approach can be of great help in finding the required blade shape and allow the designer to concentrate on the flow behaviour rather than on the geometric shape.

Furthermore as also mentioned in the introduction, the inverse design can be divided into two main categories. The first category is optimisation that iteratively modifies a set of geometrical parameters until the desired blade with the minimum "cost" function is found. This method works through minimising the error, for examples between the surface velocity distribution and the target velocity distribution (Fan, 1998), isentropic Mach number distribution (Pierret et. al., 1998), and profile loss (Trigg et. al., 1999).

The optimisation techniques are mainly gradient-based methods and exploratory algorithms. There are several optimisation methods that have been developed such as control theory (Lewis et. al., 1996), hill-climbing (Shelton et. al., 1993), simulated annealing (Pierret et. al., 1998 and Ingber,

1993) and genetic algorithm (Fan, 1998 and Trigg et. al., 1999). The control theory method is a gradient-based method. This model is powerful for minimisation of smooth and continuous function space.

Simulated annealing is an exploratory method. The term "annealing" refers to special process of heat treatment and then reducing the temperature slowly. Hence, allowing to reach global minimum of internal energy state. For example, consider a mountain range, with direction as a parameter. We wish to find the lowest valley. Simulated Annealing approach can be easily imagined as a ball, which is bouncing over mountains from valley to valley with 'parameters' direction. We first start at high "temperature" where the ball is permitting to make very high bounces over any mountain to access any valley. Then as "temperature" is relatively colder, the ball is bouncing relatively lower. We found the valley from the last saved lowest valley. Therefore, this method can find the global solution which is hidden among local extreme.

The genetic algorithms (GAs) are categorised to exploratory method. It can be said as natural selection and Darwin's main principle: survival of the fittest. The GAs works with a population of individuals (i.e. blade profiles) which have different features or characteristics. They are coded into a binary string that can be said as the genetic code or the chromosome of the profile blades. Then the blades are analysed and selected for the best one in the required environment: the specified flow conditions. The newly selected individuals are arranged in pairs or mated in order to have a new generation using cross over technique. Final evolution was made by random mutation at a given mutation rate. However, the genetic algorithm has disadvantage in the CPU (Central Processing Unit) time due to the large computational requirement and it is very time consuming as many "genetic mutation" should be done. This method is not appropriate for the long running solver. Therefore, that is the reason why Fan (1998) used Artificial Neural Network (ANN). In his paper, it can be shown that the design time using ANN is 15 times faster than using conventional solver. However, the reliability of the ANN depends on the number of training or the 'skill' of the network.

The optimisation algorithm should be incorporated with other code in order to analyse objective function. This code is very important for optimisation algorithm to know the quality of the given candidate or to see if the given blade profile meets the required criteria. For example, Pierret (1998) employed Navier-Stokes code developed by Arnone et. al. (1994) and Trigg et. al., (1999) applied a two dimensional viscous solver (Dawes, 1983). Some researchers find another alternative to predict the objective function such as Fan (1998) who employed Back Propagation (BP) Neural Network to predict surface velocity distribution. The reason of using ANN can be seen in the previous paragraph.

Furthermore, many optimisation methods require a set of parametric representation of the problem and geometry. These parameters are usually the subject of separate studies due to its criticality and sensitivity. For example, the optimiser program should have a set of parameters that can represent the aerofoil shape accurately and in a sensible manner. The parameters that do not produce a sensible profile will cause problem in the flow analysis.

I.1.9 Inverse Method

The second category is inverse method. In this method the initial blade (i.e. the physical model) is required and modified using the result from the flow calculations until the difference between the computed and prescribed design specification is close enough. The blade geometry is usually modified using a geometry modification algorithm or blade boundary condition such as slip condition at the wall. The design parameters are not as many as optimisation method, allowing it much faster design process.

Many inverse methods have been developed in all flow calculations. A large number of potential flow inverse methods are available, for example Lighthill

(1945), Hawthorne et. al. (1984), Tan et. al. (1984), Sanz (1988), Yang et. al. (1993), and Zangeneh (1991) for compressible flow. The viscous effect is introduced (Zangeneh, 1994) by viscous-inviscid interaction that are calculated using three dimensional Dawes code (1988). Dang (1992) extended the scheme to the transonic flow regime by replacing the Fourier expansion technique into finite volume method. The method was modified for blades with finite thickness as proposed by Jiang et. al. (1997). However, the potential inverse method is limited to shock-free irrotational flows.

Recently, most of the inverse method publications are devoted to inviscid calculation using Euler solver. A lot of research has been presented by Zannetti (1987), Giles et al. (1987) with capabilities for transonic flow, Leonard et. al. (1991), and Demeulenaere et. al. (1998) for three-dimensional design. Dang et. al. (1995) represented the blade by a periodic array of discrete body forces, which is included in the equation of motion. There has been an effort to combine with viscous model such as Tiow et. al. (1998) and Damle et al. (1999).

The Navier-Stokes inverse methods are provided by Demeulaere et. al (1997). This method is an extension previous work of Leonard et. al. (1991) to a two dimensional viscous inverse method using two-dimensional multiblock upwind finite-volume Navier-Stokes solver coupled with Baldwin-Lomax turbulence model. This method will provide a 'metallic' geometry without any effort to subtract the boundary layer thickness from the 'inviscid' geometry. Unlike the previous inviscid method, the well-posedness of permeable wall boundary condition is questionable. Therefore, the flow field is updated with impermeable blade walls (i.e. the prescribed pressure is not explicitly imposed along the blade). The same blade modification algorithm is applied, but with the tangential velocity along profile is obtained from the outer edge of the boundary layer.

Most of the works of inverse methods are first made in two-dimensional calculation and require several simplification, and therefore restrictive assumptions. The examples of two-dimensional blade-to-blade inverse

method are Hawthorne et. al. (1984), Giles et. al. (1987), Leonard et. al. (1991), and Demeulaere et. al. (1997). The two dimensional design methods are not accurate for turbomachine applications and the important phenomena such as secondary flows, three-dimensional shock structures, and tip clearance effects can not be modelled. The three dimensional method has been developed by Smith (1987) using a quasi three-dimensional approach. The full three-dimensional design methodologies have been shown by Tan et. al. (1984), Zangeneh (1991), Dang (1993), Yang et. al. (1993) and Demeulenaere et. al. (1998).

In the early stage of development inverse method, the design specifications are mostly the surface velocity (or Mach Number) or pressure such as Giles et. al. (1987) that specified pressure distribution along most of the suction surface or Leonard et. al. (1991), and Demeulenaere et. al. (1998) that specified pressure distribution on the suction and pressure surface. These design specifications are usually chosen to avoid flow separation on the certain parts of the blade surface and flow condition. For three-dimensional flow problem, although this design philosophy can be adequate for external flow applications such as the design of aircraft wing, they may not be easily adapted to three-dimensional internal-flow applications. The main reason is the potential effect of rotating flow (e.g. secondary flow, tip-clearance flow). It is difficult to predict constraint surface velocity in the three-dimensional turbomachinery structure flow. The other complication with this choice of prescribed flow quantity is the question of how arbitrarily one can specify such the blade-surface pressure distributions at the different spanwise locations.

The useful design specifications that can be compatible with the flow distribution and work distribution are mean swirl distribution $r\overline{V_\theta}$ for three-dimensional axial blade. The prescribed pitchwise averaged tangential velocity, $\overline{V_\theta}$ with constant radii, for example hub (inner) or tip (outer) radii can be defined as,

$$\overline{V} = \frac{B}{2\pi} \int_0^{2\pi/B} V \partial\theta \tag{I.1}$$

Where the integral is taken over the constant blade pitch, so that including the blade. In the two dimensional calculations the above equations is modified for the integration along the pitch (i.e. s=2π/B).

The mean swirl distribution method is the first development of a theory in which the effect of the blade is represented by a distribution of bound vorticity whose strength is determined from the prescribed tangential velocity along the assumed blade profile (Hawthorne et. al., 1984). The blades are assumed to have zero thickness and incidence so that there are no stagnation points at the leading edge. The pitchwise averaged tangential velocity is prescribed at all points along the blade. The new blade profile is expressed by iteration procedure using the blade surface boundary condition (i.e. no flow normal to the blade surface).

$$\mathbf{V}_{bl} \cdot \nabla\alpha = 0 \tag{I.2}$$

Some examples of this method are Zangeneh (1991, 1994), Dang (1992, 1995), Yang et. al. (1993), and Smith (1987) for unducted fan. The pitch-average velocity is an attractive prescribed flow quantity since turbomachinery blades extract and supply energy from or to the fluid from the angular momentum exchange. Moreover this prescribe distribution is appropriate quantity to remove swirl (in a compressor) or add swirl (in a turbine) to the flow.

Tan et. al. (1984) described the Kutta-Joukowski relation between lift and circulation, i.e. the relation between the lift force and the pressure between upper and lower surfaces which result in

$$\overline{V}_{bl}.\nabla r\overline{V}_{\theta} = -\frac{B}{2\pi}\frac{\left(p^{-}-p^{+}\right)}{\rho} \tag{I.3}$$

In another literature Dang and Isgro (1995) derived the pressure loading distribution from a periodic array of discrete body forces which is included in the equation of motion,

$$\Delta P = P^{+} - P^{-} = \dot{m}\frac{d\tilde{V}_{y}}{dx} \tag{I.4}$$

where

$$\tilde{V}_{y}(x) = \frac{1}{\dot{m}}\int_{0}^{s} V_{y}\left(\rho V_{x} dy\right) \tag{I.5}$$

Tan et. al. (1984), Zangeneh (1991), Yang et. al. (1993), Dang et. al. (1995), and Tiow et. al. (1998) have also shown that the rate of change of the mean tangential velocity is related to the blade loading.

One of the popular blade geometry modification algorithms for the prescribed pressure loading distribution is based on the transpiration principle. The solver is modified by replacing the slip boundary condition at the wall into a permeable wall boundary condition Hence, the imposed pressure loading at the wall will result in a normal velocity through the blade, which can be used to modify the blade geometry. More explanation of this method can be found on the inverse literature such as Leonard et. al. (1991), Demeuleaere et. al. (1997), and Tiow et. al (1998),

One of the advantages of inverse method is the possibility to improve the flow field such as impeller exit flow. Zangeneh et .al. (1996b) described the reduction of impeller exit flow nonuniformity by reducing the secondary flows on the blade suction surface. To suppress secondary flows, the impeller blades were designed by suitable choice of the design specification such as

loading distribution and stacking condition. As the choice of loading distribution to some extent are limited by the cavitation reduction criteria, the location of stacking has significant effect on the blade reduced static pressure, whose spanwise gradients are correlated directly to the meridional secondary flows in the impeller.

In 1998 Zangeneh et. al. presented a set of guidelines for the systematic design of mixed flow and centrifugal compressors and pumps with suppressed secondary flows and a uniform exit. These guidelines were validated experimentally and it also showed the inverse design impeller had 5 percent higher at the peak efficiency point as compared with the conventional one. Recently, the guidelines for the systematic design of diffuser are also presented by Zangeneh et. al. (1999). These guidelines are also validated experimentally by oil visualisation

Chapter II Theory of Inverse Method

This chapter will provide the theoretical background of two-dimensional Euler-based inverse method developed by the author. It begins from the development of grid generator, the Euler solver, and then the new blade generator. As discussed in the previous chapter each of them is an integral part of the inverse method procedure.

A structured C-type grid is chosen as it has many advantages. The choice of structured grid is mainly due to the simplicity and the speed for calculation. It provides the simplicity in the solver development and in the way of new blade geometry generated as the calculation is simple and short. Hence, it gains the advantage of speed in the calculation. Meanwhile, the C-type grid is the best choice as it has capability to treat blunt leading edges. Consequently, it gives better reliability on the calculation of blade geometry modification. Some advantages and comparison to the others type of grid can be seen in the literature survey.

The new blade modification algorithm is based on the slip condition where the velocity on the surface of the blade is required. This blade modification method has been widely used for inverse method such as Zangeneh (1994), Dang (1995) and Tiow (1998).

The slip condition restriction can only be satisfied by the inviscid solver. A cell vertex Euler solver was developed in order to satisfy this restriction. The Euler equation is the most complete description of inviscid flows and the highest level of approximation for the non-viscous fluids.

II.1 Grid Generator

The discretization of differential equations needs some organisation for the solution thereon to be efficient (i.e. it must be possible to identify the neighbouring points) and conform to the boundaries of the region so that it can be accurately represented.

At the present time, the boundary-conforming co-ordinate system is the most appropriate and used method for organisation of the discretization of the field for general regions (i.e. arbitrary regions). This curvilinear co-ordinate system covers the field and has co-ordinate lines coincident with all boundaries (i.e. without need of interpolation). Therefore, this technique frees the computational simulation from restriction to certain boundary shapes and allows the codes to be written in which the boundary shape is specified simply by input.

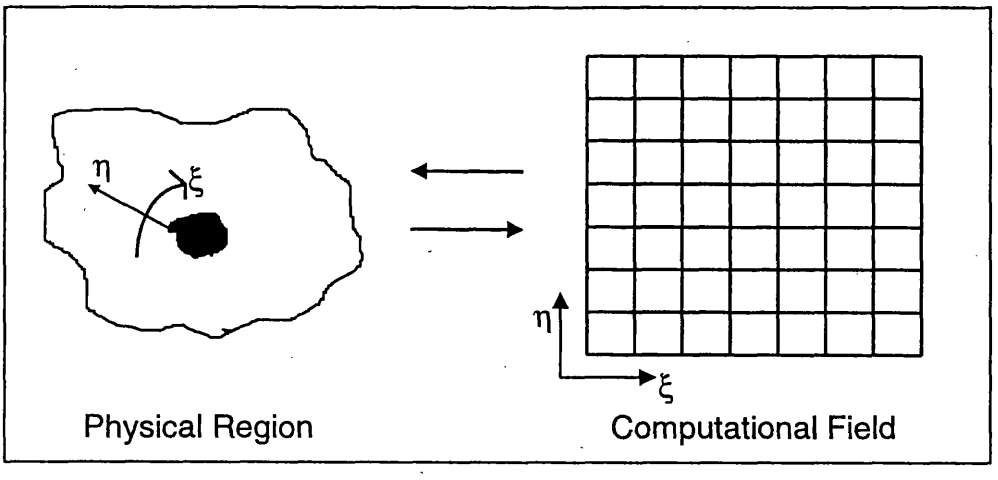

Figure 2.1. Domain transformation

The use of the curvilinear co-ordinate system allows all computation to be done on a fixed square grid in the computational field by transforming the partial differential equations of interest so that the curvilinear co-ordinates (ξ,η) replace the cartesian co-ordinates (x,y) as the independent variables. The resulting equations are more complicated, although the same types as the original ones. On the other hand, the domain is greatly simplified since it is transformed to a fixed rectangular region with a simple boundary condition regardless of the shape and configuration of the physical region.

The interval of curvilinear co-ordinate system may be normalised to any different units. However, It is convenient to define the increments of all the curvilinear co-ordinates to be uniformly unity with interval $[1,N^{(i)}]$ where $N^{(i)}$ is the total number of grid points in the ξ^i direction (for 2D i=1 and 2).

One of the methods used to generate grid is an elliptic system of partial differential equations. The use of an elliptic partial differential equation gives certain advantages. For example, the grid will be smooth even if the boundary of the domain has a slope discontinuity. In contrast, the hyperbolic partial differential equation will generate any slope discontinuities in the interior boundary.

The elliptic partial differential system that exhibits a considerable smoothness is the Laplace system:

$$\nabla^2\xi^i = 0 \quad (i = 1,2 \text{ or } 3) \tag{2.1}$$

This system guarantees a one to one mapping for boundary conforming curvilinear co-ordinate system and equally spaced in the absence of boundary curvature because of the strong smoothing effect of the Laplacian. However, it will become more closely spaced over convex boundaries, and less over concave boundaries. Hence, to control the co-ordinate line distribution in the field, the elliptic generating system is generalised to Poisson equations:

$$\nabla^2\xi^i = P^i \quad (i = 1,2 \text{ or } 3) \tag{2.2}$$

where P^i is the "control functions" to control the spacing and orientation of the co-ordinate lines.

As described previously, computation must take place in a rectangular domain with uniform grid spacing where the spatial derivatives at all points in the transformed domain can be presented by conventional finite-difference. Hence, in order to make use of a general boundary-conforming curvilinear co-ordinate system, the equations must first be transformed to the curvilinear co-ordinate by interchanging the dependent and independent variables. Then, the system becomes a quasi-linear elliptic system,

$$\alpha x_{\xi\xi} - 2\beta x_{\xi\eta} + \gamma x_{\eta\eta} = -J^2(P^1 x_\xi + P^2 x_\eta) \qquad (2.3)$$

$$\alpha y_{\xi\xi} - 2\beta y_{\xi\eta} + \gamma y_{\eta\eta} = -J^2(P^1 x_\xi + P^2 x_\eta) \qquad (2.4)$$

Where

$$\alpha = x^2{}_\eta + y^2{}_\eta \qquad \beta = x_\xi x_\eta + y_\xi y_\eta \qquad \gamma = x^2{}_\xi + y^2{}_\xi \qquad J = x_\xi y_\eta - y_\xi x_\eta$$

The control functions are expressed by Thompson (1985) in 2D as,

$$P^1(\xi,\eta) = -\sum_{i=1}^{N} a_i \; sign(\xi - \xi_i) \; \exp(-c_i \; |\xi - \xi_i|)$$

$$-\sum_{i=1}^{M} b_i \; sign(\xi - \xi_i) \; \exp\{-d_i \; [(\xi - \xi_i)^2 + (\eta - \eta_i)^2]^{0.5}\) \qquad (2.5)$$

where (a_i, b_i, c_i and d_i are constant)

and an analogous form for $P^2(\xi,\eta)$ with ξ and η interchanged. In the P^1 function, the effect of a_i, is to attract ξ-lines toward the ξ_i-line, and b_i is to attract ξ-lines toward the single point (ξ_i,η_i). The attraction decays with distance in ξ-η space according to the decay factors, c_i and d_i.

Another expression of control functions are described by Sorenson (1980) in two-dimensional as,

$$P^1(\xi,\eta) = p(\xi)e^{-a\eta} + r(\xi)e^{-c(\eta_{\max}-\eta)} \tag{2.6}$$

$$P^2(\xi,\eta) = q(\xi)e^{-b\eta} + s(\xi)e^{-d(\eta_{\max}-\eta)} \tag{2.7}$$

As seen in (2.6) and (2.7), Sorenson define the control functions in terms of four new variables with four positive constants. In order to avoid the confusion with derivative of η, the indices k is introduced. In the first line that contains the body points, the x and y derivative can be calculated by,

$$x_\eta\big|_{k=1} = \left[\frac{s_\eta\left(-x_\xi\cos\theta - y_\xi\sin\theta\right)}{\left(x_\xi{}^2 + y_\xi{}^2\right)^{0.5}}\right]_{k=1} \tag{2.8}$$

$$y_\eta\big|_{k=1} = \left[\frac{s_\eta\left(-y_\xi\cos\theta + x_\xi\sin\theta\right)}{\left(x_\xi{}^2 + y_\xi{}^2\right)^{0.5}}\right]_{k=1} \tag{2.9}$$

where $s_\eta\big|_k$ is the spacing next to the desired k line with the angle θ. While for the outer boundary (or periodic boundary for internal flow) can be calculated by

$$x_\eta\big|_{k=k\max} = \left[\frac{s_\eta\left(-x_\xi\cos\theta - y_\xi\sin\theta\right)}{\left(x_\xi{}^2 + y_\xi{}^2\right)^{0.5}}\right]_{k=k\max} \tag{2.10}$$

$$y_\eta\big|_{k=k\max} = \left[\frac{s_\eta\left(-y_\xi\cos\theta + x_\xi\sin\theta\right)}{\left(x_\xi{}^2 + y_\xi{}^2\right)^{0.5}}\right]_{k=k\max} \tag{2.11}$$

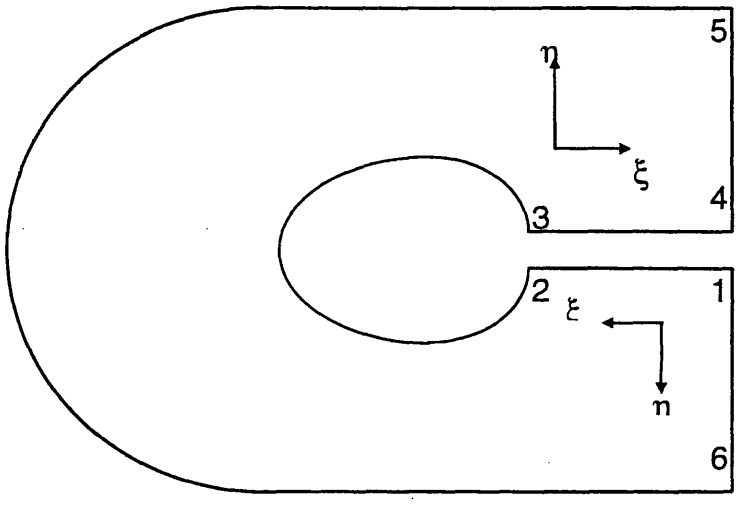

Figure 2.2 Physical region

Conceptually, the physical region can be considered to be opened at the branch cut and then deformed into a rectangle to form the transform region to help clarify the correspondence between the physical and transformed fields. Then, opening the physical field,

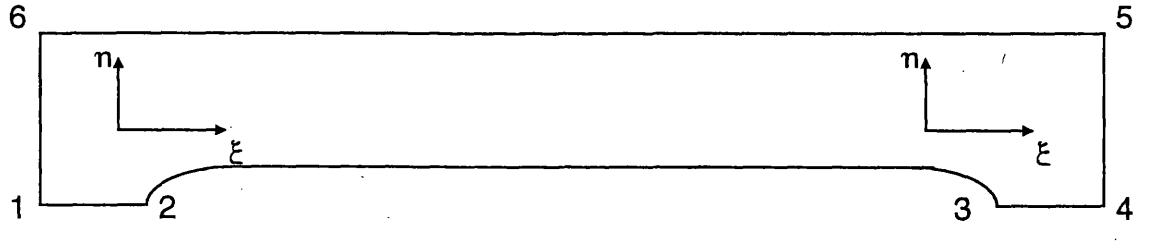

Figure 2.3 Deformed physical region

with 1-2-3-4 to flatten to the bottom of the rectangle. Here the blade points are distributed along the line 2-3. While, the lines 1-2 and 3-4 forming the branch cut which are both on the same side of the transformed region. Hence, the points located at line 1-2 coincide with the points along the line 3-4. However, continuity across the branch cut is still maintained. The configuration of the points at the branch cut can be seen as follows:

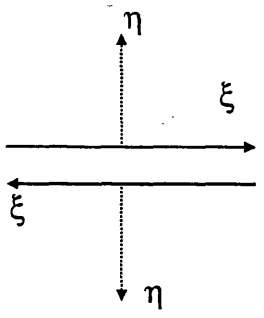

Figure 2.4 Direction on the "branch cut"

where it is indicated that ξ varies to the right on the upper side of the branch cut, but to the left on the lower side. The direction of η also reverses at the branch cut, so that although the lines are continuous across the branch cut, the direction of variation reverses.

Therefore, the use of "branch cut" allows general physical regions to be transformed to rectangular blocks in the computational field. The complicated physical region, especially in three dimensions can be configured appropriately using the branch cut. It is also possible to embed computational subfield, such as OCH-type mesh, in the overall computational field.

Then these algebraic equations are then solved iteratively using a Gauss-Siedel method.

II.2 Euler Flow Solver

The Euler solver is the core part of the inverse design procedure. The choice of Euler solver is suitable for inverse method as it enables one to apply the inviscid slip condition to compute the blade shape. However, the Euler solver fails to account for viscous effects.

The two-dimensional unsteady Euler equations satisfy continuity, momentum, and energy with assumption of flow media as an ideal gas. The equations are integrated using finite-volume time-marching method on the two-dimensional domain. The solver works on the two-dimensional multiblock fixed grid.

The Euler solver is developed using a cell vertex approach which is appropriate and easily implemented for inverse method. The approach employs central difference scheme with added artificial viscosity and a Runge-Kutta integrator proposed by Jameson et. al. (1981). The local time-stepping is implemented for convergence acceleration.

The background theory of the developed solver is fully described on the following section.

II.2.1 The Governing Flow Equations

The Euler governing equations assume that the friction phenomena and thermal conduction are neglected. The flow is regarded as a continuum and the fluid is treated as an ideal gas with absolute quantities.

The unsteady Euler equations for two dimensional compressible inviscid flow can be illustrated as a first order equation:

$$\frac{dw}{dt}+\frac{df}{dx}+\frac{dg}{dy}=0 \qquad (2.12)$$

Where,

$$w=\begin{pmatrix}\rho\\ \rho u\\ \rho v\\ \rho E\end{pmatrix},\ f=\begin{pmatrix}\rho u\\ \rho u^2+P\\ \rho u v\\ \rho u H\end{pmatrix},\ \text{and}\ g=\begin{pmatrix}\rho v\\ \rho v u\\ \rho v^2+P\\ \rho v H\end{pmatrix}$$

and E is total energy, which is obtained from internal energy and kinetic energy,

$$\text{i.e. } E=\frac{P}{(\gamma-1)\ \rho}+0.5\ (u^2+v^2)$$

with γ is ratio of specific heat.

Total enthalpy, H can be calculated from $H=E+\frac{\rho}{P}$

As mention before, the developed Euler solver is for compressible flow calculation. Therefore, the mass conservation, momentum equations, and energy equation can be linked together by equation of state.

II.2.2 Finite Volume Scheme: Cell Vertex Method

The basic feature of this schemes is the computation of the flux balance for each cell, where the quantity of the independent variables are specified at grid points (i.e. cell vertices) rather than at cell centre like Jameson et al. (1981). The advantage of cell vertex scheme is that it does not need any extrapolation on the wall boundary and as mention by Hall (1985) this scheme has second order spatial accuracy for flux balanced even at boundaries and with non-smooth grids.

The Euler equations, (Eq. 2.12) can be integrated over control volume in order to be discretized using Finite Volume method, and applying Green's theorem for a region Ω with boundary dΩ,

$$\text{i.e. } \frac{d}{dt}\iint_{\Omega} w\,dx\,dy + \oint_{d\Omega}\left(f\,dy - g\,dx\right) = 0 \qquad (2.13)$$

(the complete derivative of this equation can be seen in the appendix A).
Hence, the Euler equation for each quadrilateral cell can be assumed as follows,

$$\frac{d}{dt}(hw) + Qw = 0, \qquad (2.14)$$

where h is the cell area and Q represents an approximation to the boundary integral of the second term (Eq. 2.13). This operator Q can be defined for each side of the cell as Q_k . Finally, the equation (2.14) becomes

$$\frac{d}{dt}(hw) + \sum_{k=1}^{4}(Q_k\, w) = 0 \qquad (2.15)$$

With $Q_k = \Delta y_k\, u_k - \Delta x_k\, v_k$

Where Δy_k and Δx_k is the increment of y and x along side k of the cell.

Then, the first order change in w can be written in another different form, for example for cell C on Fig. 2.5,

$$\Delta w_C = -\begin{pmatrix}(f_3 - f_1)(y_2 - y_4) + (f_4 - f_2)(y_3 - y_1) + \\ (g_1 - g_3)(x_2 - x_4) + (g_2 - g_4)(x_3 - x_1)\end{pmatrix}\frac{\Delta t}{2\,\Delta A_C} \qquad (2.16)$$

The same expressions are applied for cell A, B, and D, while the changes of Δw in cell vertex 1 can be obtained from the weighted average from cell A, B, C, and D.

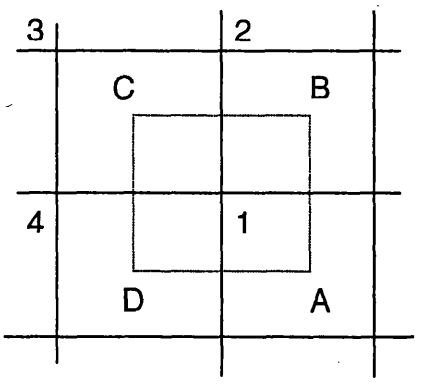

Figure 2.5 Geometry of cell-vertex scheme for single cell

II.2.3 Artificial Viscosity

Artificial viscosity can be found generally in the explicit methods. The artificial dissipative terms are added to the finite volume scheme in order to suppress the tendency for odd and even point decoupling and to prevent the appearance of wiggles in regions containing severe pressure gradients in the neighbourhood of shock waves or stagnation points.

The artificial viscosity terms are introduced explicitly in the equation (2.14) as follows

$$\frac{d}{dt}(hw) + Qw - Dw = 0 \qquad (2.17)$$

where D is the dissipative operator. The term Dw is a blend of second and fourth differences with coefficients, which depend on the local pressure gradient. It can be defined as follows,

$$Dw = D_x w + D_y w \qquad (2.18)$$

$$\text{with } D_x w = d_{i+1,j} - d_{i-1,j} \qquad (2.19)$$

$$\text{and } D_y w = d_{i,j+1} - d_{i,j-1}. \qquad (2.20)$$

The terms on the right is similarly calculated as

$$d_{i+\frac{1}{2},j} = \frac{h_{i+\frac{1}{2},j}}{\Delta t}\left(\varepsilon^{(2)}_{i+\frac{1}{2},j}\left(w_{i+1,j} - w_{i,j}\right) - \varepsilon^{(4)}_{i+\frac{1}{2},j}\left(w_{i+2,j} - 3w_{i+1,j} + 3w_{i,j} - w_{i-1,j}\right)\right) \quad (2.21)$$

where,

$$\varepsilon^{(2)}_{i+\frac{1}{2},j} = \kappa^{(2)} \max\left(v_{i+1,j}, v_{i,j}\right) \quad (2.22)$$

$$\varepsilon^{(4)}_{i+\frac{1}{2},j} = \max\left(0 , \left(\kappa^{(4)} - \varepsilon^{2}_{i+\frac{1}{2},j}\right)\right) \quad (2.23)$$

The scaling h/Δt in equation (2.21) conforms to the inclusion of the cell area h in the dependent variables of equation (2.17). Then,

$$v_{i,j} = \frac{\left|P_{i+1,j} - 2P_{i,j} + P_{i-1,j}\right|}{\left|P_{i+1,j}\right| + 2\left|P_{i,j}\right| + \left|P_{i-1,j}\right|} \quad (2.24)$$

Jameson et al. (1981) has found that in smooth regions of the flow, the scheme is not sufficiently dissipative unless the fourth differences are included, with the result that calculations will generally not converge to a completely steady state. Instead, the oscillation of low amplitude continues when it has reached an almost steady state. These appear to be induced by reflections from the boundaries of the computational domain.

II.2.4 Local Time Step

The time-stepping method is adapted to ensure stability and enhance the rate of convergence. The permissible maximum of local time step varies from cell to cell, depending on the local geometry of the cell and the local flow conditions. The following equations are used to calculate local time step for cell C (figure 2.5):

$$\Delta t \leq \min\left(\frac{\Delta A_C}{\left|u\,\Delta y^l - v\,\Delta x^l\right| + a\,\Delta l}, \frac{\Delta A_C}{\left|u\,\Delta y^m - v\,\Delta x^m\right| + a\,\Delta m}\right) \qquad (2.25)$$

where

$$\Delta x^l = 0.5\left(x_2 + x_3 - x_1 - x_4\right) \quad , \qquad \Delta x^m = 0.5\left(x_1 + x_2 - x_4 - x_3\right) \, ,$$

$$\Delta y^l = 0.5\left(y_2 + y_3 - y_1 - y_4\right) \quad , \qquad \Delta y^m = 0.5\left(y_1 + y_2 - y_4 - y_3\right) \, ,$$

$$\Delta l = \left(\left(\Delta x^l\right)^2 + \left(\Delta y^l\right)^2\right)^{1/2} \, , \qquad \Delta m = \left(\left(\Delta x^m\right)^2 + \left(\Delta y^m\right)^2\right)^{1/2} \, ,$$

and $a = \sqrt{\frac{\gamma P}{\rho}}$

Then, the local time step (lts) at point 1 is set to be the minimum of the lts at cell A, B, C, and D.

$$\text{i.e. } \left(\Delta t\right)_1 = \min\left(\left(\Delta t\right)_A, \left(\Delta t\right)_B, \left(\Delta t\right)_C, \left(\Delta t\right)_D\right) \qquad (2.26)$$

II.2.5 Boundary Conditions

The boundary conditions should be well treated in order to avoid serious errors and instability. Special treatments usually are needed for inflow, outflow and wall boundary. The complete example of boundary conditions for CH-type grid can be seen on **Appendix B**, which shows four types of boundary condition.

II.2.5.1 Periodic Boundary

In order to fully guarantee conservation of mass, momentum and energy, the flux across periodic boundaries are treated like interior boundaries. The periodic boundary calculates the average value of flux on the cell, which are on the two sides of the face. Phantom cells are applied to calculate the average cell, local time step, and artificial damping terms (see figure 2.6, 2.7, and 2.8).

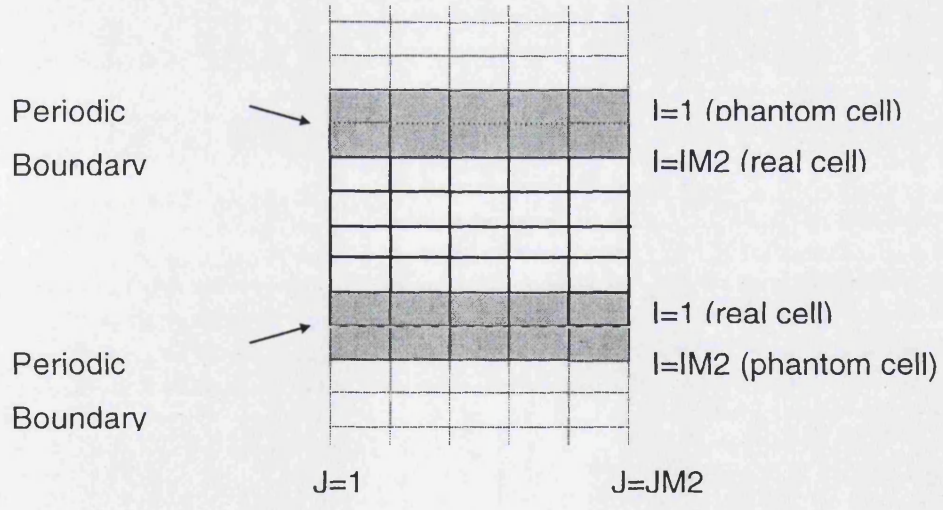

Figure 2.6 Periodic boundary on the far upstream region

Figure 2.6 shows the upstream region. The periodic condition is applied for lower line (i=1) and upper line (i=im). Therefore the calculation for those cells depends on the properties on the cell i=2 and i=im2.

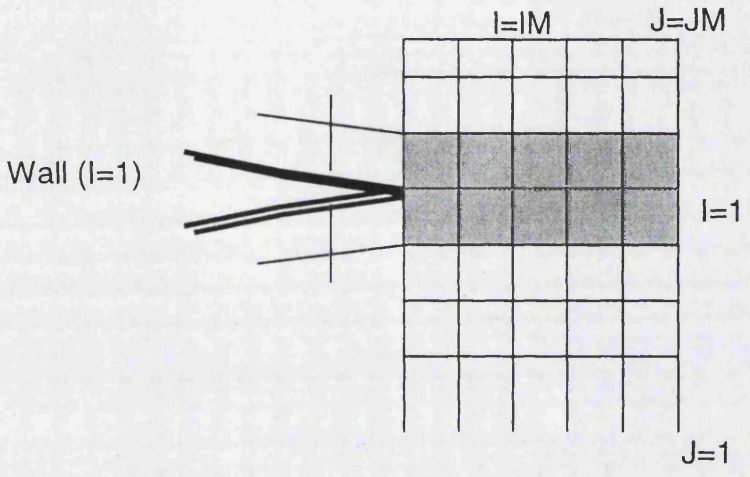

Figure 2.7 Periodic boundary near trailing edge region

Figure 2.7 shows two lines (computational domain, see fig 2.3) are treated as a periodic line. This periodic line connects the "branch cut" for c-type grid (see figure 2.2).

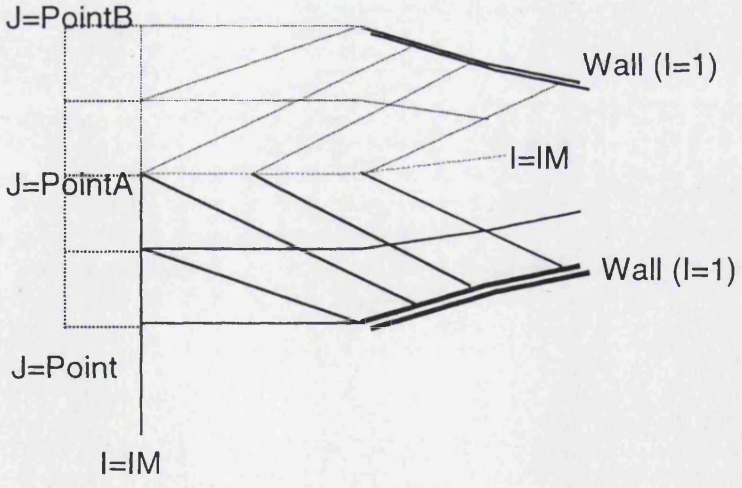

Figure 2.8 Periodic boundary near leading edge

The region near leading edge can be seen on figure 2.8. The treatment of periodic boundary (i=im) can be easily imagine by drawing two blades on this region. The wall (i=1) on the lower part is the upper blade (i.e. suction side),

while the other wall on the upper part which are drawn using dash line is pressure side of the blade.

II.2.5.2 Solid Wall Boundary

The advantage of cell vertex method can be seen on this type of boundary as pressure and momentum at the wall can be computed without approximation. For the inviscid fluxes, the momentum fluxes due to the pressure remain, but all the other inviscid fluxes vanish. The condition that the flow be tangential to the body surface is also implemented on the trailing edge.

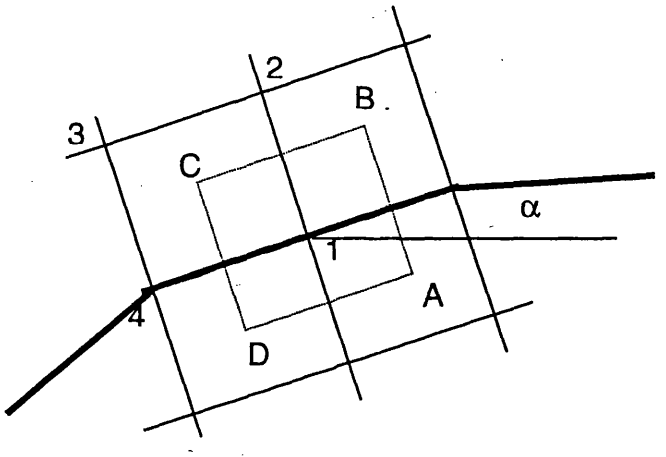

Figure 2.9Geometry of cell vertex scheme on the blade surface

Figure 2.9 shows the cell vertex 1, with cell D and A inside the solid wall boundary and cell B and C in the interior of the field. Firstly, the quantities of the cells around point 1 are calculated, except cell A and D, where w_A and w_D are equal to zero. Then for multi-stage scheme the flow tangency condition of cell 1 is calculated by

$$(\rho q_t)_1 = (\rho u)_1^{n+1} \cos\alpha + (\rho v)_1^{n+1} \sin\alpha \qquad (2.27)$$

where q_t is the velocity component tangential of the surface. The new corrected value of ρu_1^* and ρv_1^* are

$$(\rho u)_1^* = (\rho q_t)_1 \cos \alpha \quad (2.28)$$

$$(\rho v)_1^* = (\rho q_t)_1 \sin \alpha \quad (2.29)$$

II.2.5.3 Inflow Boundary

According to the theory of characteristics, the flow angle, total pressure and total temperature are specified at the subsonic inlet. Then the remaining flow variables such as static pressure are extrapolated from interior. While, for supersonic inflow condition, all characteristic directions are propagated from the boundary toward the domain. Hence, all primitive variables, P_{01}, T_{01}, V_1, and β_1 are specified.

Figure 2.10 Inlet and outlet boundaries

The non-reflecting boundary condition, which would eliminate waves, is applied by calculating the pressure P as follows,

$$P_{I,1}^{n+1} = P_{I,1}^{n} + PRF\left(P_{I,2}^{n+1} - P_{I,1}^{n}\right) \tag{2.30}$$

The value of PRF can be chosen between 0.0 and 1.0. In the program, we use the value of PRF equal to 0.5. The other variables are calculated from the new calculated pressure value.

The inflow boundary can be seen on figure 2.10

II.2.5.4 Outflow Boundary

Like the inlet boundary, the theory of characteristics is also applied on the exit boundary (see figure 2.10). At the subsonic flow condition, one condition should be specified (i.e. the exit static pressure).

For parallel stream then $\partial P/\partial y=0$, so that the static pressure at outflow boundary is specified directly by

$$\text{i.e. } P = P_{outlet} \tag{2.31}$$

The energy and enthalpy components at (I,JM) are calculated using extrapolation from the interior.

While if the outflow is supersonic, there is no boundary condition should be specified. Hence, all primitive variables are extrapolated from the interior values.

II.3 Multiblock

In the non-moving geometries, the simplest approach is to arrange blocks to be patched along pre-defined interface lines (Kelemenis 1994). The arrangement of blocks has great effect for block boundary. A block boundary may consist of either one or several types of boundary conditions, depending on whether it interfaces one or several blocks; for examples:

1. An interior boundary of block one maps to the complete edge of an interior boundary of block two.

Figure 2.11 Two blocks are completly connected

2. An interior boundary of block one consists of two block boundary conditions.

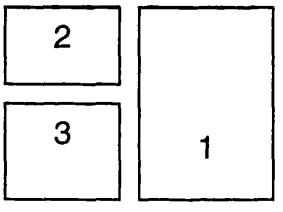

Figure 2.12 A block is connected to two blocks in one surface

3. An interior boundary of block one consists of the complete boundary of block three and part of the boundary of block two.

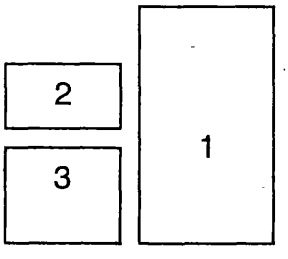

Figure 2.13 A block is partially connected

In the multiblock grid generation scheme adopted for the developed solver, the physical space is divided into non-overlapping regions or blocks, which can be mapped to rectangular computational domain. Many researchers apply the above strategy such as proposed by Norton (1984). The most important advantage gained with this strategy is the ability to implement a mixed topology grid system which requires no interpolation, especially for the solver and inverse calculation. This strategy is different with that implemented by Demeulenaere (1997) or Arnone (1996) that the grids do not match which requires special treatments and makes the calculations more complicated.

In the first stage of the scheme, the way in which the space is divided, the topology of the block structure is specified. This specified topology determines the form of grid that will be generated. The objective is to specify a topology that will suit the configurations and enable a satisfactory grid to be to be generated throughout the field. Moreover, it also will lead to a desired form of the grid around the component, for example an 'O' or 'C' type grid around a turbine blade. The chosen topology may lead to a grid that contains irregular points, eventhough within each block the grid is regular. In two dimensions, a normal point of the grid is surrounded by four cells, but the irregularity manifest itself by the appearance of the points surrounded by five, six, or more cells. Therefore, the solver code must detect and treat points appropriately

The multiblock scheme that we implemented here has two features that
1) the grid lines continue across the block boundaries and
2) the boundary conditions that apply on each block are the same.
The last condition is very important when we meet a periodic boundary.

For a large number of blocks and complex configurations, it is apparent that, the grid is structured locally. However globally, the relationship between blocks is not necessarily of a direct structured nature. It is necessary to define a communication between the grids in terms of a connectivity matrix. In this

sense, the so-called multi-block grids are pseudo-unstructured. The connectivity matrix for this code is defined as follows:

- BB(NB,4)=INTEGER

This matrix identifies the neighbouring block.
NB: current block number.
INTEGER: neighbouring block number. If the neighbouring block is a physical boundary, the value of integer is 0.

- SB(NB,4)=INTEGER

This array identifies the neighbouring edge.
INTEGER= 0, if the neighbouring edge is physical boundary.

- BCB(NB,4)= 0, 1, 2, or 3

The boundary of the block is defined by this matrix with a number from 0 to 3, which is defined as
0: solid boundary,
1: interior boundary,
2: inlet boundary,
3: outlet boundary.

The solver code is made general in order to meet large variation of block such as different number of points and co-ordinate directions. So that it should be able to calculate the flow over any configuration, given a grid of the multiblock type. All the information data of the block are held in the computer memory. The blocks may be numbered in order, but the information about the block numbers and relative orientation of adjacent blocks should be stored in memory. The dependent flow variables and the grid co-ordinate are also stored in the computer memory.

This has additional advantage that calculations can be performed on the same solver code, so that comparisons between the types of grid can be assessed.

II.4 Inverse Design Methodology

This section is concerned with the development of inverse method which the blade shape is designed subject to a specified mass-averaged tangential velocity and thickness distribution. The current method is restricted to the assumption of the slip condition on the wall.

The background theory of inverse method has been described in the literature survey. Hence, most of the inverse design theory will not be repeated here. Further details on the use of mass-averaged tangential velocity and inviscid slip condition can be found in chapter one.

The developed method has many features, such as:

1. Easily implemented (i.e. there is no modification of the grid generator and flow solver).
2. Applicable to a large range of flow conditions (e.g. subsonic, transonic, shock)
3. Design specification: mass-averaged tangential velocity and finite thickness
4. The C-type grid allows a large or blunt leading edge and more accurate calculation on that region.

As mention above, the developed technique is easily implemented. It can be easily coupled with any solvers without any modification such as permeable wall boundary.

The next section will describe the procedure and some background theory of the developed method such as initial blade geometry and the calculation method in C-type grid.

II.4.1 Inverse Methodology Procedure

The developed grid generator and solver, which have been described in the previous sections are coupled with the developed blade update algorithm.

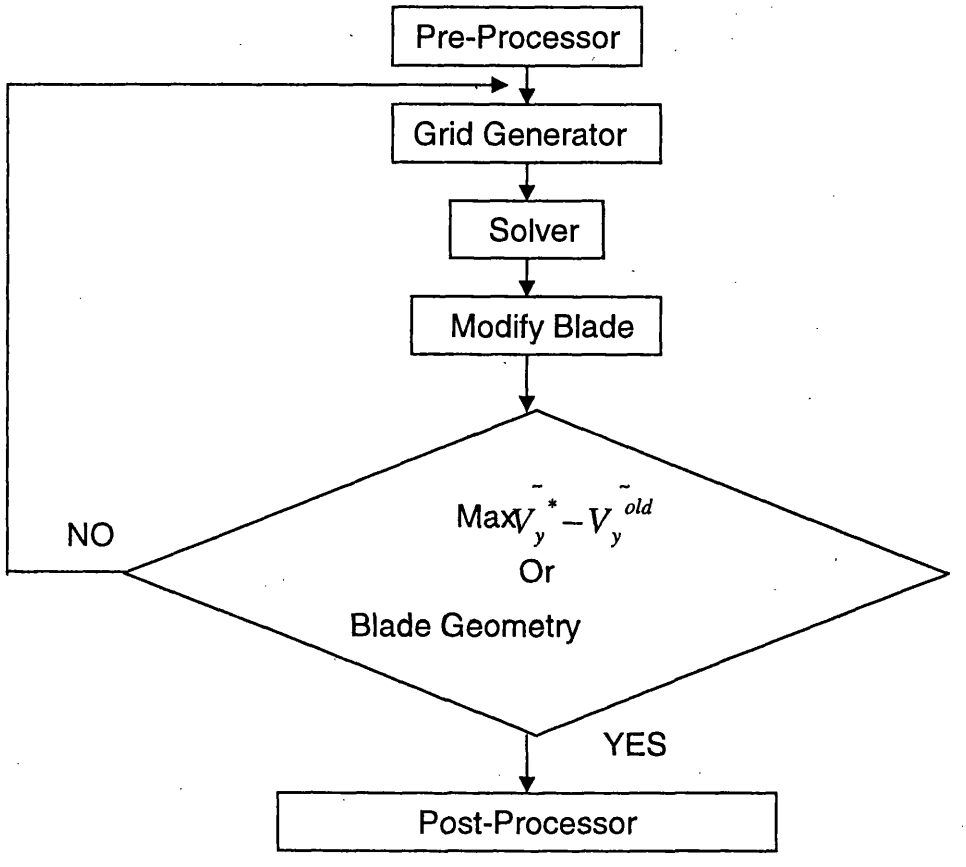

Figure 2.14 Flowchart of developed inverse method

Firstly, a grid for the initial blade is generated. It is important for inverse method to have an initial blade geometry as it will be used for the calculations (please see literature survey for further details on inverse and optimisation method). Therefore, it is important to provide an initial blade geometry. The initial blade geometry algorithms will be described in the initial blade section.

Secondly, the blade performance is analysed by the Euler flow solver. The required flow properties, such as tangential velocity, are given to the blade modification algorithm.

The blade modification algorithm will calculate the current mass averaged tangential velocity and compare it to the target distribution. Using those differences, this algorithm produces a new blade geometry.

The procedure continues iteratively as shown on figure 2.14. The designed blade geometry can be found after it meets certain value of convergence criteria, which will be explained further in the last section.

II.4.2 Blade Modification Algorithms

The blade surface can be presented as

$$\alpha^{\pm} = y - f^{\pm}(x) = nS \tag{2.32}$$

where S is the pitch and n=0 or integer.
The superscript (+) represents the upper surface and (-) for the lower surface of the blade. The $f^{\pm}(x)$ defines the shapes of the upper and lower surface of the blade,
i.e. $f^{+}(x) = f + 0.5 * t_{\theta}$ and $f^{-}(x) = f - 0.5 * t_{\theta}$
where f is the camber line and t_{θ} is the thickness of the blade

For inviscid case at solid wall must satisfy the slip condition as follows

$$\vec{V}^{\pm} \cdot \nabla \alpha^{\pm} = 0 \tag{2.33}$$

Where **V** represents the velocities on the upper and lower surface of the blade.

Then, the equation (2.33) can be extended as

$$V_x^{\pm} \cdot \frac{d(f \pm \frac{t_\theta}{2})}{dx} = V_y^{\pm} \tag{2.34}$$

Where f is the camber line and t_θ is the thickness of the blade.

Then, applying equation 2.34 to an initial camber line, f^{old} for both upper and lower surface and adding them, hence it becomes,

$$\left(V_x^{+old} + V_x^{-old}\right)\frac{df^{old}}{dx} + \frac{dt_\theta}{dx}\left(\frac{V_x^{+old} - V_x^{-old}}{2}\right) = \left(V_y^{+old} + V_y^{-old}\right) \tag{2.35}$$

or

$$V_{x\,bl}^{old} \cdot \frac{df^{old}}{dx} + \frac{1}{4}\frac{dt_\theta}{dx}\Delta V_x^{old} = V_{y\,bl}^{old} \tag{2.36}$$

Where

$$V_{x_{bl}} = \frac{1}{2}\left(V_x^{+} + V_x^{-}\right)$$

$$V_{y_{bl}} = \frac{1}{2}\left(V_y^{+} + V_y^{-}\right)$$

$$\Delta V_x = \frac{1}{2}\left(V_x^{+} - V_x^{-}\right)$$

The subscript bl represents the average value of upper and lower surface variable.

For the new camber line, but the same thickness distribution, we can write as

$$V_{x\,bl}^{\,old}\cdot\frac{df^{new}}{dx}+\frac{1}{4}\frac{dt_\theta}{dx}\Delta V_x^{\,old}=V_{y\,bl}^{\,old}+\tilde{V}_y^{\,*}-\tilde{V}_y^{\,old} \qquad (2.37)$$

The equation (2.37) can be explained further details in Tiow's thesis (2000).

$\tilde{V}_y^{\,*}$ is the specified mass-averaged tangential velocity and $\tilde{V}_y$ can be calculated as

$$\tilde{V}_y=\frac{\int_0^S V_y(\rho V_x)\,dx}{\int_0^S(\rho V_x)\,dx} \qquad (2.38)$$

Finally, subtracting equation (2.37) with equation (2.38), we obtain

$$V_{x\,bl}^{\,old}\cdot\frac{d(f^{new}-f^{old})}{dx}=\tilde{V}_y^{\,*}-\tilde{V}_y^{\,old} \qquad (2.39)$$

The new camber line, f^{new} can be found by integrating equation (2.39) along the blade. Subsequently, the new blade is generated using equation (2.40).

$$f^{\pm}=f\pm\frac{t_\theta}{2} \qquad (2.40)$$

II.4.3 Initial Blade

As mention before, the inverse method requires an initial blade geometry. For most cases, the initial blade geometry is available. However, in some cases the initial blade geometry does not exist and an initial blade geometry has to be computed in order to start the inverse design process. This usually can be found for a completely new design with a given a certain design specification.

In fact, there is no restriction how to make an initial blade geometry. It is possible to use an arbitrary camber line to generate an initial blade. However, this is not a good idea and can result in time consuming iteration. The following method provides a good initial blade geometry for mass averaged tangential velocity as design specification.

The initial blade shape is predicted based on the simplified equation (2.36), which ignores the second term (i.e. thickness term) Hence, the equation becomes,

$$\frac{df^0}{dx} = \frac{\tilde{V}_y^*}{\tilde{V}_x^0} \qquad (2.41)$$

The value of $\tilde{V}_x^0$ is obtained from the specified mass flow and assuming a constant density. The initial blade can be generated using the obtained value of f^0 for the equation (2.40).

II.4.4 Implementation on the C-type Grid and Multiblock

This inverse method is more complicated when it is applied for C-type grid compares to H-type grid. Since it has to calculate the mass-averaged tangential velocity, which is not automatically provided on the C-grid. Therefore some interpolation is needed in order to have those values and that interpolation is taking place in a boundary conforming co-ordinate system for accurate result. The boundary conforming co-ordinate theory is not difference as applied for grid generator (see figure 2.1). Therefore, some variables are already calculated and can be used for blade modification algorithm. This is one of the advantages of using this method for the developed inverse method.

However, in the multiblock solver, the calculations become more difficult as the required data might be provided in the other block or across boundary. Moreover, it should also be careful with the direction and the determination of the block where the interpolation will be taken.

II.4.5 Convergence Criteria

The blade modification algorithm is carried out after the solver achieved the allowed value of percentage mass error (< 0.8%) and root-mean square error on velocity (of order < 10^{-9}) of the flowfield. This value is a compromise result from the experience to give the lowest computational cost with an acceptable solver convergence criterion.

Finally, the blade geometry is updated at n-th iteration after the differences between the specified and obtained mass-averaged tangential velocities reach a certain tolerance (<1%). This value is found adequate and can be seen on the examples of this method.

Chapter III Application of Inverse Method

Some examples of inverse method can be seen in this chapter. However, firstly the validation of cell vertex Euler solver is presented. The Euler flow solver is validated by two well known of turbomachinery test cases.

Firstly, the Euler solver is validated for a low speed turbine stator blade. The experimental data is provided by Dring (1982). Then the flow solver is validated for subsonic and transonic flows. The experimental results are presented by Consigny (1981) for a turbine rotor blade.

In this chapter, some examples of grid generations are shown together with some multiblock structures. A computational result from another Euler flow solver (cell-centre method) is also compared with the cell-vertex Euler solver. The cell-centre Euler solver is based on Jameson et. al. (1981) which is extended to C-type solver by the Author.

III.1 Turbine Stator Blade

The turbine model (0.8 hub/tip ratio) had three rows of airfoils; first vane, first blade and second vane, but only the first vane (stator) and the first blade (rotor) were installed. The experiment was accomplished at the United Technologies Research Centre (UTRC). Details of experiment can be seen in Dring et. al. (1982). This blade geometry and experimental data are commonly used for the simulation of a multistage turbine, such as Admcyzk et al. (1990), or for code validation such as Amano (1996) and Tiow (1998).

The following validations compare the numerical results with experimental results obtained from the midspan of turbine stator blade in the following condition:

P_1 /(10^5 Pa)	β_1	P_2 /(10^5 Pa)	P_o /(10^5 Pa)	T_o (K)
0.99	0^o	0.96308	1.00	288

Table 3.1 Flow conditions for Dring Blade

The multiblock CH-type grid is presented together with H-type grid and CH-type grid for cell-centre Euler solver. The blunt leading edge is kept but the trailing edge is modelled by short wedges simulating the unsteady flow zone near the trailing edge.

The use of "cusp" at the trailing edge is already known and quite popular amongst the CFD researchers. Some examples in the turbomachinery area can be found in Leonard (1991), Amano (1996), Tiow (1998), and Xiao (2000).

Denton and Dawes (1999) described more details on the effect of the real flow at a blade trailing edge which is always unsteady with regular vortex shedding for numerical analysis. The use of cusp will avoid the misleading numerical solution such as wrong exit angles and high trailing edge loss. In the same paper, both authors strongly recommend that a "cusp" should be placed at the trailing edge of the blade so that the flow leaves the blade smoothly.

III.1.1 H-Type Grid (Cell Centre)

A simple inviscid H-type grid is generated with 91 x 20 mesh points (see fig. 3.1). The number of mesh points on the suction side is 52, which is the same as on the pressure side. The calculation of the steady solution of the cell centre scheme on this grid took about 8'27 minutes on the digital computer Turbo2 (433 MHz).

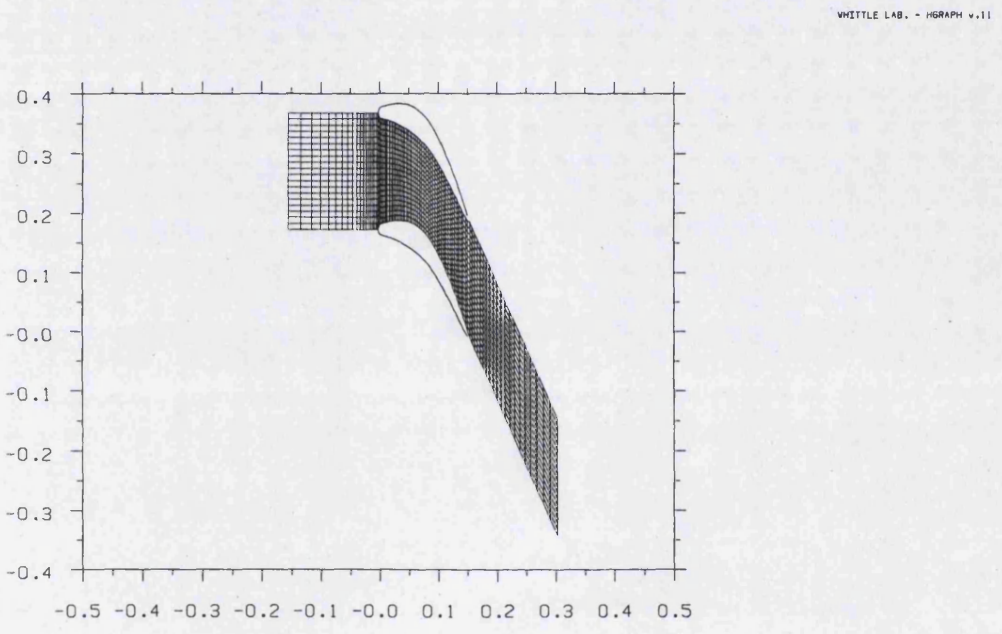

Figure 3.1 H-type grid for Dring blade

III.1.2 CH-Type Grid (Cell Centre)

The C-type grid wraps the turbine stator blade with 131 x 13 mesh points. The number of points along the blade is 104, which is one point more than the previous test. The upstream is treated with general H-grid, which is 31 mesh points in the pitch-wise and 8 grid points in the streamwise direction (fig. 3.2). The solver code is cell centre scheme. Converged solution on this grid was obtained in about 6'48 minutes on the same computer.

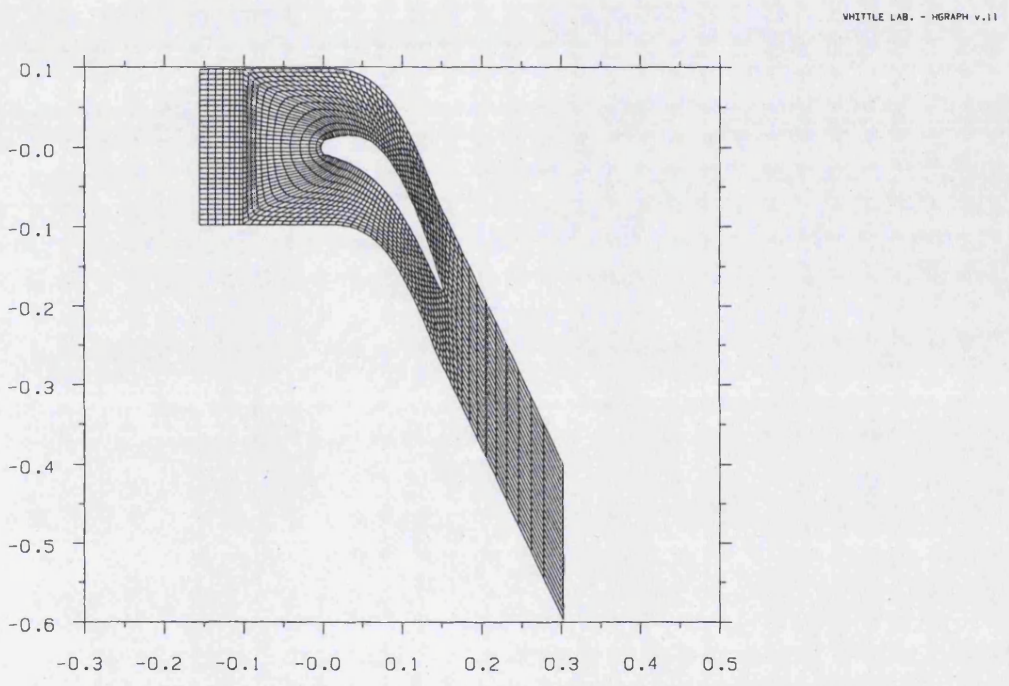

Figure 3.2 CH-type grid for Dring blade

III.1.3 CH-Type Grid Multiblock (Cell Vertex)

Another model for upstream and downstream is applied. The multiblock grid has 138 x 12 mesh points on the C-grid topology and 13 x 32 mesh points on the H-grid (fig. 3.3). The total number of block is 8 with 6 blocks around the blade and 2 blocks at upstream. The blade has the same number of points as the previous H-type grid. The suction surface has the same number of block and mesh points as on the pressure side, which are 2 blocks and 65 mesh points respectively. The computation was completed in about 4'33 minutes at the same computer.

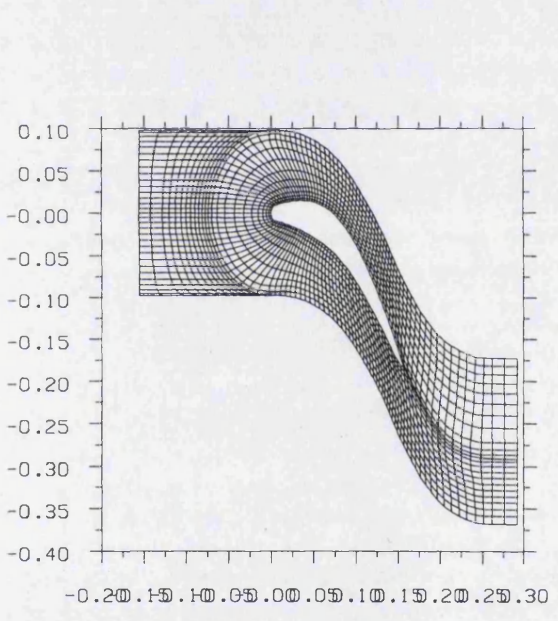

Figure 3.3 CH-type multiblock grid

III.1.4 Overall Results

The numerical results of pressure coefficient, Cp along the suction and pressure sides are compared with the experimental as shown in figure 3.4.

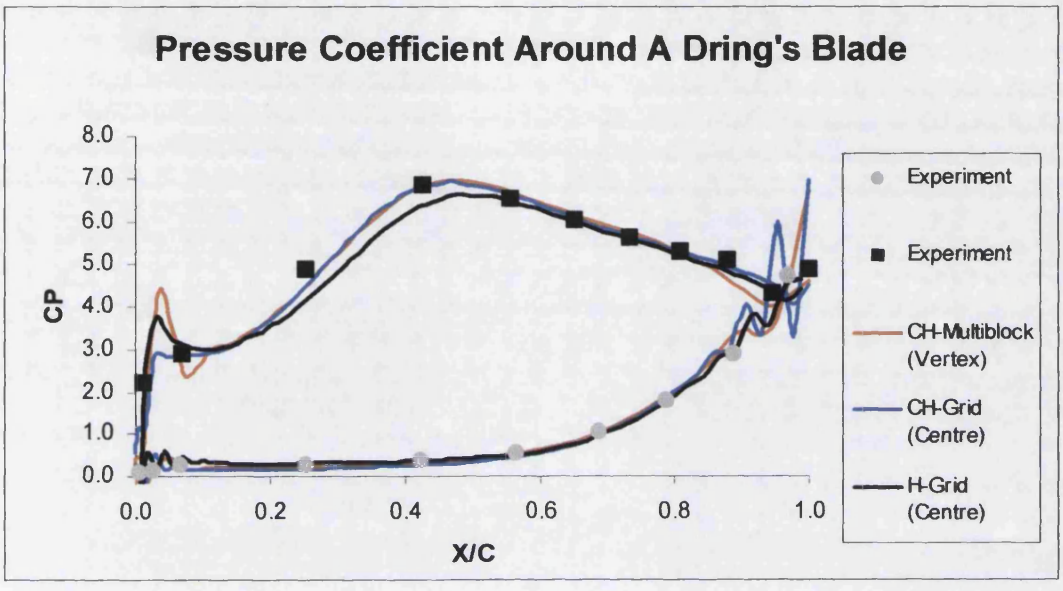

Figure 3.4 Overall results

III.1.5 Discussion

The computed results show that for the same number of point on the surface of the blade (figure 3.4), both cell centre and cell vertex scheme have a good agreement with the experimental result, especially for CH-type grid. The CH-type grid for both schemes has less oscillation on the leading edge. The reasons of these could be explained due to the better treatment on the leading edge and the aspect ratio of the grids on that region, which is better than H-type grid.

All numerical results show the peak near the leading edge on the suction surface. It is difficult to see the reasonable value of this peak since there are no experimental results on this region. However, Dring (1982) compared the experimental result with a theoretical distribution based on potential flow

method, which showed peak as well on this region. There is no explanation or discussion of this peak on his publication. Meanwhile, the peak showed up on other publications (e.g. Adamcyk (1990) and Tiow (2000)), which used the same Dring's blade, with the value of the peak about 4.

The multiblock solver performance is not bad as seen in table 3.2. Although, it has the highest number of mesh points, the speed of convergence is still better compare to the other monoblock solver.

Type of Grid	Solver Scheme	Grid Point	CPU Time/min
H	Cell Centre	1820	8:27
CH	Cell Centre	1951	6:48
CH	Cell Vertex	2072	4:33

Table 3.2 Grid comparisons for Dring blade

The cell vertex scheme should produce better results than cell centre scheme. Since, the independent variables are specified at the grid points, especially on the boundary. It is different with the cell centre scheme that stores the quantities of boundary variable on the centre of the nearest cell to the boundary line. For example, the cell centre scheme uses the value at the centre of the cell, which is adjacent to the solid wall boundary. Simply because they do not have the value of variables on the wall except by interpolation from the interior boundary, which can be found further details on Hall (1985).

The curvy shape of the outer line of the upstream C-type grid is better than the straight one. It can reduce the skewness on the upstream region, so that the grid is smoother. Nevertheless, this shape is just only good for inlet angle equal to zero and has an adverse effect on the smoothness of the periodic boundary. Hence, this shape can not be used for inverse method, which should be able to handle any changes of the blade profile.

III.2 Turbine Rotor Blade

In the next validation exercise, the cell vertex multiblock Euler solver is validated using the experimental results (subsonic and transonic flow) and the geometry of the VKI turbine rotor blade provided by Consigny (1981). The test facility used for the experiment is the VKI isentropic light piston tunnel CT2. The operation of this short duration wind tunnel follows the principle of isentropic compression of the test gas by a light-weight piston driven by compressed air until the desired total pressure and hence temperature are obtained.

Beside the heat transfer rate investigation by Consigny, the VKI CT2 blade is also used for the film-cooled transonic turbine blade experiment (Camci et al. 1990), its aerodynamics computation (Camci et al. 1991) and numerical analysis of the effect of hole physics (Garg et al. 1998).

The following validation was performed at the condition of test A and B (table 3.3), which is subsonic and upper transonic case respectively. The other details of the flow conditions are described in Consigny's paper.

Test Case	M_1	$M_{2_{IS}}$	β_1	P_o /(10^5 Pa)	T_o (K)
A	0.240	0.622	30°	1.275	419
B	0.278	1.150	30°	2.070	419

Table 3.3 Flow conditions for VKI blade

Both test cases were run with three different types of multi-block computational mesh. The details of these multi-block meshes can be found in Appendix C.

III.2.1 H-Type Multiblock Grid

This H-type grid is developed by 14 blocks (see app. C.1.) The total number of mesh points is 3674 with 96 points along the upper surface of the blade (app C.2.). The computation was completed in about 10'54 minutes for subsonic case and 7'34 minutes for transonic case.

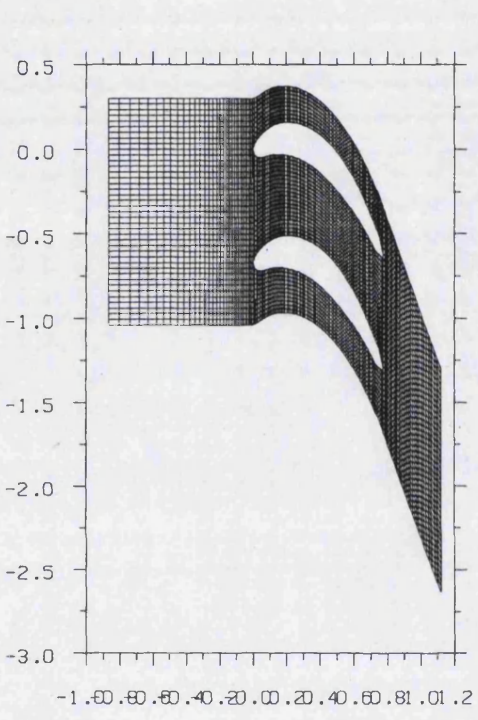

Figure 3.5 H-type multiblock grid

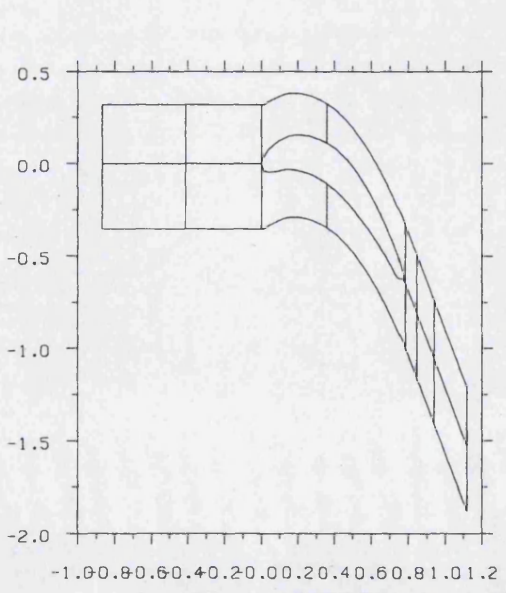

Figure 3.6 H-type multiblock

III.2.2 CH-Type Multiblock Grid

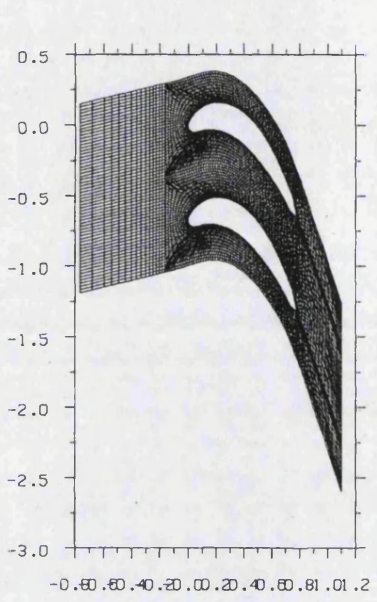

Figure 3.7 CH-type multiblock grid

The total number of blocks is eight with two blocks at the upstream, downstream, suction and pressured side (app. C.3.). The number of grid points at the upper and lower surfaces are the same as that used for the H-type grid and the total number of mesh point is 3732 (app C.4). The steady solution converged after 6'15 minutes for subsonic case and 6'12 minutes for transonic case.

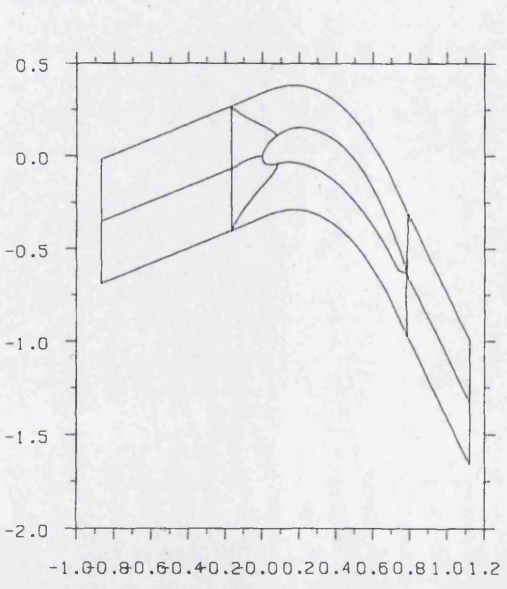

Figure 3.8 CH-type multiblock

III.2.3 OCH-Multiblock Grid

The VKI turbine rotor blade is wrapped by O-grid topology, which is divided by 5 blocks. Then, six blocks of C-grid topology covered the inner grid with one block addition for the trailing edge. The other kind of grid is added at the upstream of C-grid. This mesh has 3687 grid points with 72 on the upper surface (app C.6.). The computational solution is taken in about 3'23 mins for sub. and 2'30 mins for transonic case.

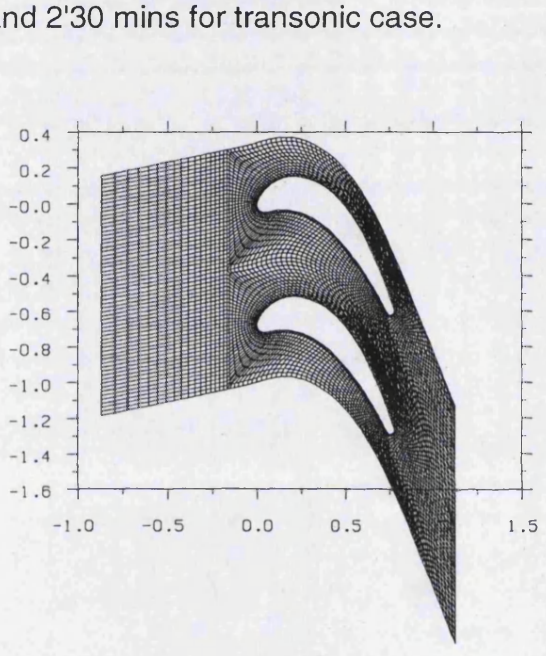

Figure 3.9 OCH-multiblock grid

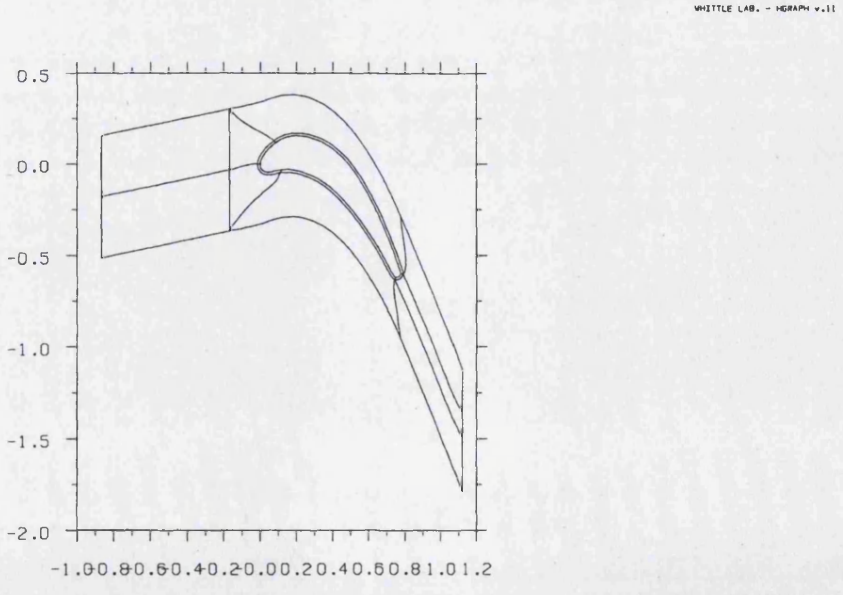

Figure 3.10 OCH-multiblock

III.2.4 Overall Results

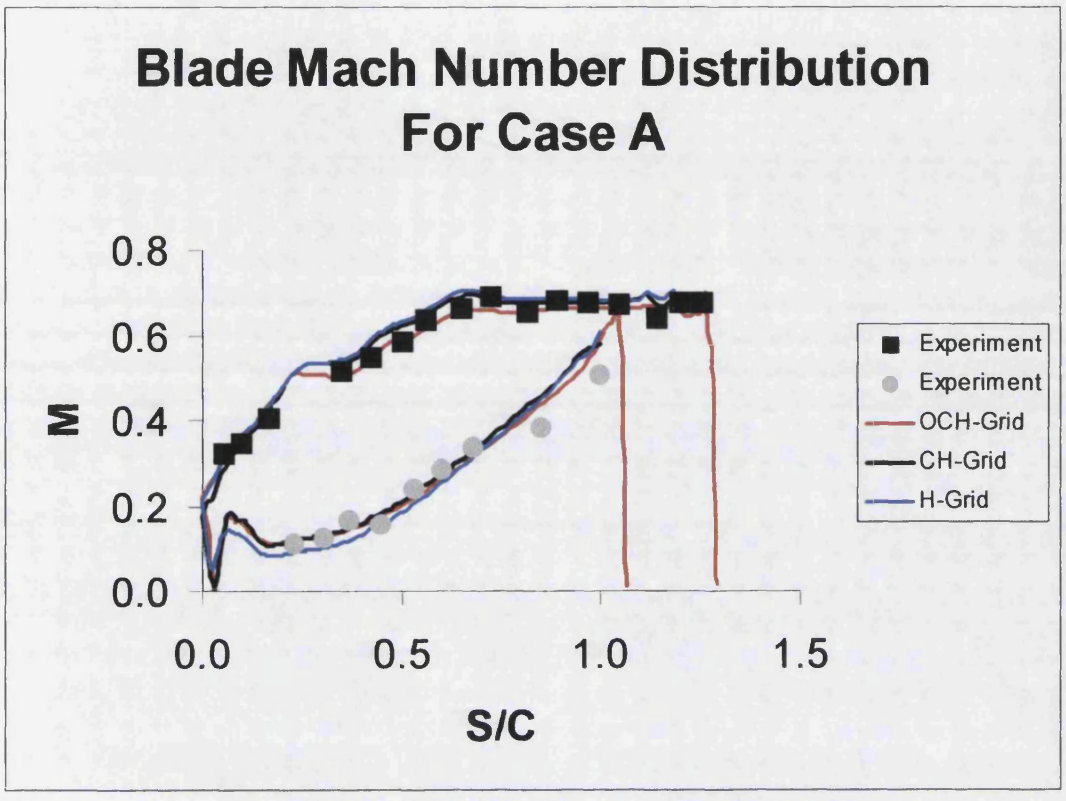

Figure 3.11. Mach Number results (case A)

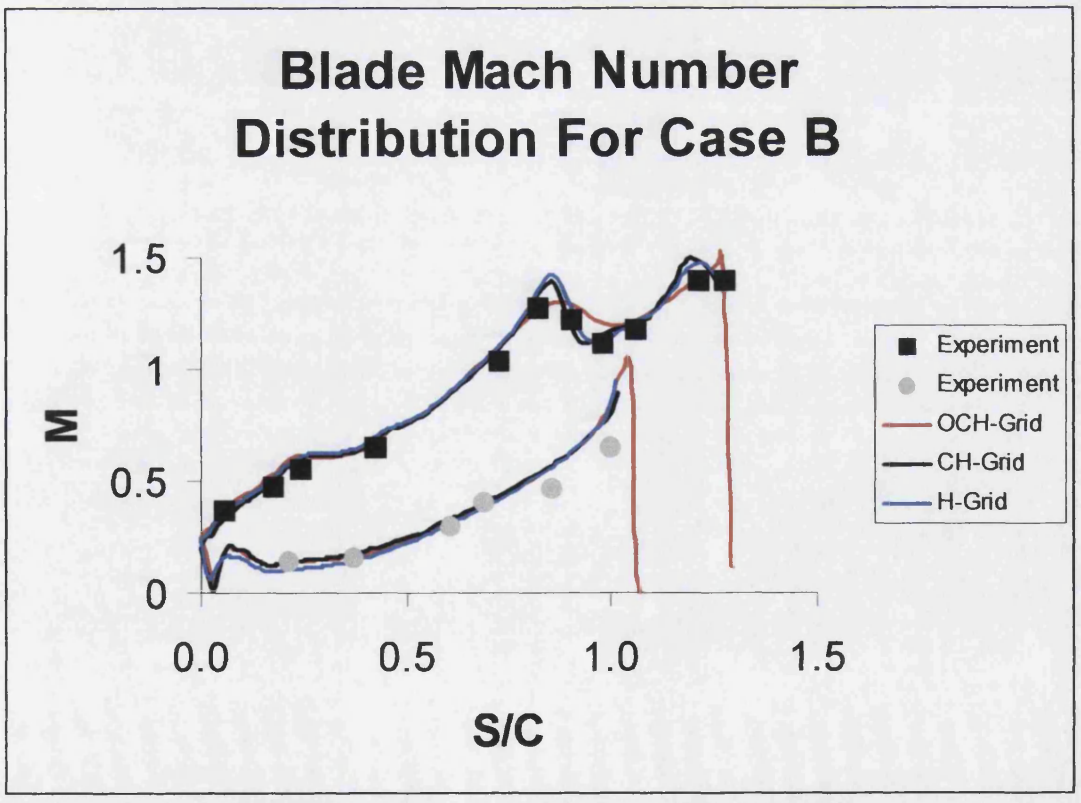

Figure 3.12. Mach number results (case B)

III.2.5 Discussion

The validations were performed using the same multiblock cell vertex Euler scheme, even though the grid topology is not the same. This is made possible by the advantage of multiblock. Therefore, besides the validation, the results can also be compared between the predicted solutions of those grids.

For both subsonic and transonic cases, all the numerical results show an excellent agreement with the experiments. The CH-type and OCH-type grids give better results in the leading edge region and it can capture the stagnation point well. However, the H-type and CH-type grids, which have 192 points on the blade are better in capturing the shock than OCH-type grid which only has 142 points on the blade. The reason to have large number of grid points, especially in the leading edge region is intended to have a better result around leading edge region for H-type grid. But the obtained H-type grid result at those regions is not as good as the other types of grid.

Of course, it is not fair to compare this H-grid result with the other type of grid. However, for the blade such as compressor, and particularly for a fan, the leading edge is often quite sharp and the leading aspect geometry is the high stagger and twist. Therefore, the use of H-type grid is the most efficient at this condition. This is why Arnone (1994) implemented H-grid rather than his usual C-grid for compressor blade.

Hence, every type of grid has some special features, which is not covered by the others type of grid. It could depend on the shape of the blade or other conditions that have been explained in the previous chapter (i.e. introduction and literature survey). Using this multiblock solver, we can easily employ the desired type of grid for certain type of blade. Furthermore, it allows us to mix the grid structure, such as presented by Arnone (1996) for his investigation on rotor-stator analysis. He use C-type grid for stator and H-type structure for the PTG2 turbine rotor blade

Then, all the results are similar with the numerical results provided by Consigny (1981) and they are better than the inviscid calculations made by Camci (1990) or some viscous calculations computed using commercial package TASC Flow. The results are summarised on the following table:

Type of Grid	Test Case	Grid Point	CPU Time/min
H	A	3674	10:54
CH	A	3732	6:15
OCH	A	3687	3:23
H	B	3674	7:34
CH	B	3732	6:12
OCH	B	3687	2:30

Table 3.4 Grid comparisons for VKI blade

From table 3.4. we can say that the time needed to obtain a convergence solution for transonic case is faster than the subsonic one. The speed of the CH-type grid is comparable with the H-type grid, although it has more mesh points.

III.3 Inverse Design

In this section, the validation and some examples of the inverse method are presented. The inverse method is validated by reproducing of an existing VKI turbine rotor blade. Two examples of inverse method are demonstrated by producing new blade designs with C4 thickness and large leading edge.

III.3.1 Numerical Validation

Firstly, the inverse method is validated by reproducing the VKI turbine rotor blade in the upper transonic flow condition. This test is very challenging as this blade has quite large leading edge, high camber, and strong shocks in the blade passage.

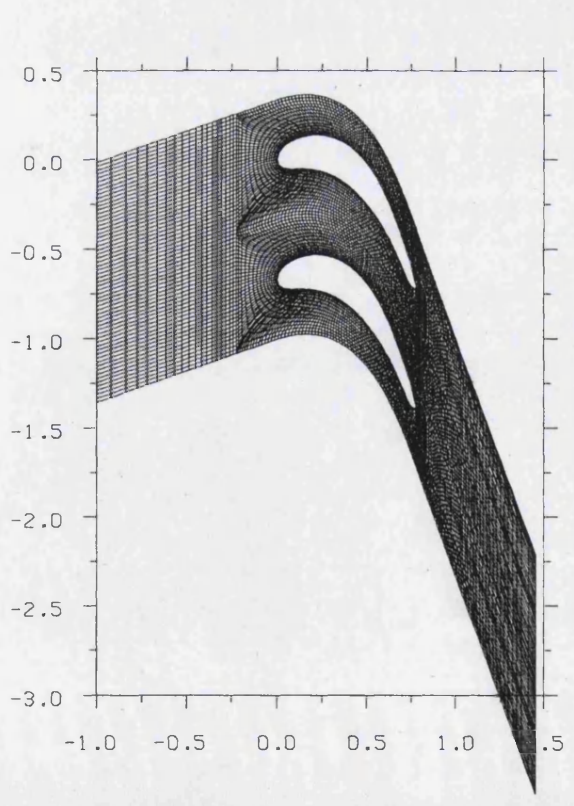

Figure 3.13 Initial blade

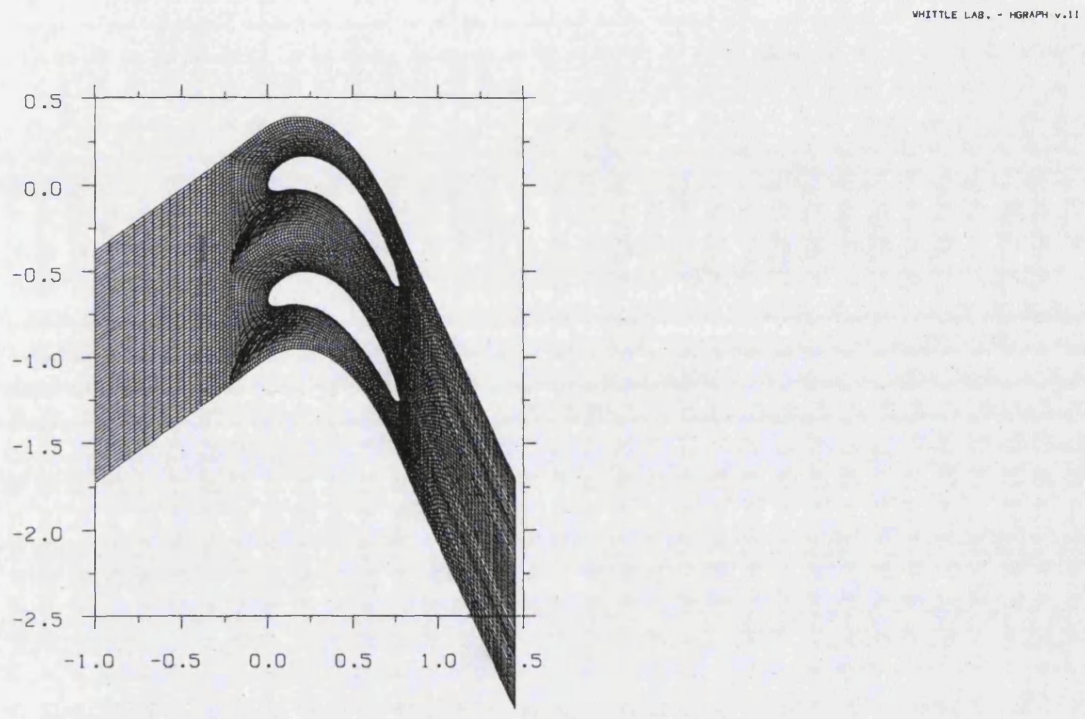

Figure 3.14 Final Blade

The specified design parameter, mass-averaged tangential velocity distribution is obtained from the direct analysis and the inverse method is performed with the same flow condition. The initial and final mesh can be seen on figure 3.13 and 3.14 respectively.

The computational mesh employed in this validation comprises 5568 mesh points. The blade is finally reproduced after 70 minutes. The initial and reproduced turbine rotor blades are shown on figure 3.15. Then, the comparison of original and reproduced blades is shown on figure 3.16.

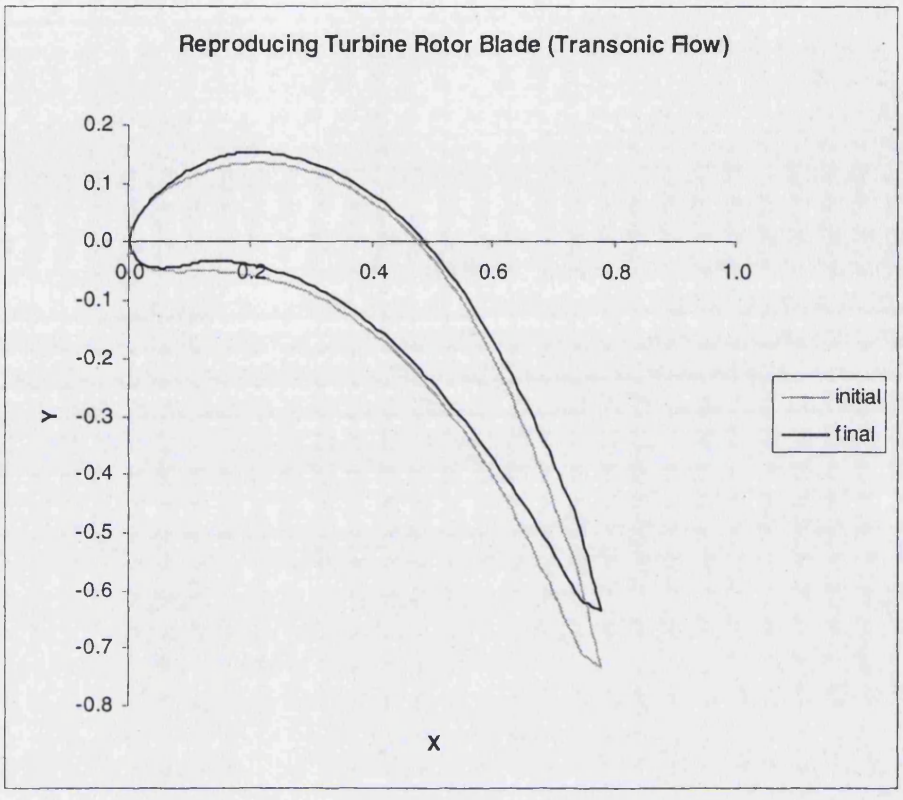

Figure 3.15 Initial and Reproduced blade

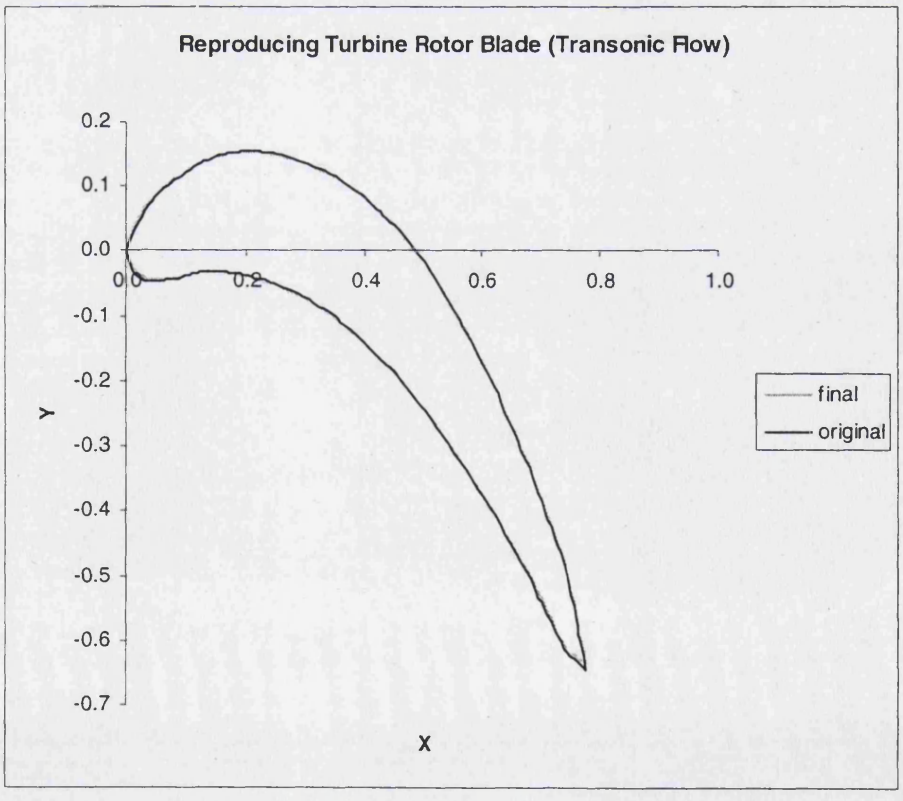

Figure 3.16 Original and Reproduced blade

III.3.2 Inverse Method Example I

The C4 thickness distribution is used to design a subsonic stator blade. A multiblock Euler solver is employed and CH-type grid is applied with 3438 total mesh points. The C-type grid topology has 87 grid points in the streamwise direction and 34 grid points in the pitchwise direction.

The blade model has a pitch to chord ratio of 1.0 with inlet flow angle equal to 0 degree. The flow pressure ratio, P_2/P_0 is set to 0.8. The prescribed mass-averaged tangential velocity is taken from the parabolic relation

$$\frac{\partial \tilde{V}_y^*}{\partial x} = A\,X(1-X) \qquad (3.1)$$

which has the maximum loading located at midchord. The value of $\frac{\partial \tilde{V}_y^*}{\partial x}$ is equal to zero at the leading edge and trailing edge as explained in previous chapter. The required inlet mass-averaged tangential velocity is set at 0 m/s and the outlet is 120 m/s. Hence the overall change in the circumferential mass-averaged tangential velocity is set at 120 m/s.

The initial and final mesh can be seen on figure 3.17 and 3.18 respectively.

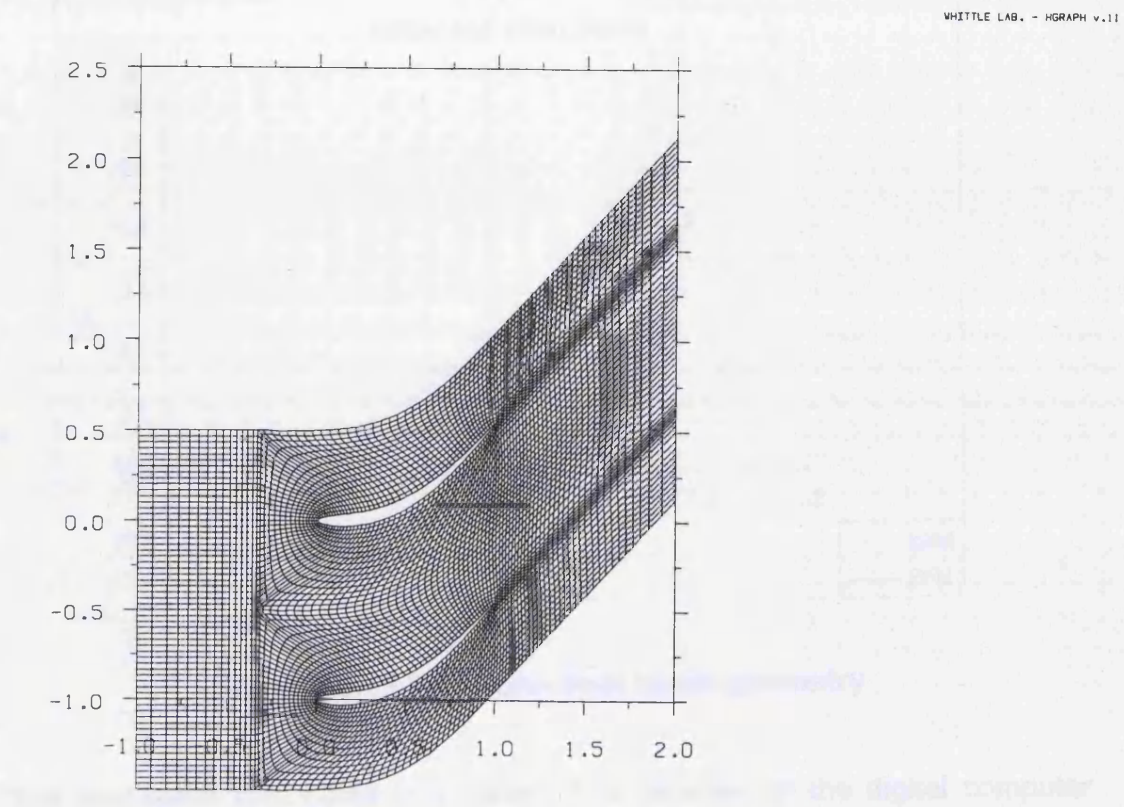

Figure 3.17 Initial blade

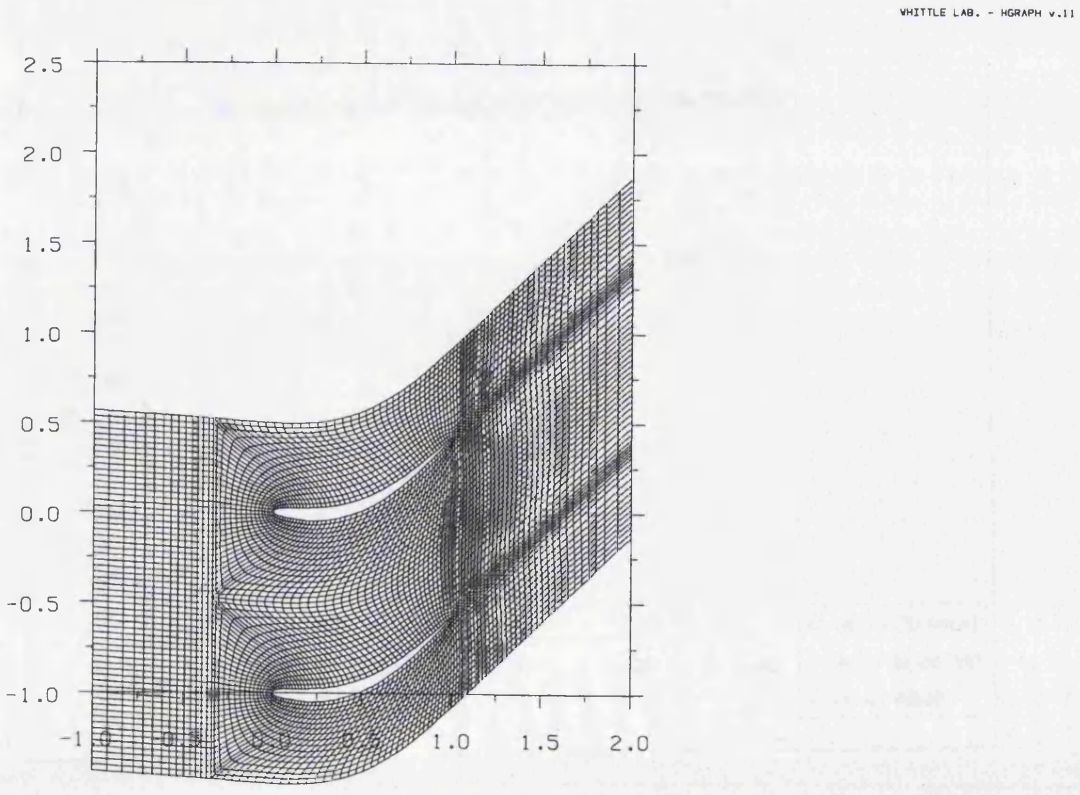

Figure 3.18 Final Blade

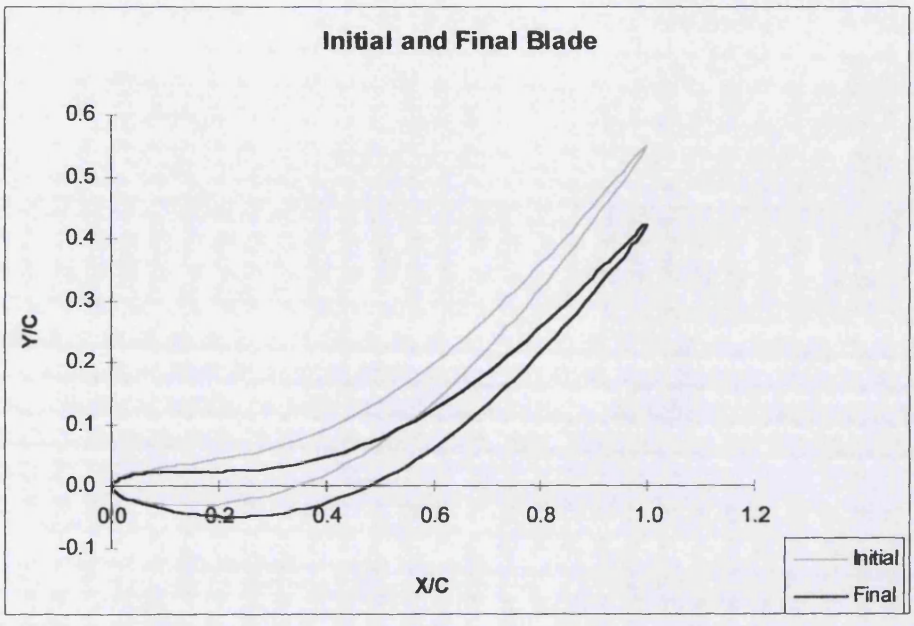

Figure 3.19 Initial and final blade geometry

The final blade was obtained in about 9'42 minutes on the digital computer turbo2 (433 MHz). The obtained blade is compared with the initial one on figure 3.19.

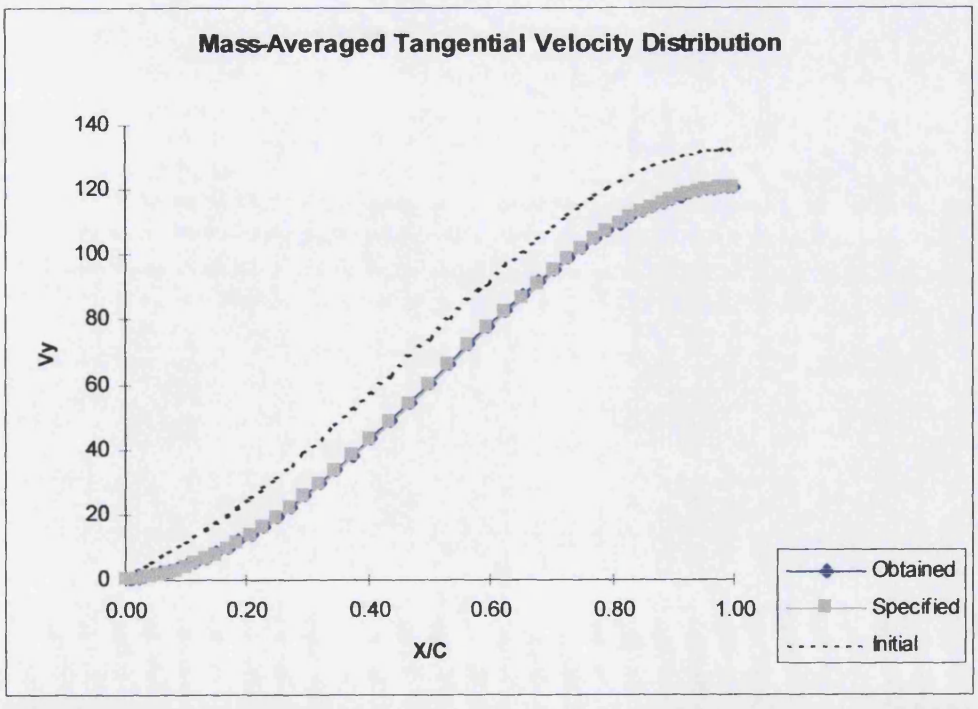

Figure 3.20 Mass-averaged tangential velocity distribution

The design was set within 1% tolerance, which gives the exit tangential velocity about 120.5819 m/s. The specified (black line) and the obtained (grey line) mass-averaged tangential velocities are shown on figure 3.20

The loading distribution of the obtained blade is shown on figure 3.21. Consequently, the Mach number of the obtained blade is shown on figure 3.22.

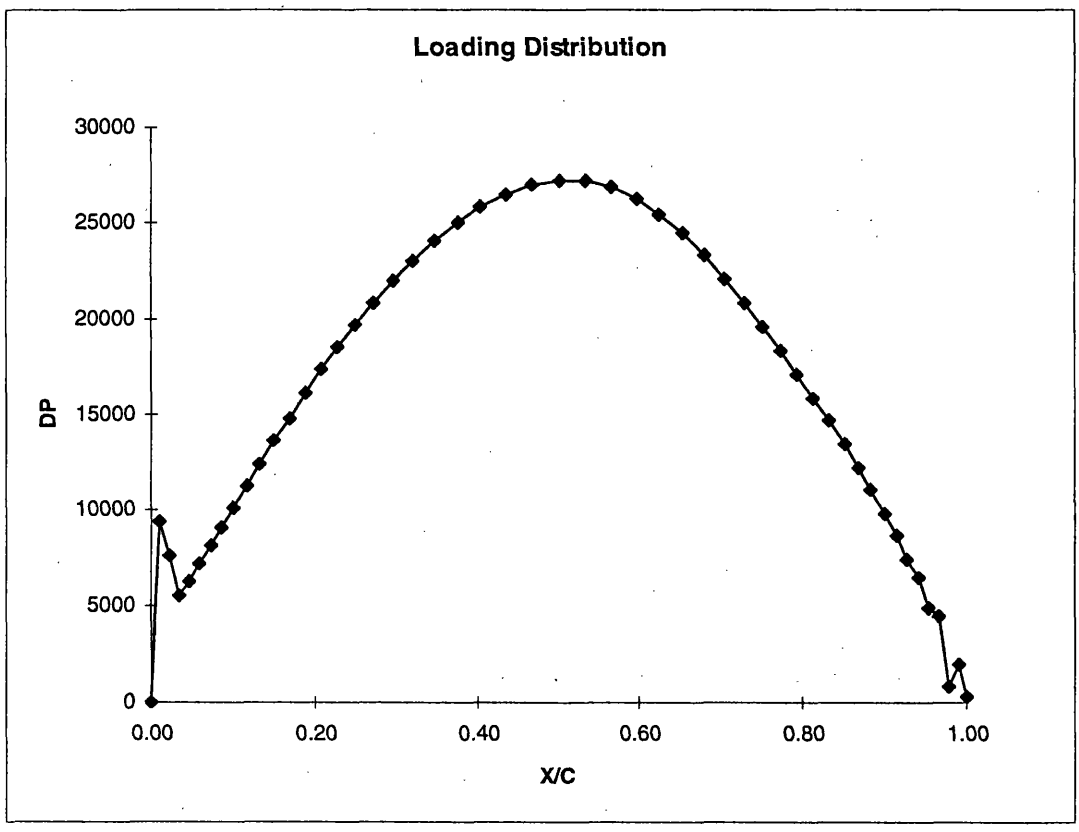

Figure 3.21 loading distribution

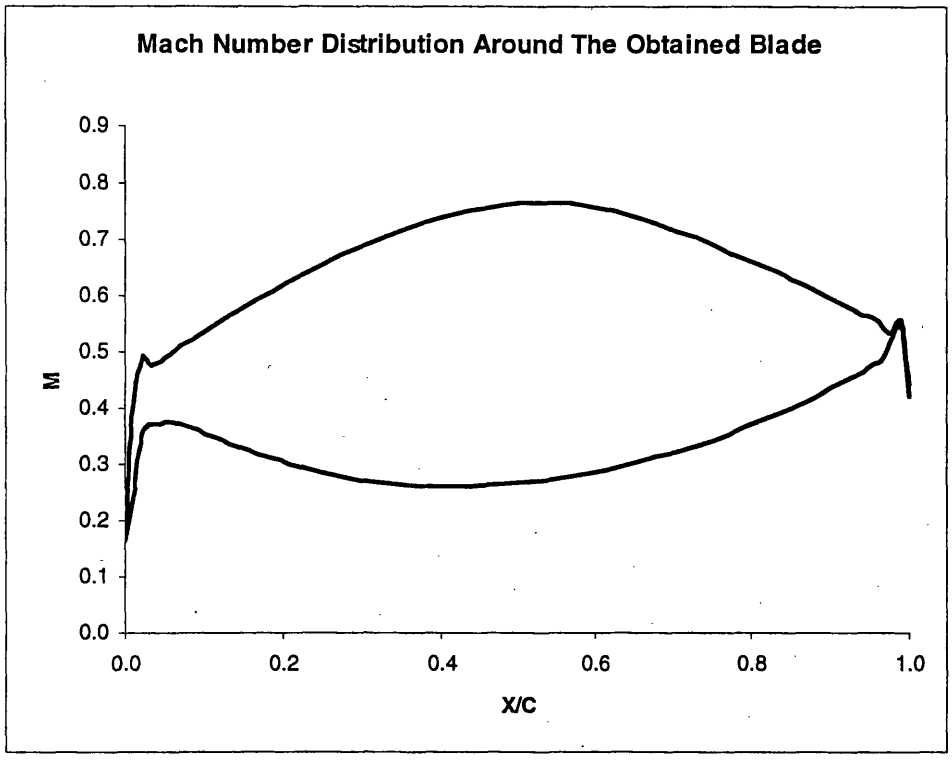

Figure 3.22 Surface Mach Number

III.3.3 Inverse Method Example II

In order to see the reliability of the method, the other subsonic stator blade is demonstrated with a large thickness distribution (Zangeneh, 1999). The thickness distribution is generated using the following equation

$$t_\theta(x) = \sqrt{x\,(1-x)} \qquad (3.2.)$$

The above prescribed thickness distribution corresponds to a symmetrical blade profile with rounded leading edge. The flow condition and the other design specifications are set the same as the first example.

The mesh for initial blade is shown on figure 3.23 and figure 3.24 for the final blade. There are no changes on the number of mesh points and grid generator parameters.

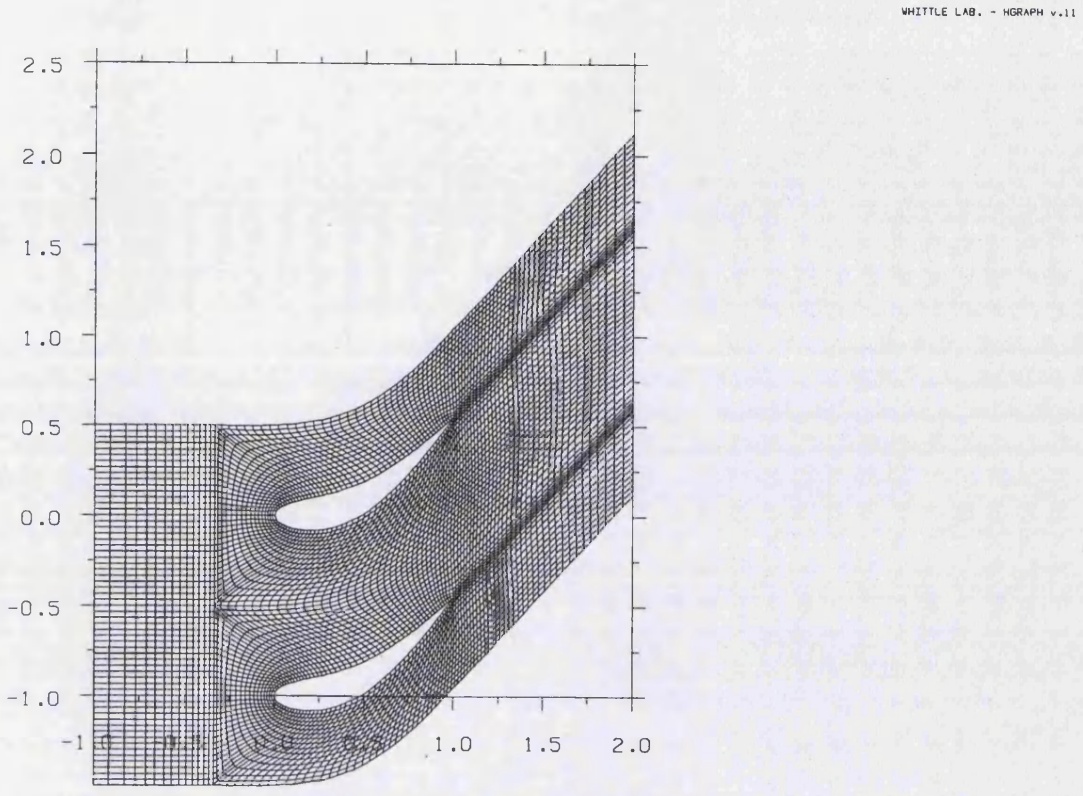

Figure 3.23 Initial blade geometry

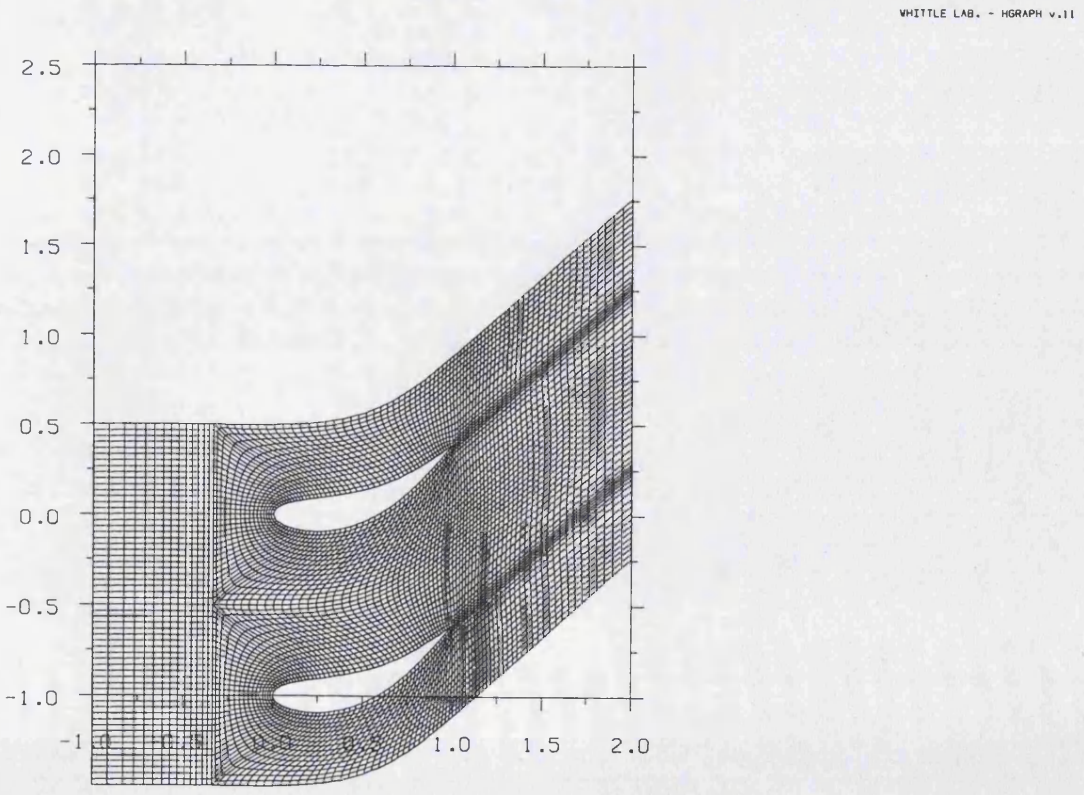

Figure 3.24 Final Blade Geometry

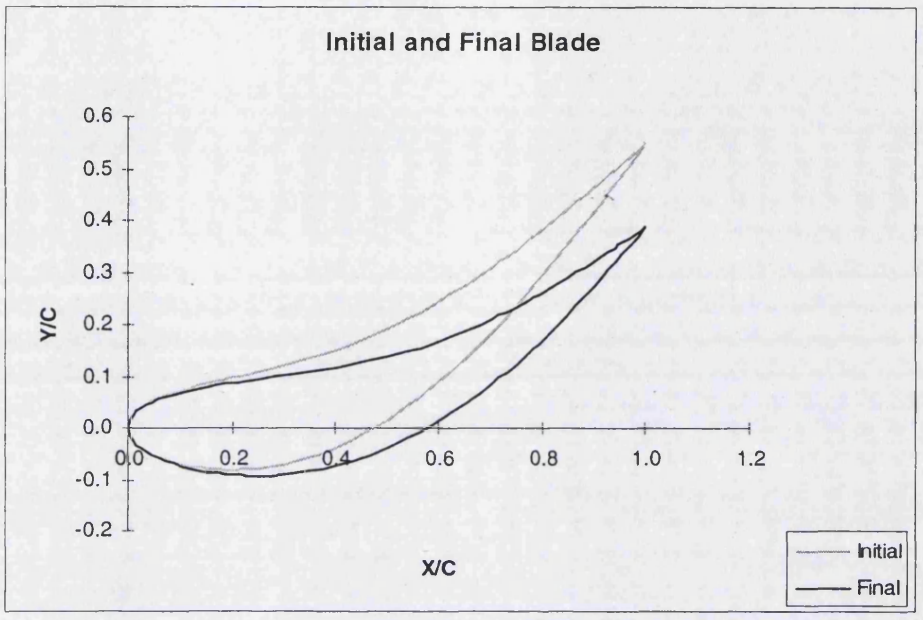

Figure 3.25 Initial and final blade geometry

Figure 3.25 illustrates more clearly the shape of the blade with a given thickness distribution and also a comparison between the initial and final blade geometry.

The obtained mass-averaged tangential velocity is shown on figure 3.26 together with the initial and the specified ones. The final blade was obtained in about 16 minutes on the same computer (i.e. turbo2, 433 MHz) and the exit tangential velocity is 120.6819 m/s as the design tolerance is set to 1%.

As the previous example, the corresponding loading distribution and the Mach number around the surface of the blade are presented (fig. 3.27 and fig. 3.28)

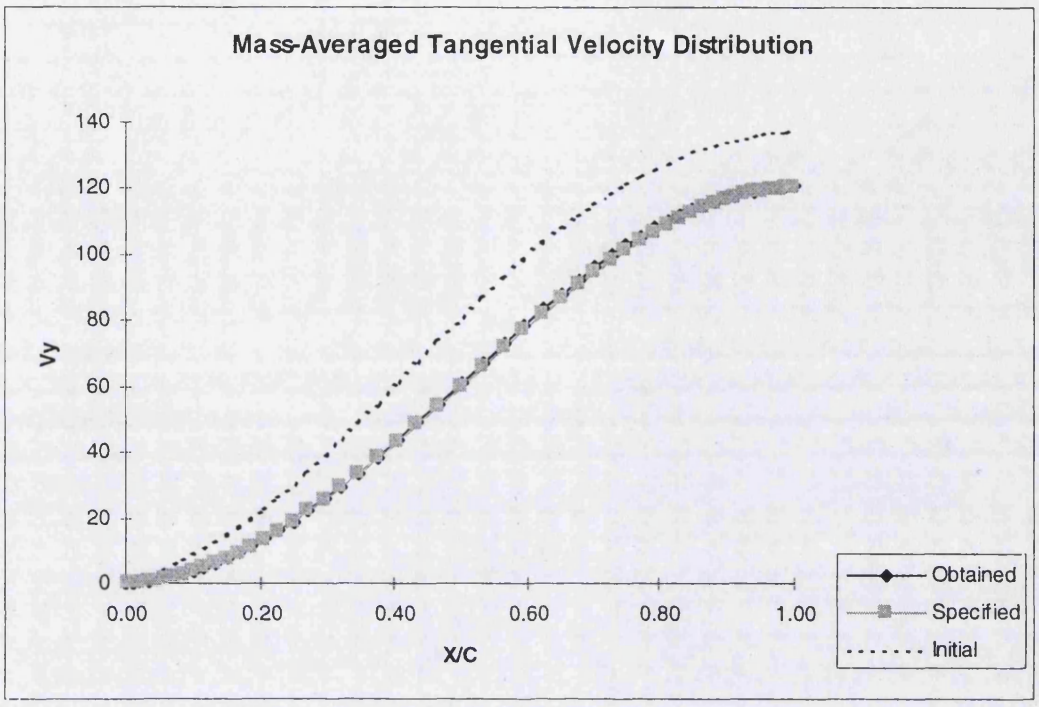

Figure 3.26 Initial, final, and specified mass-averaged tangential velocity

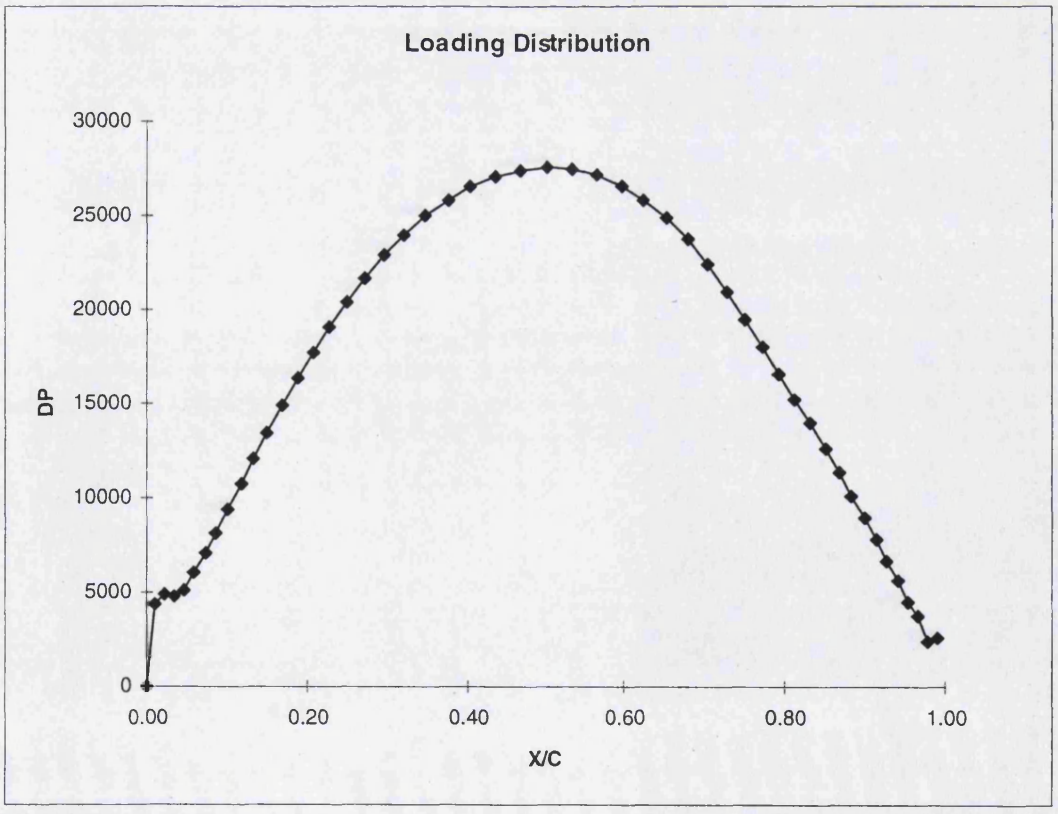

Figure 3.27 Loading distribution around a design blade

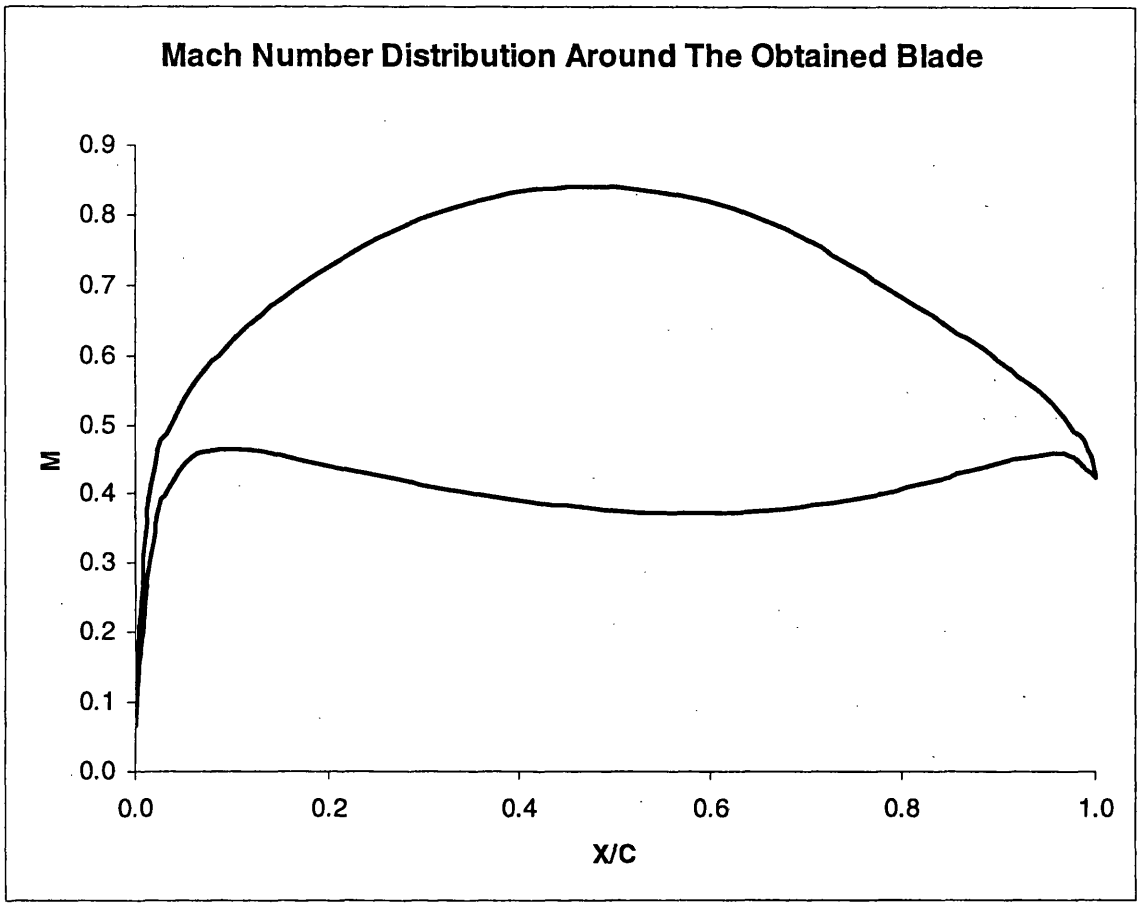

Figure 3.28 Mach Number around a designed blade

III.3.4 Discussion

Figure 3.16 illustrates the method has been successfully validated using VKI CT2 turbine rotor blade in upper transonic flow condition. This test is complicated since the blade profile has a quite large leading edge and thickness distribution. Moreover, the blade is tested in the upper transonic flow condition, which consequently produces strong shocks in the blade passage made the problem more complicated. Therefore, the blade should be modified in this complicated environment, where, of course there will be so much changes of the flow characteristics, such as pressure, velocity, and the shocks as some part of the blade profile is modified. However, in this

inverse method, the whole of large blade profile is modified, even the leading edge, which we know has a great influence in the transonic flow.

Moreover, after the blade is modified, it is possible to have some part of the blade shape that producing mass-averaged tangential velocity to the nearest design specification. The computer time required to design the desired blade profile in the transonic flow condition should be slower than subsonic flow since the changes of shape of the blade have the great effects on the entire flow field in the transonic flow.

Then, in the design example I, a C4 thickness distribution is used to design a subsonic stator blade. As shown on figure 3.20, the desired blade is successfully obtained with the mass-averaged tangential velocity very close to the specified one. Nevertheless, the loading distribution is not fully parabolic as specified, especially on the leading edge region. This problem happens due to the main design specification is mass-averaged tangential velocity and the obtained blade will be within the design tolerance. In the high gradient region such as leading edge (at x=0 and x=0.1), very small difference value of mass-averaged tangential velocity will result in the high difference in loading distribution as shown on figure 3.21.

The generated grid successfully follows the changing of the blade geometry. As seen on figure 3.18. the grid in the upstream downstream changes and the grid in the downstream moves lower. Therefore, there are no difficulties to generate the grid for all modified blades. It takes less than a second (Turbo2, 433 MHz) to generate the grid and even faster on the advanced computer such as Turbo6.

The next design example is intended to design a subsonic stator blade with a large thickness and leading edge. The design specification, flow conditions, and the grid parameters are kept fixed.

The desired blade is successfully produced as shown on figure 3.25. and 3.26. The time required to design this blade is about 16 minutes. It is longer

than the first example (i.e. the blade with C4 thickness distribution), which take about 10 minutes. It shows that for the same number of mesh points and flow conditions, the blade with a large thickness need more time to converge than the thin one. Since the changes of the large blade will have a great effect on the flow field rather than the thin blade.

Therefore, from the discussion in this section we can conclude that the time required to produce the desired blade will depend on the flow condition and the size of leading edge and the thickness of the blade.

Chapter IV Theory of Optimisation Method

The developed optimisation methodology is to design a turbomachinery blade with a surface heat transfer coefficient distribution as a design specification. The main impetus of this work is to find the possibilities of re-designing a turbomachinery blade with reduced heat transfer coefficient distribution on a certain part of blade surface.

In this methodology, the blade geometry is explored until the difference between an actual and specified heat transfer distribution is minimised. This type of approach is a kind of 'inverse method' as the blade geometry is designed to the design specification on the suction and pressure surface of the turbomachinery blade.

The optimisation procedure is basically the same as inverse methodology as described in chapter 2. The optimisation method needs grid generator, flow solver, and blade update algorithm. The same grid generator used for inverse method is also used for this optimisation method. Therefore, the theoretical background about grid generator will not be described here and can be found in chapter 2.

IV.1 Navier-Stokes Flow Solver

The developed cell vertex Euler solver which is employed in the inverse method, was extended to Navier-Stokes Equation. The extension of the flow solver is essential for heat transfers simulation which will be used for design specification. However, the addition of the viscous and heat conduction terms consumes more computer resources and time for calculation.

The Reynolds-averaged Navier-Stokes equations are closed with Baldwin-Lomax turbulent model (1978) as the convenient choice for aerodynamics and thermal simulation, and of course, for optimisation. The turbulence level in most turbomachinery flow is high, but the boundary layer profile is originally laminar at the leading edge of the blade and then develops into turbulent boundary layer downstream. The Abu-Ghannam and Shaw transition model (1980) is incorporated to treat transition, hence improving the prediction of heat transfer. Both turbulence and transition model are an algebraic model, which are economical to run and have already been well-known and most commonly used in both industry and university.

IV.1.1 The Governing Flow Equations

The two-dimensional unsteady Reynolds-averaged Navier-Stokes equations can be written in a Cartesian coordinate system as

$$\frac{dw}{dt}+\frac{df}{dx}+\frac{dg}{dy}=\frac{dr}{dx}+\frac{ds}{dy} \tag{4.1}$$

Where,

$$w=\begin{pmatrix}\rho\\ \rho u\\ \rho v\\ \rho E\end{pmatrix},\ f=\begin{pmatrix}\rho u\\ \rho u^2+P\\ \rho u v\\ \rho u H\end{pmatrix},\ g=\begin{pmatrix}\rho v\\ \rho v u\\ \rho v^2+P\\ \rho v H\end{pmatrix}$$

$$r = \begin{pmatrix} 0 \\ \tau_{xx} \\ \tau_{xy} \\ r_4 \end{pmatrix}, \quad g = \begin{pmatrix} 0 \\ \tau_{yx} \\ \tau_{yy} \\ s_4 \end{pmatrix}$$

and

$\tau_{xx}=(\lambda+2\mu)u_x+\lambda v_y$

$\tau_{yy}=(\lambda+2\mu)v_y+\lambda u_x$

$\tau_{xy}=\tau_{yx}=\mu(u_y+v_x)$

$r_4=u\tau_{xx}+v\tau_{xy}+kT_x$

$s_4= u\tau_{yx}+v\tau_{yy}+kT_y$

In the present scheme, the flow is regarded as a continuum and only ideal gas with absolute quantities will be considered.

The calculations of viscous flux terms require the values of first derivatives of U, V, and T with respect to X and Y. These values can be obtained from the cells adjacent to the required edge. For example, the value of first derivative U at cell-edge BC can be obtained from the auxiliary cell FGHI (see figure 4.1).

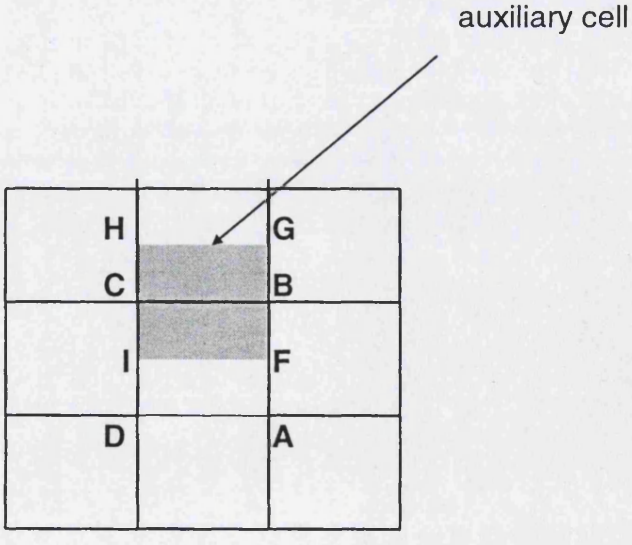

Figure 4.1 Typical auxiliary cell for viscous flux computation

The bulk viscosity, λ is taken to be $-2/3\mu$. The effect of turbulence is taken into account by using the eddy-viscosity hypothesis. Hence, the dynamic viscosity, μ and the thermal conductivity k are replaced with

$$\mu=\mu_l+\mu_t \tag{4.2}$$

$$k = C_p\left[\left(\frac{\mu}{Pr}\right)_l + \left(\frac{\mu}{Pr}\right)_t\right] \tag{4.3}$$

The laminar dynamic viscosity, μ is obtained from the Sutherland's law

$$\mu = \mu_0\left(\frac{T}{T_0}\right)^{\frac{3}{2}}\frac{T_0+110}{T+110} \tag{4.4}$$

IV.1.2 Baldwin-Lomax Turbulence Model

The implemented turbulence model is the well-known and most commonly used in both industry and university. The Baldwin-Lomax model is an algebraic turbulence model scheme its capabilities and limitations are already well known.

This two-layer algebraic turbulence model defines the nondimensional turbulent viscosity as

$$\mu_t = \begin{cases} (\mu_t)_{inner} & y \le y_{crossover} \\ (\mu_t)_{outer} & y_{crossover} < y \end{cases} \tag{4.5}$$

where y is the normal distance from the wall and the subscript crossover refer to distance at which the values of $(\mu_t)_{inner}$ and $(\mu_t)_{outer}$ are equal.

The inner eddy viscosity is determined using Prandtl-Van Driest formulation,

$$(\mu_t)_{inner} = \rho\, l^2 |\omega| \tag{4.6}$$

where the turbulence length scale l is given by $l = kyD$

The Van Driest damping factor is defined as

$$D = 1 - \exp\left(\frac{-y^+}{A^+}\right) \tag{4.7}$$

The magnitude of vorticity $|\omega|$ is given by

$$|\omega| = \left|\frac{\partial u}{\partial y} - \frac{\partial v}{\partial x}\right| \tag{4.8}$$

and the law of the wall coordinate y^+ is

$$y^+ = \frac{\sqrt{\rho_w \tau_w}\, y}{\mu_w} \tag{4.9}$$

For the outer region the eddy viscosity is calculated by

$$(\mu_t)_{outer} = K\, C_{CP}\, \rho\, F_{WAKE}\, F_{KLEB}\, (y) \tag{4.10}$$

Where K is the Clauser constant, C_{CP} is an additional constant, and F_{WAKE} is

$$F_{WAKE} = \min\left(y_{max} F_{max}, C_{WK}\, y_{max} \frac{U_{DIF}^2}{F_{MAX}}\right) \tag{4.11}$$

The quantity U_{DIF} is the difference of the maximum and minimum total velocity that occurs across the layer,

$$U_{DIF} = \left(\sqrt{u^2 + v^2}\right)_{MAX} - \left(\sqrt{u^2 + v^2}\right)_{MIN} \tag{4.12}$$

while the value of F_{MAX} is obtained from the function

$$F(y) = y|\omega|D \tag{4.13}$$

and y_{max} is the normal distance at which F_{MAX} occurs. In wakes, the Van Driest damping factor is taken as one.

The function $F_{KLEB}(y)$ represents the Klebanoff intermittency factor, which is defined by

$$F_{KLEB}(y) = \left[1 + 5.5\left(\frac{C_{KLEB}\, y}{y_{MAX}}\right)^6\right]^{-1} \tag{4.14}$$

The values of the constants appearing in the above equations are

A^+ = 26

C_{CP} =1.6

C_{KLEB} = 0.3

C_{WK} = 1.0

k = 0.4

K = 0.0168

Pr = 0.72

Prt = 0.9

Baldwin-Lomax (1978) in their paper defined the value of constant C_{WK} to be 0.25. However, according to Swanson and Turkel (1997) the value is usually inappropriate in transonic flows because it produces oscillatory movement of a shock wave. Hence, they set $C_{WK} = 1.0$. Moreover, the determination of the maximum function of F(y) follows as mentioned in their paper that the second peak is chosen.

IV.1.3 Abu-Ghannam and Shaw Transition Model

Like the turbulence model, the transition model should be carefully studied and chosen so that it could be appropriately implemented for the use of optimisation. Sarkar (2001) reviewed a bit of the past works on the simulation of flow and heat transfer in the turbomachinery field. He deduced from his review that there are two approaches adopted to tackle the transition simulation problem: the first one is based on the use of an algebraic turbulence model coupled with an explicitly imposed transition model, and the second one is to use higher order model with proper grid refinement. More researchers, who implemented the first approach, gained more satisfactory results than the two-equation model, although some researcher find the two-equation can predict the same accuracy or uncertainty as an algebraic model. Hence, Sarkar re-examine the two approaches and concluded that the Baldwin-Lomax turbulence model with an explicitly imposed transition model (i.e. Abu-Ghannam and Shaw transition model) performs well in predicting the onset and length of transition rather than the low-Reynolds number version of the k-ε model. Furthermore, the algebraic model is computationally economical. Therefore, these important points one can conclude that the algebraic transition model is the best choice for optimisation and Abu-Ghannam and Shaw transition model is the choice as it has been widely used in the turbomachinery calculation and gives better predictions for aerodynamics and heat transfer simulation.

The transition starts when the local momentum thickness Reynolds number Re_θ is greater than the critical momentum thickness Reynolds number for the onset of transition, which can be calculated as

$$R_{\theta S} = 163 + \exp\left\{F(\lambda_\theta) - \frac{F(\lambda_\theta)}{6.91} Tu\right\} \tag{4.15}$$

Where,

$$F(\lambda_\theta) = 6.91 + 2.48\lambda_\theta - 12.27(\lambda_\theta)^2 \qquad for\ \lambda_\theta \rangle 0 \tag{4.16}$$

$$F(\lambda_\theta) = 6.91 + 12.75\lambda_\theta + 63.64(\lambda_\theta)^2 \qquad for\ \lambda_\theta \langle 0 \tag{4.17}$$

and the acceleration parameter defined as

$$\lambda_\theta = \frac{\theta^2}{\nu}\frac{dU_e}{dx} \tag{4.18}$$

The end of transition is related to the critical Reynolds number for the onset of transition

$$\mathrm{Re}_{\theta E} = 2.667\ \mathrm{Re}_{\theta S} \tag{4.19}$$

Then, the intermittency factor is defined as

$\gamma = 0.0$ ($Re_\theta < Re_{\theta s}$)

$\gamma = 1 - \exp(-5\eta^3)$ ($Re_{\theta s} < Re_\theta < Re_{\theta E}$)

$\gamma = 1.0$ ($Re_{\theta E} < Re_\theta$)

Where η is obtained from

$$\eta = \left(\frac{\mathrm{Re}_\theta - \mathrm{Re}_{\theta S}}{\mathrm{Re}_{\theta E} - \mathrm{Re}_{\theta S}}\right)^{\frac{1}{1.35}} \tag{4.20}$$

IV.2 Optimisation Methodology

This section is concerned with the theoretical background of the developed optimisation method. Like inverse method, the optimisation method has three important modules: the grid generator, the viscous flow solver and the optimisation algorithm. However in this method, the thickness distribution is not specified. Hence, another module is required to generate blade geometry.

The developed method has many features, such as:

1. Easily implemented (i.e. it can use any type of grid generator and flow solver without modification).
2. The designer can obtain an optimised blade profile with heat transfer distribution as demand
3. The designer can add another constraint of the design specification such as pressure loss, specific work and/or mass flow rate.
4. There is no need for designer to have complex knowledge of the relation between blade geometry, heat transfer distribution, and other design specifications.
5. The optimisation will give the best blade profile if the design specification does not exist in practice.

Further details are described in the next sections including the blade generator.

IV.2.1 Optimisation Methodology Procedure

The optimisation is performed in the iSIGHT framework developed by Engineous Software, Inc. The design process involves iterative processing of blade parameters input files, the running of viscous flow simulation program and the numerical results in the output files. The optimisation is completed when the numerical results satisfy the design specifications, resulting a new blade profile. It can be seen clearly on figure 4.2.

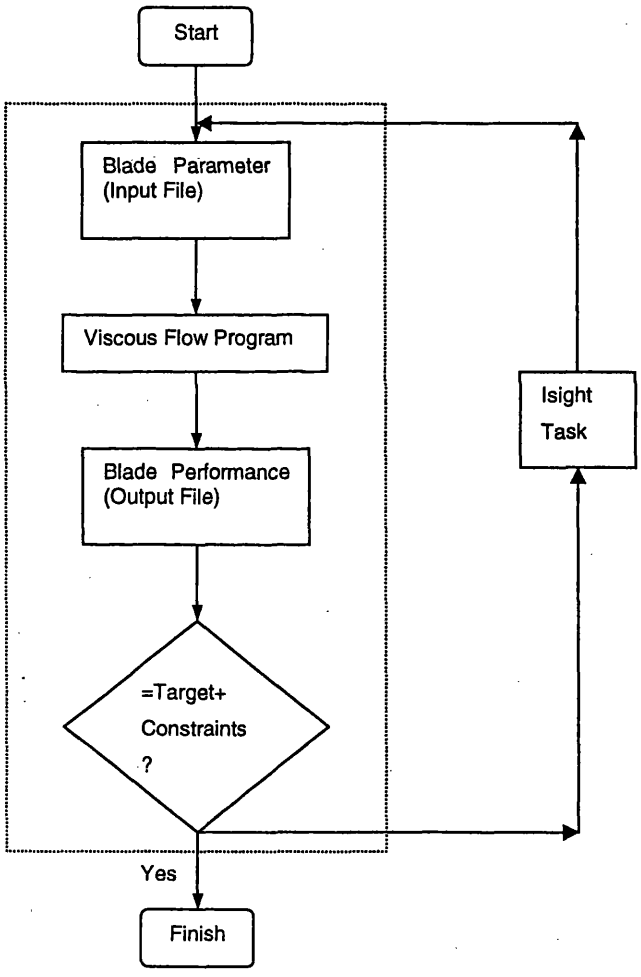

Figure 4.2 Simplified Flow Chart of optimisation method

Input File

This file stores a set of blade parameters for blade generator in order to generate a new camber line and thickness distribution. The parameter values are given by Isight for each iteration. The Isight analyses 7 parameters for thickness distribution and 5 parameters for camber line. All input parameters are controlled by input constraint.

Viscous Flow Program

This program contains blade generator, grid generator, and viscous flow solver. The blade generator read the input file in order to generate camber line, and thickness distribution, and hence the blade geometry. The grid generator creates automatically the multi-block mesh and the viscous solvers computed each problem with specified flow conditions. The solver convergence criteria are the percentage mass error (< 1 %) and root-mean square on velocity (of order 10^{-13}).

Output File

This file is the output of the viscous program, which contains the flow condition and the performance of the blade such as convergence criteria, pressure loss, mass flow rate, heat transfer distribution and $\Delta\,(r\bar{V}_\theta)$, which is related to specific work as,

$$W = \omega \Delta\,(r\bar{V}_\theta) \tag{4.21}$$

where

$$\Delta\,(r\bar{V}_\theta) = r\bar{V}_{\theta 2} - r\bar{V}_{\theta 1} \tag{4.22}$$

The $r\bar{V}_{\theta 1}$ and $r\bar{V}_{\theta 2}$ are mass-averaged swirl velocities at leading and trailing edge respectively. In the designing of turbomachinery blades, it is essential to keep the specific work or $\Delta \bar{V}_y$ (for two-dimensional) fixed with some tolerance. Then, the Isight program reads this file and analyses it according to the task

plan. The optimisation completed after all the output parameters satisfy the constraints

IV.2.2 Blade Generator

Two different approaches are considered for the blade generator. In the first approach, the blade is parameterised in terms of a leading edge and trailing edge radius together with two Bezier curves representing the upper and lower surfaces of the blades. Many authors (e.g. Trigg (1999) and Manna (2002)) have used this approach in the past for automatic optimisation studies. However, early application of this approach indicated that it did not provide enough flexibility to meet the design objectives in this study and therefore an alternative blade generator was developed. In the second approach the blade's camber line f(x) and tangential thickness $t_\theta(x)$ were each represented by a Bezier curve with six control points. The overall upper $f^+(x)$ and lower surfaces $f^-(x)$ of the blade was then constructed from:

$$\text{i.e. } f^{\pm}(x) = f_{cl}(x) \pm 0.5 * t_\theta(x) \qquad (4.23)$$

Once the new blade geometry is generated the grid generator creates automatically the multi-block mesh and the viscous solvers computed each problem with fixed flow conditions.

IV.2.3 Optimisation Algorithm

The design process involves iterative processing of blade parameters input files, the running of viscous flow simulation program and the numerical results in the output files, which are then used by the optimisation algorithm to adjust the camber line and thickness distribution. Conventional optimisation methods tend to converge more rapidly, requiring far fewer expensive viscous

computations. However, they suffer from the disadvantage that they tend to converge to the local minima, especially in multi-peak problems, which are typical of turbomachinery optimisation.

Exploratory schemes such as Genetic Algorithm (GA) or Simulated Annealing (SA) can converge to the global minimum but they require a few order of magnitude more viscous iterations. In this study the commercial optimisation algorithm ISIGHT (commercialised by Engineous Software Inc) is used. The optimisation plan is a combination of

- adaptive simulated annealing technique, which is good for searching global optimal solution in the discontinues space,
- exterior penalty technique, which is good for non linear and discontinues space and well suited for long running job,
- sequential quadratic programming, which is good for highly non-linear design

In fact, adaptive simulated annealing technique play a big role in the optimisation analysis, which is set to 700 iterations. The adaptive simulated annealing is very good to explore and to distinguish between different local optima. When minimising an objective, it can explore for certain region and it can also escape, from the local optima, to find the global solution. Then, the exterior penalty method will make sure the global optimum is correct by running only 120 iterations. Finally, the sequential quadratic programming is set to 10 iterations to check the region around the solution. From the authors' experiences, this is the best combination and should be run sequentially. The adaptive simulated annealing should be employed first in order to find the best global solution, while the exterior penalty and sequential quadratic programming could lead to the local optima or sometimes no solution at all if they were employed in the first run.

IV.2.4 Objective Function/Constraints

The main objective of the optimisation method is to minimise the difference between the specified and actual heat transfer coefficient. The objective function is defined by

$$\varphi = \frac{\sum_{j=1 to N} \left| h_j^n - h_j^* \right|}{\sum_{j=1 to N} h_j^*} \qquad (4.24)$$

Where h^* is the specified heat transfer coefficient, h^n is the heat transfer coefficient on the latest design and j is location of the mesh point and N is the total number of mesh points over which h^* is specified. In addition a number of constraints are specified. The most important constraint is to ensure that the stagnation pressure loss in the new design is at least the same as or less than that of the original blade. The other important constraint ensures that the overall turning within the blade row (i.e. the difference in tangential velocity at exit and inlet of blade row) is within 2% of that for the conventional blade

Chapter V Application of Optimisation Method

In this chapter, the developed Navier-Stokes solver is employed for the optimisation method. Hence, the validation of the solver is firstly shown. The developed Navier-Stokes solver is compared with the experimental data and commercial CFD software, such as Fluent.

Two design specifications are presented in this chapter. The first example of optimisation method is loading distribution ($\Delta P=P^{+}-P^{-}$). The main purpose is to validate the method by reproducing the existing blade. The loading distribution is generally used for designing blade geometry using inverse method.

The second examples show the optimisation of surface heat transfer distribution. The method is applied on the turbine blade in the turbulence flow condition. Two examples are presented for optimisation on heat transfer coefficient distribution.

V.1 SNECMA Stator Blade

The validation of the developed viscous code has been achieved. The code is the integration of 2D Navier-Stokes equation with the time marching method. While the flux terms is discretised based on a cell-vertex finite volume formulation. The Baldwin-Lomax turbulence model (1976) and the Abu-Ghannam and Shaw transition model (1980), is employed in this viscous code.

The blade test is a well-known high-pressure gas turbine rotor RS1S profile (Arts et. al., 1998), which was designed by SNECMA. The aerothermal

measurements were carried out in one of the two Isentropic Light Piston Compression Tube facilities of the Von Karman Institute, namely the linear cascade wind tunnel CT-2. The blade was mounted in a linear cascade arrangement; 6 blades (i.e. 5 passages) were used and the third profile was instrumented. The uncertainty of the measured quantities was in the order of ± 5%. Many numerical heat transfer coefficient validations had been performed on this uncooled blade for example Arts (1998) and Xiao (2000).

The flow was set with the following conditions:

Incidence angle I=-5 deg

Turbulence Intensity= 4%

Exit isentropic Mach Number=0.8

Inlet total temperature T_o= 420 K

Exit static pressure P_2= 1x10^5 Pa

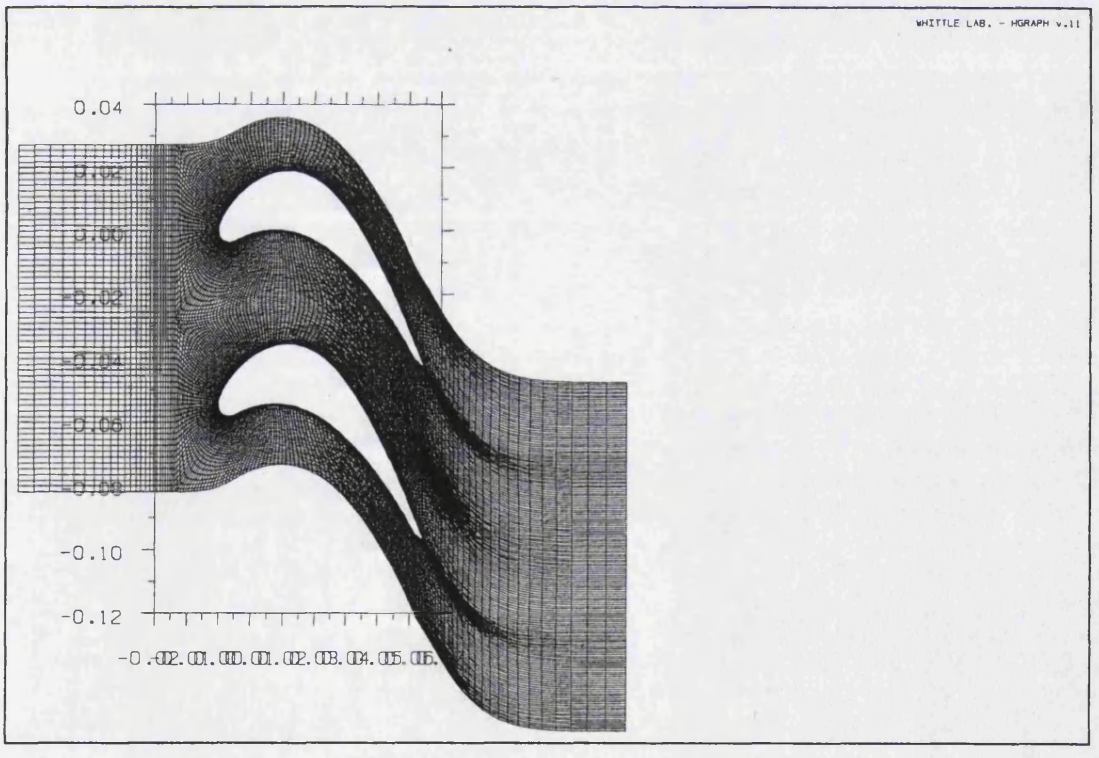

Figure 5.1 Computational multi-block mesh of the RS1S blade

The two-dimensional multi-block viscous grid was generated around the RS1S blade as illustrated in figure 5.1. The RS1S blade is wrapped by C- mesh topology (254 * 45) and the upstream region is treated by H-mesh (52 * 16), total of grid points is 12262.

The viscous code completed the calculation in about 25 minutes on turbo6. The predicted surface pressure by viscous code is compared with the commercial code Fluent's prediction as shown in figure 5.2. A similar multi-block grid domain and number of cells were also generated for Fluent, which was set to use the k-ε turbulence model.

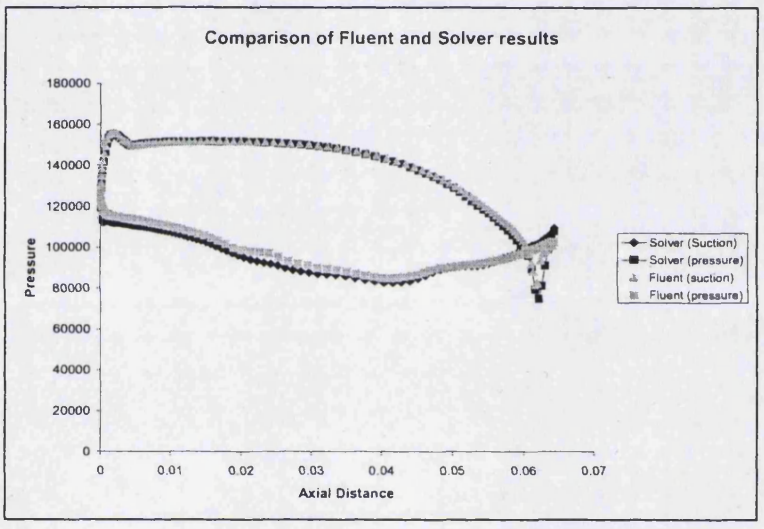

Figure 5.2 Surface pressure distribution around RS1S blade obtained from the developed solver and commercial code

Figure 5.2 shows that the predicted surface static pressure by the current flow solver, which implemented an algebraic turbulence and transition model, is in good agreement with that predicted by FLUENT. It means that the viscous code with the algebraic model is as good as the commercial code, which implemented the more sophisticated turbulence model.

	COLIBRI (T.ARTS)	CANARI (T.ARTS)	Xiao	Raharjo
Type	Quasi 3D	3D	3D	2D
Method	Runge-Kutta, cell vertex	Runge-Kutta, cell centre	Implicit Cell-centre	Runge-Kutta cell vertex
Turbulence Model	Algebraic mixing length model formulated by Michel (1969)	K-e	Baldwin Lomax	Baldwin Lomax
Type of Mesh	H-O-H	H-O-H	H	H-C
Number of Points	26,500	26,500	7869 (2D) 322,629 (3D)	13,374

Table 5.1 Viscous Solver Comparison

The result of heat transfer distribution is compared with the result of Arts (1998) and Xiao (2000) as shown in figure 5.3. The Arts code is a Runge-Kutta cell-centre scheme with a k-e turbulence model (CANARI, 3D) and an algebraic turbulence model (COLIBRI, quasi-3D), and Xiao code applied Baldwin-Lomax Turbulence model. The code and grid comparison can be seen in table 5.1

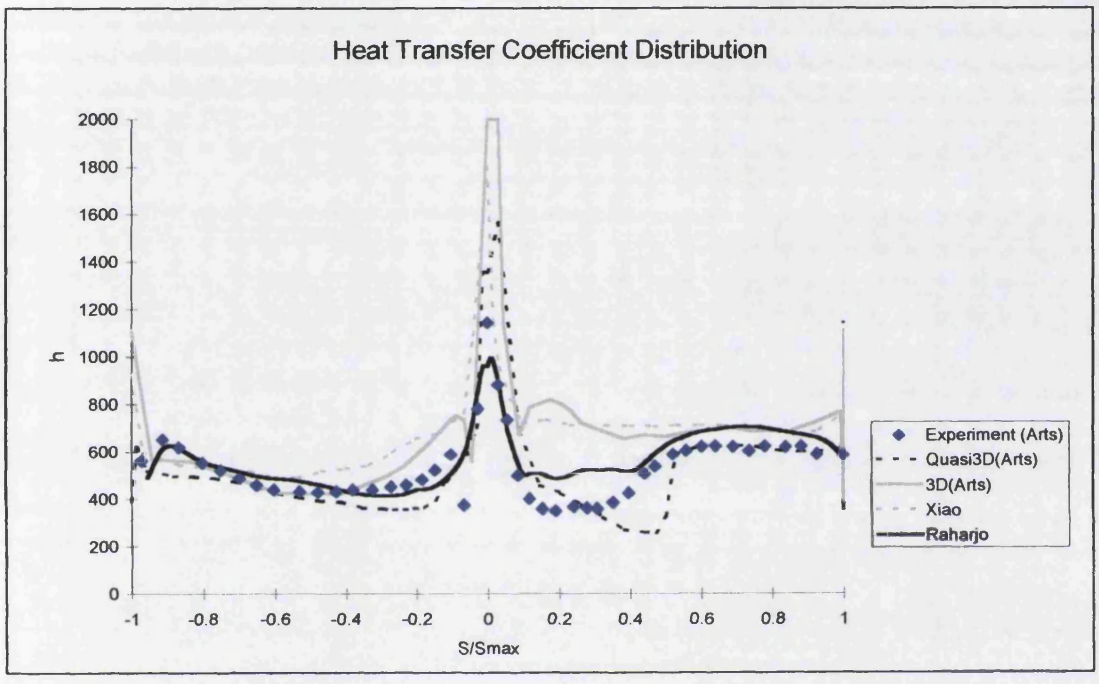

Figure 5.3 Heat transfer coefficient on the RS1S blade surface obtained from experimental and numerical results

The heat transfer coefficient (HTC), h is calculated using the heat flux on the wall, total temperature at the inlet, T_0, and the local wall temperature, T_w, as follows:

$$h = \frac{q_w}{T_0 - T_w} \tag{5.1}$$

Where, the heat flux on the wall is obtained from,

$$q_w = \left.\frac{\partial T}{\partial n}\right|_w \tag{5.2}$$

As shown in figure 5.3 the result of heat transfer coefficient (HTC) from the developed viscous code had a good agreement with the measurement and better than the other numerical method. On the pressure side, the viscous code gave the closest result on the value and trend of the curve of HTC distribution measurement.

The result on the suction surface is affected by laminar to turbulent flow model. In the fully turbulence region (i.e. from S/Smax=0.5-0.9), all numerical calculations gave a bit higher value than the measurements but they still follow the trend of the experimental line. However for S/Smax=0.1-0.5 where the transition was encountered, the results of Xiao and CANARI (Arts, k-ε model) were very poor. It seems there is a problem for two equations turbulence model to predict the heat transfer on the transition part, although it is good for aerodynamics analysis. In the paper, Xiao quoted from the Larsson's paper (1997) that two equations k-ε and k-ω models were not fully able to correctly predict the heat transfer on the suction side. Only the Launder-Sharma model could capture any laminar region. The two equations k-ω, which had been optimised for transition simulations, was also poor on predicting heat transfer. Meanwhile the developed viscous code computed better and closer to the experiment. The computed result showed clearly the transition region correctly (i.e. the starting point and the length of transition).

Furthermore, the result from the developed viscous code on the leading edge region is better although it used the smallest amount of grid size. This could be due to Xiao's code used H-mesh topology while the developed solver used C-mesh topology, which treats the leading edge better than H-mesh. However, both Arts numerical results were overshoot, although he applied O-mesh around the blade. However, as also noticed by Larsson, all two

equations models had problems around the leading edge. He modified the production term, k, resulting a bit lower heat transfer than the measurements.

Finally, this result shows that the developed viscous code has an excellent performance over all complicated codes. The most important thing is the algebraic model gives a good speed of calculation, which is needed and very critical for inverse design or optimisation.

V.2 Loading Distribution

The optimisation method was firstly tested for loading distribution. The first test aims to reproduce the RS1S blade starting from any arbitrary geometry. The pressure loading distribution of the original blade is obtained from the direct analysis and used as the target of optimisation. The loading distribution can be seen on figure 5.4.

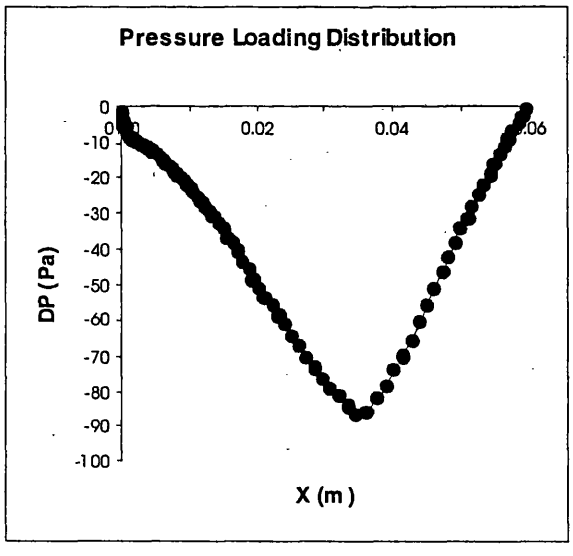

Figure 5.4 Target loading distribution

The grid and flow conditions are set as described in the previous section. The solver convergence criteria are set to be less than 1 % for percentage mass error and in order of 10^{-11} for velocity root-mean square. The optimisation task

is set to 10 iterations for adaptive simulated annealing, 120 iterations for exterior penalty technique, and 40 iterations for sequential quadratic programming. The optimisation process completed in about 7 hours and 4 minutes on turbo6. The reproduced blade matched the original one as shown on figure 5.7.

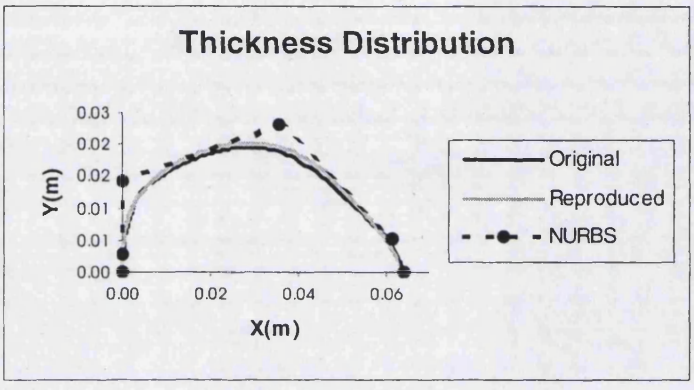

Figure 5.5 Thickness distribution

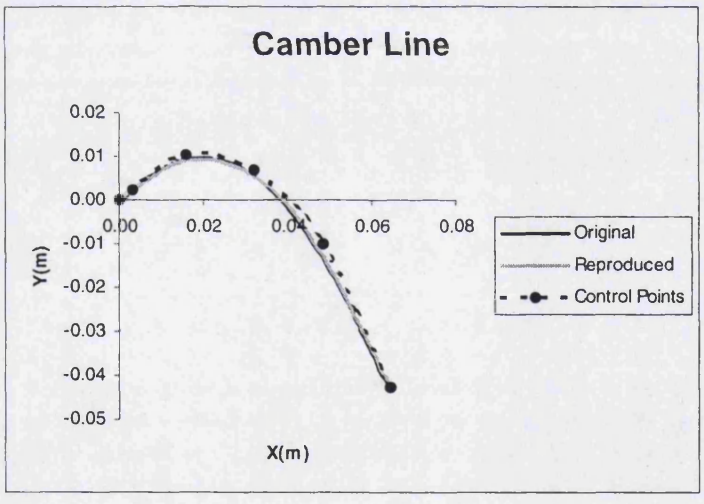

Figure 5.6 Camber line

The loading distributions as shown in figure 5.4. is smooth on the leading edge region. The treatment of C-type grid on the leading edge is better than H-type grid. The H-type grid can give an oscillation loading distribution near leading edge as shown by Tiow (1998). An oscillation on the target distribution or on numerical result can lead to a big problem for inverse design and optimisation.

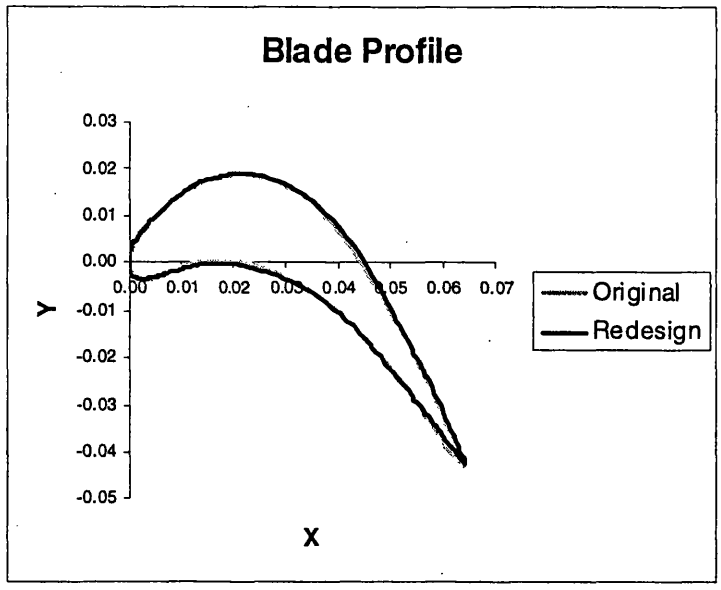

Figure 5.7 Blade profile of the original and reproduced blade

Figure 5.7 shows the blade has been successfully reproduced. The reproduced blade is match closely to the original one, but not exactly matches to the blade. The difficulty was put forth by the limitation of the blade generator and number of iteration. The blade generator produces the blade profile using the NURBS functions. These functions generate the camber line and thickness distribution with help of control points. The generated smooth curve was highly dependent on the control points. If one control points move, it will affect the production of the smooth curve. As the numbers of control points are limited, the reproduction of smooth blade can only be very close to the original one.

The camber line was produced exactly the same as original one as presented in figure 5.6. However, the thickness distribution is a slightly different in the region x=0.04 m as shown in figure 5.5. Hence, for this case the thickness distribution only can match closely to the original and so the blade profile. However, this problem can be observed in other optimisation methods (e.g. Manna (2002)) and inverse methods (e.g. Tiow (1998)), and can be solved by improving the accuracy of the NURBS representing the camber line and blade thickness. Despite that, this optimisation design is attained with a high level of closeness.

V.3 Heat Transfer Coefficient Distribution

Now the optimisation method is applied to re-design the RS1S blade profile with a heat transfer coefficient distribution as one of design parameters. In the first example, the optimisation method is used to increase the value of the heat transfer coefficient h over a large part of the blade pressure surface. Then in the second example the method is applied to reduce h close to the trailing edge on the suction surface of the blade.

V.3.1 Example I: higher heat transfer

In this optimisation, a linear target Heat Transfer Coefficient (HTC) distribution was applied. A given set of target HTC distribution has constant value of h=570 W/m^2K on the pressure surface from x= 0.00783 to x= 0.0601 m. The objective functions was set to minimise the difference of the target and the current heat transfer coefficient with several constraints on the blade geometry and several flow criteria such as pressure loss, specific work, and mass flow rate.

In this example, we imposed a mix design specification as follows:
- given a target heat transfer coefficient distribution
- less pressure loss than RS1S blade ($<$0.0425)
- mass flow rate about the same ($6.42<\dot{m}<6.69$ Kg/s)
- ΔVy should be about almost the same($-431<\Delta Vy<-414$m/s)

The flow condition and the grid size were set to be the same as shown in the previous section. The solver convergence criteria are set to be less than 1 % for percentage mass error and in order of 10^{-13} for velocity root-mean square. The blade parameter constraints can be seen on table 5.2.

No	Parameter	Lower Bound	Upper Bound
1	thcpy1	0.001	0.005
2	thcpx2	0.0	0.01
3	thcpy2	0.005	0.02
4	thcpx3	0.01	0.045
5	thcpy3	0.01	0.025
6	thcpx4	0.06	0.065
7	thcpy4	0.001	0.0075
8	clcpy2	0.0	0.005
9	clcpy3	0.0	0.015
10	clcpy4	0.0	0.015
11	clcpy5	-0.02	0.0
12	clcpy6	-0.05	-0.03

Table 5.2 Constraints of the input parameters

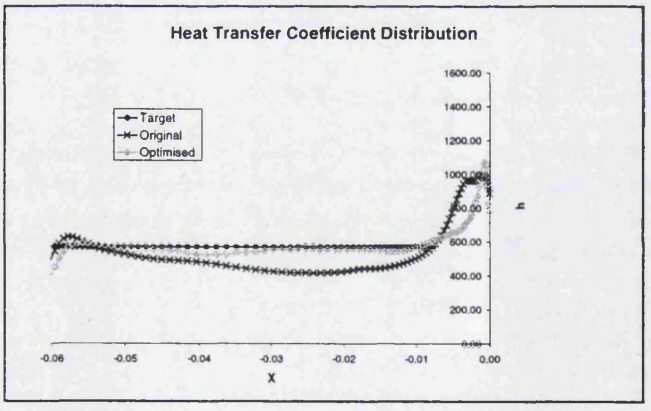

Figure 5.8 The optimised HTC distribution of the designed blade

The optimisation completed after 909 iterations for about 326 hrs 38 mins on turbo2. The designed blade had heat transfer distribution as illustrated in figure 5.8 and satisfied the design constraint as follows:

- Pressure Loss = 0.0417 (<0.0425 as specified)
- Mass flow rate = 6.6823 Kg/s (6.42< $\dot{m}$ <6.69 Kg/s)
- ΔVy = - 423.647 m/s (-431<ΔVy<-414 m/s)

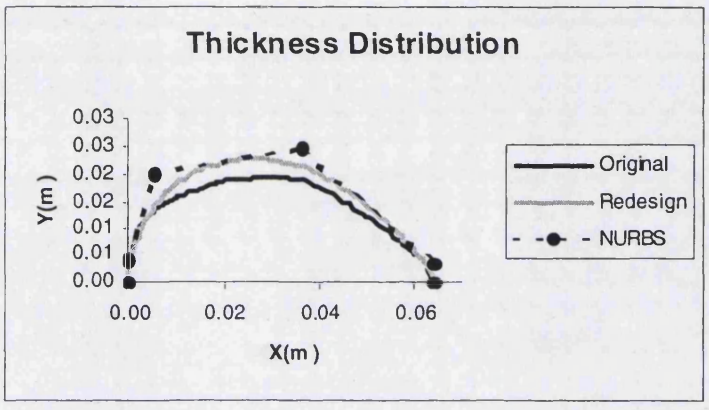

Figure 5.9 The blade thickness distribution

To illustrate the changes of blade geometry carried out in the optimisation design, the blade profile can be seen on figure 5.11 which has thickness distribution as shown in figure 5.9 and camber line profile as presented in figure 5.10. The thick dots on those figures show the position of control points.

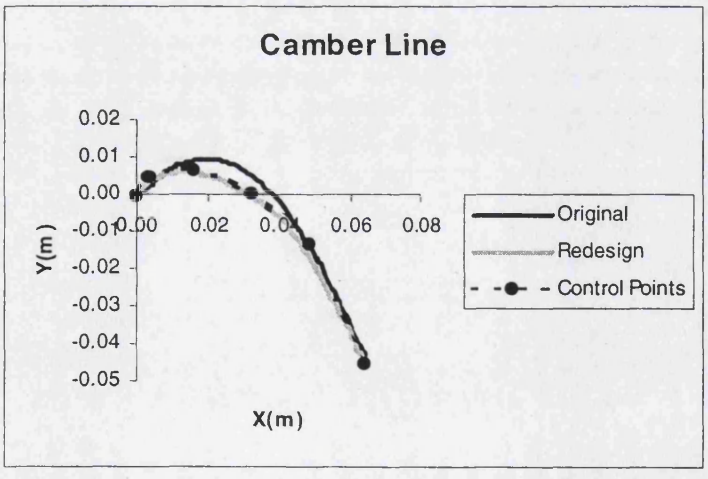

Figure 5.10 The camber line profile

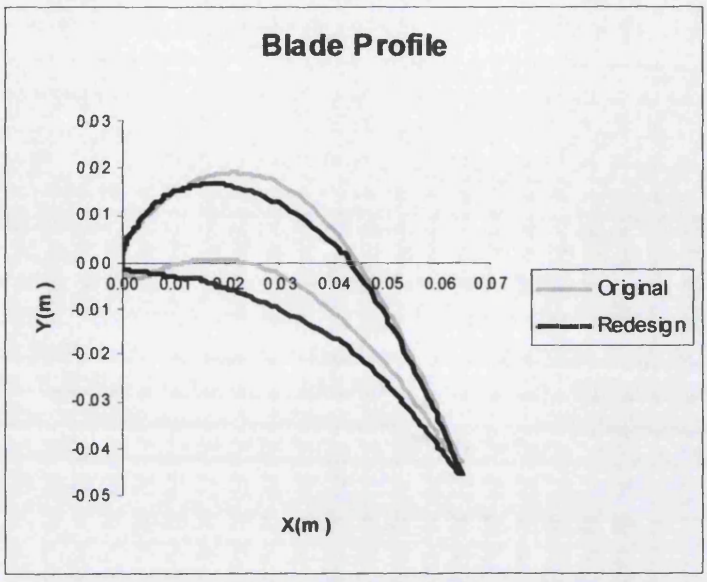

Figure 5.11 The Designed blade profile

Again, The flow through the new blade was computed by FLUENT. The surface pressure predicted by FLUENT is agree very well as presented in figure 5.12. It shows that in order to meet the specified heat transfer distribution, the blade profile changes and hence the flow field. The comparison of overall heat transfer coefficient around the designed blade is presented in figure 5.13.

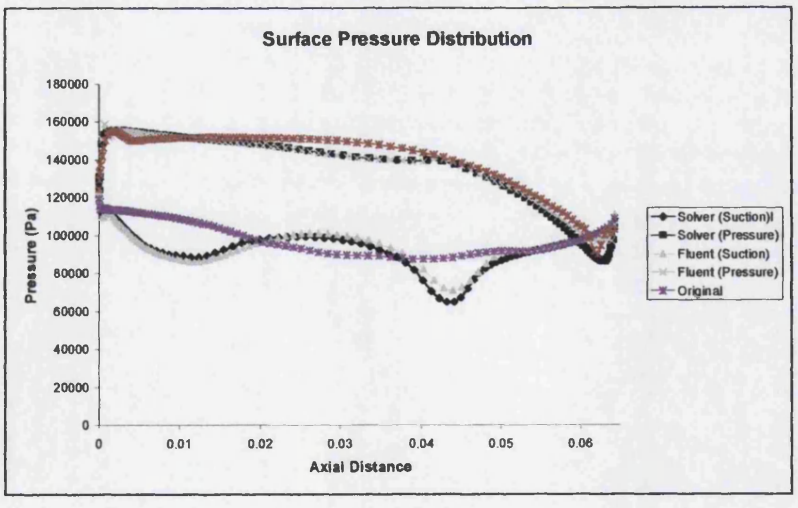

Figure 5.12 Surface pressure around designed blade

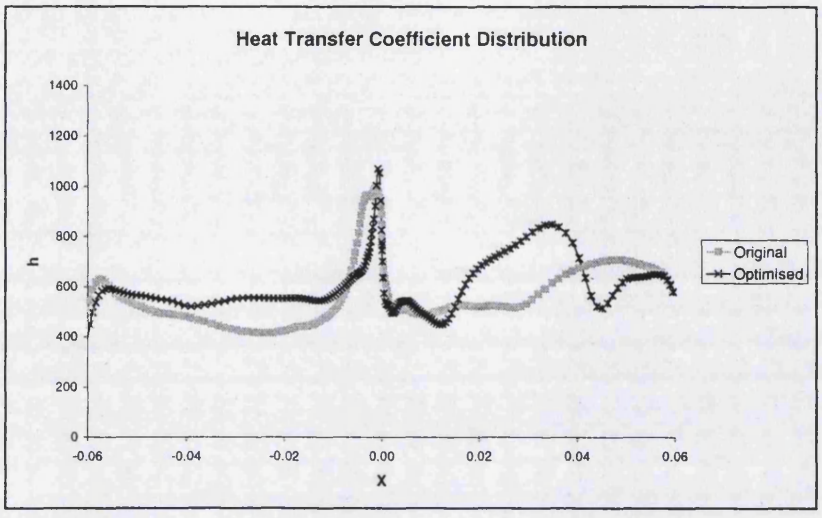

Figure 5.13 Heat transfer coefficient around designed blade

V.3.2 Example II: reduced heat transfer

In the second example, the heat transfer coefficient is reduced on the region near the trailing edge. The prediction on the original blade shows the heat transfer coefficient is increasing at this region (see figure 5.3). The selected region (i.e. the section near the trailing edge) is usually thin and difficult to design for cooling system.

For the numerical calculation the design region is now set from x= 0.04510488 m to trailing edge of the pressure surface. The specified design distribution is set to linear for simplicity with lower constant value. The value of target distribution is h= 491.6845 W/m^2K. All flow conditions and optimisation constraints are set the same as example I.

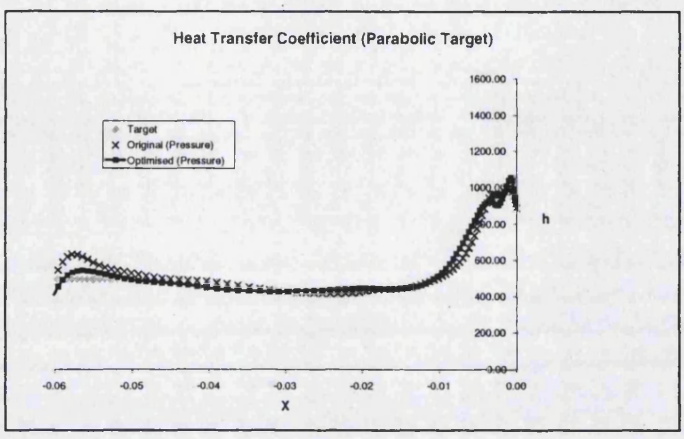

Figure 5.14 Reduced heat transfer

The optimisation process completed after 923 iterations in about 269 hours 23 mins on 50% CPU of turbo6. The heat transfer coefficient near the trailing edge of the pressure side has been successfully reduced, as presented in Fig. 5.14, while maintaining almost the same heat transfer coefficient on the rest of pressure surface. The value of h is now reduced by 15.6% from its peak value. The designed blade geometry is illustrated in figure 5.15 together with the original blade (dotted line).

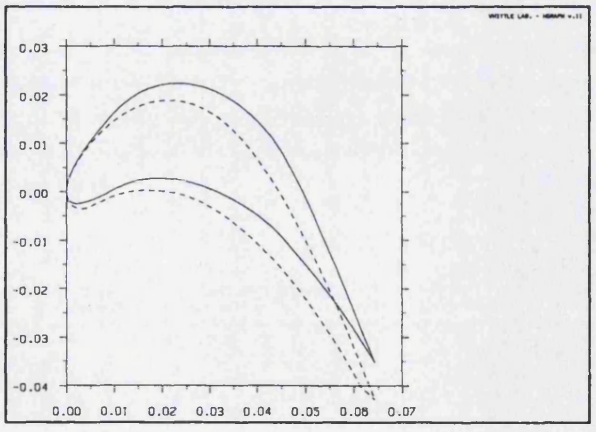

Figure 5.15 Designed blade for reduced HTC near trailing edge of pressure side

As expected this design example satisfies the design specifications as follows:

- Pressure Loss = 0.0334 (<0.0425 as specified)
- Mass flow rate = 6.539 Kg/s (6.42< $\dot{m}$ <6.69 Kg/s)
- ΔVy = - 416.434 m/s (-431<ΔVy <-414 m/s)

Finally, the surface pressure and HTC around the design blade are shown in figure 5.16 and figure 5.17 respectively.

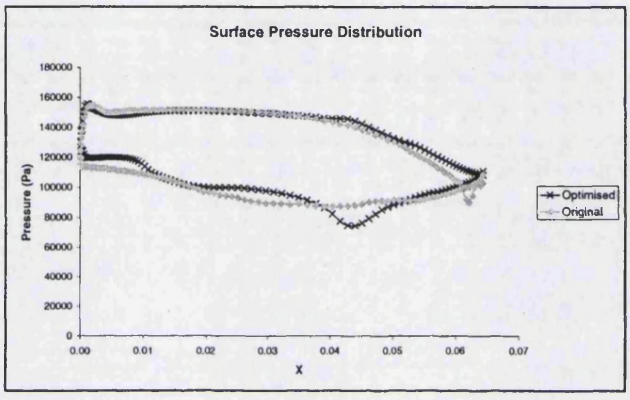

Figure 5.16 Surface pressure of designed blade

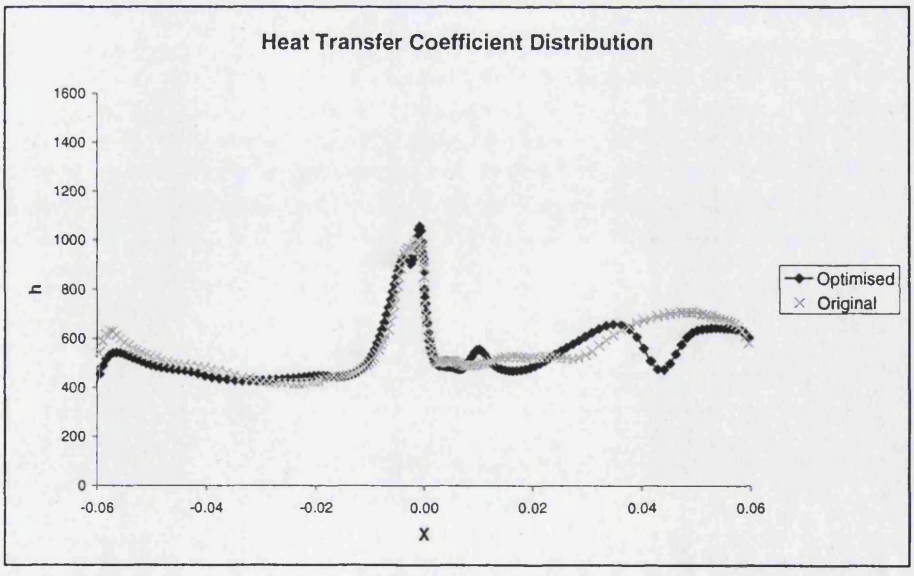

Figure 5.17 Heat transfer coefficient around the blade

Chapter VI Conclusion and Future Work

The numerical methods for designing turbomachinery blade have been presented in this thesis. Both inverse and optimisation method has several advantages, especially in comparison with traditional design approach. The following sections summarise the development of these numerical design methods and outline the possible further extension of both methods.

VI.1 Conclusion

The use of boundary conforming co-ordinate system is the appropriate choice for inverse and optimisation method for generating grid around any shape of the modified blade geometry. Moreover, the elliptic Poisson equations ensure the grid is always smooth and the use of Sorenson scheme provide the grid can be generated faster and saving more time in the optimisation and inverse method.

The grid generator has been developed in the multiblock method, which has some advantages as follows

- Reducing the complexity of the problem (e.g. the need to use H-type grid for upstream boundary)
- The grid can be employed easily for inverse and optimisation method with any type of flow solver.
- For further work this grid generator can be easily implemented for multistage, cooling system, and three dimensional analysis

The multiblock cell-vertex Euler solver has been validated using experimental results of Dring turbine stator blade and VKI turbine rotor blade in subsonic

and upper transonic flow. The novel viscous solver with turbulence and transition model had also been validated. The viscous solver was validated with the result of surface pressure and heat transfer coefficient distribution of RS1S blade. A good correlation was obtained between the result of the developed solver and from both experimental and numerical calculation of commercial software.

The inverse method has been developed with the prescribed design specification, mass-averaged tangential velocity distributions follows the theory in the papers that are summarised in section I.2.2. The other primary design specification, blade thickness distribution ensures the obtained blade satisfies the structural and manufacturing requirement.

The developed method employs a two-dimensional CH-type grid and a multiblock inviscid solver. Using this type of grid, it is possible to design a blade with blunt leading edge accurately such as turbine blade. The problem to calculate the mass-averaged tangential velocity is solved in the boundary conforming co-ordinate system. Some examples have been presented including a blade with large leading edge.

It was shown that the time required to get the desired blade depends on the shape of the blade and the flow conditions. The blade with large thickness distribution and hence leading edge will take longer time than a thin blade. Moreover, in transonic flow conditions especially when shocks exist, the blade convergence is slower than in subsonic case.

The author has investigated the possibility of designing turbine blade with a surface heat transfer distribution as a design parameter using optimisation method. The camber line and thickness distribution seems a proper choice for optimisation design and can easily generate any shape of blade geometry.

An optimisation design procedure addressing the enhancement of the combined aero-thermal blade performance has been outline. Some examples on the loading distribution and heat transfer coefficient are presented. The

results of heat transfer optimisation especially has shown that it is possible to optimise the heat transfer distribution on the certain part of the blade where required.

Obviously, this method can find a blade geometry that can change the flow, which will affect the aerodynamics and heat transfer performance. Moreover, the examples show that it is also possible to add some design criteria as constraints. This would allow us to have some several flow conditions on the designing of the blade. However, it needs a lot of time to complete the heat transfer optimisation, since it requires viscous solver with several models and viscous grids (i.e. more grid points). However, as the computer speed is continuously increasing, the optimisation method can be extended to three-dimensional flow in the future. This method will open a new era of designing a turbomachinery blade, especially turbine blade.

VI.2 Future Work

VI.2.1 Inverse Method

The inverse design method can be enhanced by improving the component involved, such as the solver. The speed of inverse design could be improved by implementation of multi-grid technique and other convergence accelerations.

The presented inverse method can produce two-dimensional blade profile. The method can be extended to three-dimensional inverse method by modifying all the inverse tools to three dimensional. It is possible since the method implements structured grid. However the big jobs are to extent the three dimensional grid generator and Euler solver.

There is possibility to extent the inverse method to model the viscous effect. The solver can be modified to solve Navier-Stokes equation. However, the problem is how to update the blade geometry as the presented method based on the slip condition. If the blade update algorithm for non-slip conditions can be found, the solver can be further enhanced by adding turbulence and even transition model. However, there are many other possibilities to involve the viscous effect, such as viscous model proposed by Denton or inviscid-viscous interaction. The author does not feel convenience with the method proposed by Demeuleaere et. al. (1997) that the slip condition is moved to the edge of boundary layer as the boundary layer characteristic is not as simple as we thought. Demeuleare admitted that he face some problem in updating blade profile, especially on the region near trailing edge. However, from those any possible method, the implementation of Navier-Stokes equation is the best idea.

The inverse method can also be extended to design the blade in a multi-stage arrangement. The multiblock grid generator and multiblock solver made the method to be easily extended for this design method. However, the main

problem could be the multi-stage calculation that could remove the unsteadiness from the flow through consecutive blade rows.

Furthermore, the inverse method can also be modified in order to be used for hydraulic applications, such as water pump. However, the working fluid has constant density, which means the time derivative of the density should be modified. Hence, the presented solver should be modified to incompressible solver.

Finally, the inverse method can be combined with optimisation method. The distribution of $\tilde{V}_y^*$ can be optimised for certain design parameter, for example to minimise loss. There is no significant modification necessary. It works by integrating the grid generator, solver, and blade updater to an optimisation algorithm.

VI.2.2 Optimisation Method

Similar as inverse method, this optimisation approach can be extended to three-dimensional method. There is no big work or problem on modifying grid generator or the Navier-Stokes solver. The main concern is the computational time. As has been described in the previous chapter, the heat transfer optimisation could be completed in about 10 days. Hence, the three-dimensional heat transfer optimisation should lasts for more than ten days. Therefore, the three dimensional work should be appropriately performed using faster computer. Nevertheless, as the computer speed increasing rapidly, the author can predict that this job can be run using home computer. It can be seen easily as the speed of new computer is now already seven times faster than the computer used for the research.

However, there is another possibility to increase the speed of optimisation. As we have been noticed, the speed of the optimisation depends mainly on the speed of solver to calculate the flow. Hence, in order to reduce the computer

cost, it is worth to implement the multi-grid method and other convergence accelerations.

Furthermore, the optimisation method can also be used for hydraulic applications, such as water pump. Therefore, the viscous program should be modified for incompressible flow program. The program should be validated using incompressible test blade.

Finally, the method can also be extended to a multi-stage optimisation method. The multiblock method made the grid generator and solver can be easily extended to this method. Again, the main concern is the computational cost. However, the author believed that when the development of the viscous program to solve the multi-stage calculations for the optimisation completed, the new fast computer will be ready in the market.

REFERENCES

Abid, R., Vatsa, V. N., Johnson, D. A., and Wedan, B.W. 1990. Prediction of Separated Transonic Wing Flows. AIAA Journal 28(8): 1426-1431.

Abu-Ghannam, B. J. and Shaw, R. 1980. Natural Transition of Boundary Layers - The Effects of Turbulence, Pressure Gradient, and Flow History. Journal of Mechanical Engineering Science 22(5): 213-228.

Adamczyk, J.J., Celestina, M.L., Beach, T.A., and Barnett, M. 1990. Simulation of Three-Dimensional Viscous Flow Within a Multistage turbine. Journal of Turbomachinery 112:370-376.

Adamczyk, J.J. 2000. Aerodynamic Analysis of Multistage Turbomachinery Flows in Support of Aerodynamic Design. Journal of Turbomachinery 122:189-217.

Ahmadi, M., and Ghaly, W.S. 1998. Aerodynamic Design of Turbomachinery Cascade Using a Finite Volume Method on Unstructured Meshes. Journal of Inverse Problems in Engineering 6:281-298.

Amano, R. S. Rieger, N. F., and Hesler, S. 1996. An Aerodynamic analysis of Turbine Cascade by Using a Second Order Closure of Turbulence. Int. J. Heat and Fluid Flow 17:276-282.

Anderson, D.A., Tannehill, J.C. and Pletcher, R.H. 1984. Computational Fluid Mechanics and Heat Transfer. London: Hemisphere Publishing Corporation.

Arnone, A., Liou, M. S., and Povinelli, L. A. 1991. Multigrid Calculation of Three Dimensional Viscous Cascade Flows. AIAA Paper No. AIAA-91-3238-CP.

Arnone, A. and Swanson, R.C. 1993. A Navier-Stokes Solver for Turbomachinery Applications. Journal of Turbomachinery 115:305-313.

Arnone, A. 1994. Viscous Analysis of Three Dimensional Rotor Flow Using a Multigrid Method. Journal of Turbomachinery 116:435-445.

Arnone, A. and Benvenuti, E. 1994. Three Dimensional Navier-Stokes Analysis of a Two-Stage Gas Turbine. ASME Paper No. 94-GT-98.

Arnone, A. and Pacciani, R. 1996. Rotor-Stator Interaction Analysis Using the Navier-Stokes Equations and a Multigrid method. Journal of Turbomachinery 118:679-689.

Arts, T., Duboue, J.-M., and Rollin, G. 1998. Aero-Thermal Performance Measurements and Analysis of a Two-Dimensional High Turning Rotor Blade. Journal of Turbomachinery 120:494-499.

Baldwin, B. and Lomax, H. 1978. Thin-Layer Approximation and Algebraic Model for Separated Turbulent Flows. AIAA Paper 78-257.

Birch, N.T. 1987. Navier-Stokes Predictions of Transition, Loss, and Heat Transfer on a Turbine Cascade. ASME Paper 87-GT-22.

Borges, J.E. 1990. A Three-Dimensional Inverse Method in Turbomachinery: Part 2-Experimental Verification. Journal of Turbomachinery 112:355-361.

Boyle, R. J. 1991. Navier-Stokes Analysis of Turbine Blade Heat Transfer. Journal of Turbomachinery 113:392-403.

Boyle, R. J., and Giel, P.W. 2001. Prediction of Relaminarization Effects on Turbine Blade Heat Transfer. ASME Paper NO. 2001-GT-0162.

Camci, C. and Arts, T. 1990. An Experimental Convective Heat Transfer Investigation Around a Film-Cooled Gas Turbine Blade. Journal of Turbomachinery 112:497-503.

Camci, C. and Arts, T. 1991. Effect of Incidence on Wall Heating Rates and Aerodynamics on a Film-Cooled Transonic Turbine Blade. Journal of Turbomachinery 113:493-501.

Cumpsty, N.A. 1989. Compressor Aerodynamics. England: Longman Scientific & Technical.

Consigny, H. and Richards, B. E. 1981. Short Duration Measurements of Heat Transfer Rate to a Gas Turbine Rotor Blade. ASME Paper 81-GT-146

Compton, W. B. 1996. Comparison of Turbulence Models for Nozzle-Afterbody Flows with Propulsive Jets. NASA Technical Paper 3592.

Damle, S., Dang, T., Stringham, J., and Razinsky, E. 1999. Practical Use of Three-Dimensional Inverse Method for Compressor Blade Design. Journal of Turbomachinery 121:321-325.

Dang, T. Q. 1992. Design of Turbomachinery Blading in Transonic Flows by The Circulation Method. Journal of Turbomachinery 114:141-146.

Dang, T. Q. 1993. A Fully Three-Dimensional Inverse Method for Turbomachinery Blading in Transonic Flows. Journal of Turbomachinery 115:354-361.

Dang, T. and Isgro, V. 1995. Euler-Based Inverse Method for Turbomachinery Blades: Part 1 – Two-dimensional Cascades. AIAA Journal 33(12):2309-2315.

Dannenhoffer, J.F., and Baron, J.R. 1986. Robust Grid Adaptation for Complex Transonic Flows. AIAA Paper No. 86-0495.

Dawes, W.N. 1983. Computation of Viscous Compressible Flow in Blade Cascades Using an Implicit Iterative Replacement Algorithm. TPRD/M/1377/N83.

Dawes, W.N. 1988. The Development of a 3D Navier-Stokes Solver for Application to All Types of Turbomachinery. ASME Paper No. 88-GT-70.

Dawes, W.N. 1998. Development of a 3D Navier Stokes Solver for Application to all Types of Turbomachinery. ASME paper 88-GT-70.

Demeulenaere, A., Leonard, O., and Van den Braembussche, R. 1997. A Two Dimensional Navier-Stokes Inverse Solver for Compressor and Turbine Blade Design. Proceedings of International Mechanical Engineers Vol. 211 Part A 299-307.

Demeulenaere, A., and Van den Braembussche, R. 1998. Three-Dimensional Inverse Method for Turbomachinery Blading Design. Journal of Turbomachinery 120:247-255.

Denton, J.D. 1974. A time Marching Method for Two and Three Dimensional Blade to Blade Flows. ARC Report and Memoranda No. 3775.

Denton, J.D. 1992. The Calculation of Three-Dimensional Viscous Flow through Multistage Turbomachines. Journal of Turbomachinery 114:18-26.

Denton, J.D. and Dawes, W.N. 1999. Computational Fluid Dynamics for Turbomachinery Design. Proc Instn Mech Engrs 213 Part C: 107-124.

Dring, R.P., Joslyn, H.D., Hardin, L.W., and Wagner, J.H.. 1982. Turbine Rotor-Stator Interaction. ASME Paper No. 82-GT-3.

Elliott, J., and Peraire, J. 1996. Practical 3D Aerodynamic Design and Optimization Using Unstructured Meshes. AIAA Paper No. AIAA-96-4170.

Fan, H-Y. 1998. An Inverse Design Method of Diffuser Blades by Genetic Algorithms. Proceedings of International Mechanical Engineers 212:261-268.

Fletcher,C.A.J.1987. Computational Techniques for Fluid Dynamics Vol 1&2. London: Springer-Verlag.

Furukawa, M., Yamasaki, M., and Inoue, M. 1991. A Zonal Approach for Navier-Stokes Computations of Compressible Cascade Flow Fields Using a TVD Finite Volume Method. Journal of Turbomachinery 113:573-582.

Furukawa, M., Nakano, T., and Inoue, M. 1992. Unsteady Navier-Stokes Simulation of Transonic Cascade Flow using an Unfactored Implicit Upwind Relaxation Scheme with Inner Iterations. Journal of Turbomachinery 114:599-606.

Garg, V. K. and Rigby, D. L. 1998. Heat Transfer on a Film-Cooled Blade – Effect of Hole Physics. NASA Report No. CR-1998-206609.

Garg, V. K. and Ameri, A. A. 2001. Two-Equation Turbulence Models for Prediction of Heat Transfer on a Transonic Turbine Blade. ASME Paper No. 2001-GT-0165.

Gerolymos, G.A., Neubauer, J., Sharma, V.C., and Vallet I. 2001. Improved Prediction of Turbomachinery Flows Using Near-Wall Reynolds-Stress Model. ASME Paper No. 2001-GT-0196.

Ghaly, W.S.S. 1990. A Parametric Study of Radial Turbomachinery Blade Design in Three-Dimensional Subsonic flow. Journal of Turbomachinery 112:338-345.

Gier, J. Ardey, S. and Heisier, A. 2000. Analysis of Complex Three Dimensional Flow in A Three-Stage LP Turbine By Means of Transitional Navier-Stokes Simulation. ASME Paper No. 2000-GT-645.

Giles, M.B. and Drela M. 1987. Two-Dimensional Transonic Aerodynamic Design Method. AIAA Journal 25(9):1199-1206.

Goto, A., Takemura, T., and Zangeneh, M. 1996. Suppression of Secondary Flows in a Mixed-Flow Pump Impeller by Application of Three Dimensional Inverse design Method: Part 2 – Experiment Validation. Journal of Turbomachinery 118:544-551.

Hall, E.J. 1998. Aerodynamic modelling of multistage compressor flow fields: Part 1 – analysis of rotor-stator-rotor aerodynamic interaction. Proceedings of International Mechanical Engineers 212 Part G: 77-89.

Hall, M.G. 1985. Cell-Vertex Multigrid Schemes for Solution of the Euler Equations. In Morton, K.W. and Baines, M.J., editors. Conference on Numerical Methods for Fluid Dynamics. Reading, United Kingdom.

Hawthorne, W.R., Wang, C., Tan, C.S., and McCune, J.E. 1984. Theory of Blade Design for Large Deflections: Part I – Two-Dimensional Cascade. Trans. ASME, Journal of Engineering for Gas Turbine and Power. 106:346-353.

Heiser, W.H. 1978. Modern Turbine Technology in Turbomachinery Fluid Mechanics. Iowa State University Lecture Notes.

Hirsch, C. 1995. Numerical Computational of Internal and External Flows Vol. 1 & 2. England: John Wiley & Sons.

Ingber, L. 1993. Adaptive Simulated Annealing (ASA). Lester Ingber Research, Chicago. URL http://www.ingber.com.

Jameson, A., Schmidt, W., and Turkel, E. 1981. Numerical Solution of the Euler Equations by Finite Volume Methods Using Runge-Kutta Time-Stepping Schemes. AIAA Paper 81-1259.

Jiang, J. and Dang, T. 1997. Design Method for Turbomachine Blades With Finite Thickness by The Circulation Method. Journal of turbomachinery 119:539-543.

Johnson, D.A. and King, L. 1985. A Mathematically Simple Turbulence Closure Model for Attached and Separated Turbulent Boundary Layers. AIAA Journals 23(11):1684-1692.

Johnson, D.A. 1987. Transonic Separated Flow Predictions with an Eddy-Viscosity/Reynolds-Stress Closure Model. AIAA Journal 25(2):252-259.

Johnson, M.W. 2002. Predicting Transition without Empiricism or DNS. ASME Paper No. GT-2002-30238.

King, D.A. and Williams, B.R. 1988. Development in computational methods for high-lift aerodynamics. Aeronautical Journal 92:265-288.

Kelemenis, G.I. 1994. Approaches to multi-block methods in CFD [MSc dissertation]. Manchester: University of Manchester, Institute of Science and Technology (UMIST). 92p.

Lakshminarayana, Budugur. 1996. Fluid Dynamics and Heat Transfer of Turbomachinery. New York: John Wiley & Sons.

Larsson, J. 1997. Turbine Blade Heat Transfer Calculations Using Two-Equation Turbulence Models. Proceedings of International Mechanical Engineers 211:253-262.

LeJambre, C.R., Zacharias, R.M., Biederman, B.P., Gleixner, A.J., and Yetka, C.J. 1998. Development and Application of a Multistage Navier-Stokes Flow Solver: Part II – Application to a High-Pressure Compressor Design. Journal of Turbomachinery 120:215-223.

Leonard, O. and Van Den Braembussch. 1991. Design Method for subsonic and Transonic Cascade with Prescribed Mach Number Distribution. ASME Paper No. 91-GT-18.

Lewis, J.C. and Agarwal, R.K. 1996. Airfoil Design via Control Theory using full potential and Euler Equations. AIAA Paper No. 96-2483-cp.

Lighthill, J.M. 1945. A New Method of Two-Dimensional Aerodynamic Design. ARC R&M 2112.

Manna, M. and Tuccillo.2002. Improving the Aerothermal Characteristics of Turbomachinery Cascades. ASME Paper GT-2002-30596.

Menter, F. R. 1992. Performance of Popular Turbulence Models for Attached and Separated Adverse Pressure Gradient Flows. AIAA Journal 30(8):2066-2072.

Nakamura, Shoichiro. 1991. Applied Numerical Methods With Software. New Jersey: Prentice Hall.

Ni, R.H., and Bogoian, J. 1989. Prediction of 3-D Multi-Stage Turbine Flow Field Using a Multiple-Grid Euler Solver. AIAA Paper No. AIAA-89-0203.

Noguchi, Y. 1994. Behaviour of the Johnson-King Turbulence Model in Axisymmetric Supersonic Flows. AIAA Journal 32(7):1394-1398.

Norton, R.J.G., Thompson, W.T., Haimes, R. 1984. Implicit Finite Difference Schemes with Non-simply Connected Grids-A Novel Approach. AIAA Paper No. AIAA-84-0003.

Pierret, S. and Van den Braembussche, R.A. 1998. Turbomachinery Blade Design Using a Navier-Stokes Solver and Artificial Neural Network. ASME Paper 98-GT-4.

Raharjo, F. J. and Zangeneh, M. 2003. Design of Turbomachinery Blades for Specified Heat Transfer Distribution. To be published.

Rai, M. M. and Madavan, N.K. 1990. Multi-Airfoil Navier-Stokes simulations of Turbine rotor-Stator Interaction. Journal of Turbomachinery 112:377-382.

Raithby, G.D. 1976. Skew upstream differencing schemes for problems involving fluid flow. Comput. Methods Appl. Mech. Eng. 9:153-164.

Rhie, C.M., Gleixner, A.J., Spear, D.A., Fischberg, C.J., and Zacharias, R.M. 1998. Development and Application of a Multistage Navier-Stokes Solver: Part I – Multistage Modelling Using Body forces and Deterministic Stresses. Journal of Turbomachinery 120:205-214.

Roach, P.E., and Brierley, D.V. 2000. Bypass Transition Modelling: A New Method Which Accounts for Free-Stream Turbulence Intensity and Length Scale. ASME Paper No. 2000-GT-278.

Rumsey, C. L. and Vatsa V. N. 1993. A Comparison of the Predictive Capabilities of Several Turbulence Models Using Upwind and Central-Difference Computer Codes. AIAA Paper 93-0192.

Sanz, J.M. 1988. Automated Design of Controlled Diffusion Blades. Journal of Turbomachinery 110:540-544.

Sarkar, S. 2001. Analysis of Transitional Flow and Heat Transfer over Turbine Blades: Algebraic versus Low-Reynolds number Turbulence Model. Proceedings of International Mechanical Engineers 215:1003-10018.

Shelton, M.L., Gregory, B.A. Lamson, S.H., Moses, H.L. Doughty, R.L., and Kiss, T. 1993. Optimisation of a Transonic Turbine Airfoil Using Artificial Intelligence, CFD and Cascade Testing. ASME Paper No. 93-GT-161.

Smith, G. C., Hilditch, M.A., and Wood, N.B. 2001. Heat Transfer Computations for High Pressure Turbines. ASME Paper 2001-GT-0172.

Smith, L.H. 1987. Unducted Fan Aerodynamic Design. Journal of Turbomachinery 109:313-324.

Smith, R.J. 1996. Automatic grid generation for compressible Navier-Stokes solvers in Aerodynamic design for complex geometry [EngD thesis]. Manchester: University of Manchester, Institute of Science and Technology (UMIST). 168p.

Sorenson, R.L. 1980. A Computer Program to Generate Two-Dimensional Grids About Airfoil and Other Shapes by The Use of Poisson's Equations. NASA technical memorandum 81198.

Swanson, R.C. and Radespiel, R. 1991. Cell Centred and Cell Vertex Multigrid Schemes for the Navier-Stokes Equations. AIAA Journal 29(5):697-703.

Subramanian, S.V., and Bozzola, R. 1985. Application of Runge Kutta Time Marching Scheme For the computation of Transonic Flows in Turbomachines. AIAA Paper No. 85-1332.

Swanson, R.C. and Turkel, E. 1997. Multistage Schemes With Multigrid for Euler and Navier-Stokes Equations: Component and Analysis. NASA Technical Paper 3631.

Tan, C.S., Hawthorne, W.R., McCune, J.E., and Wang, C. 1984. Theory of Blade Design for Large Deflections: Part II – Annular Cascades. Trans. ASME, Journal of Engineering for Gas Turbine and Power. 106:354-365.

Thompson, J.F. 1984. Grid Generation Techniques in Computational Fluid Dynamics. AIAA Journal 22(11):1505-1523.

Thompson, J.F., Warsi, Z.U.A and Mastin, C.Wayne. 1985. Numerical Grid Generation: Foundations and Applications. New York. North-Holland.

Tiow, W.T. and Zangeneh, M. 1998. A Viscous Transonic Inverse Design Method for Turbomachinery Blades, Part I: 2D Cascades. ASME Paper 98-GT-125.

Tiow, W.T. 2000. Inverse Design of Turbomachinery Blades in Rotational Flow [PhD Thesis]. London: University College London.

Tiow, W.T. 1999. Turbomachinery Group, UCL. Private communication.

Trigg, M.A., Tubby, G.R., and Sheard, A.G. 1999. Automatic Genetic Optimisation Approach to Two-Dimensional Blade Profile Design for Steam Turbines. Journal of Turbomachinery 121:11-17.

Tristanto, I. Turbomachinery Group, UCL. Private communication.

Turner, M.G. and Jennions, I.K. 1993. An Investigation of Turbulence Modelling in Transonic Fans Including a Novel Implementation of an Implicit k-ε Turbulence model. Journal of Turbomachinery 115:249-260.

Versteeg, H.K. and Malalasekera, W. 1996. An introduction to Computational Fluid Dynamics: The Finite Volume Method. England: Longman.

Xiao, Yumin and Amano, R. S. 2000. Analysis of Flow and Heat Transfer in the Endwall Region of a Turbine Blade Passage. ASME Paper 2000-GT-211.

Yang, Y.L., Tan, C.S., and Hawthorne, W.R. 1993. Aerodynamic Design of Turbomachinery Blading in Three Dimensional Flow: An Application to Radial Inflow Turbines. Journal of Turbomachinery 115:602-613.

Zangeneh, M. 1991. A Compressible Three-dimensional Design Method for Radial and Mixed Flow Turbomachinery Blades. International Journal of Numerical Methods in Fluids 13:599-624.

Zangeneh, M. 1994. Inviscid-Viscous Interaction Method for Three-Dimensional Inverse Design of centrifugal Impellers. Journal of Turbomachinery 116:280-290.

Zangeneh, M. 1996a. Inverse Design of Centrifugal Compressor Vaned Diffusers in Inlet Shear Flows. Journal of Turbomachinery 118:385-393.

Zangeneh, M., Goto, A., and Takemura, T. 1996b. Suppression of Secondary Flows in a Mixed-Flow Pump Impeller by Application of Three Dimensional Inverse Design Method: Part 1 – Design and Numerical Validation. Journal of Turbomachinery 118:536-543.

Zangeneh, M., Goto, A., and Harada, H. 1998. On the Design Criteria for Suppression of Secondary Flows in Centrifugal and Mixed Flow Impellers. Journal of Turbomachinery 120:723-735.

Zangeneh, M. 1999. Turbomachinery Group, UCL. Private communication.

Zangeneh, M., Goto, A., and Harada, H. 1999. On the Role of Three-Dimensional Inverse Design Methods in Turbomachinery Shape Optimisation. Proceedings of International Mechanical Engineers Vol. 213 Part C 27-42.

Zannetti, L. 1987. Time Dependent Computation of the Euler Equations for Designing Fully 3D Turbomachinery Blade Rows. AIAA Paper No. AIAA-87-0007.

APPENDIX A

Finite Volume Discretization

The Euler equations are written in a first order equation as,

$$\frac{dw}{dt}+\frac{df}{dx}+\frac{dg}{dy}=0$$

Integrating the equation for a region Ω,

$$\iint_{\Omega} 1\left(\frac{dw}{dt}+\frac{df}{dx}+\frac{dg}{dy}\right) dx\, dy = 0$$

or $$\iint_{\Omega}\frac{dw}{dt}\, dx\, dy + \iint_{\Omega}\left(\frac{df}{dx}+\frac{dg}{dy}\right) dx\, dy = 0$$

Applying Green's theorem, $\oint_{S}\left(\overline{H} \cdot n\right) dS = \iint_{A}\left(\nabla \cdot \overline{K}\right) dA$

Hence, the Euler equation becomes,

$$\frac{d}{dt}\iint_{\Omega} w\, dx\, dy + \oint_{d\Omega}\left(\overline{H} \cdot n\right) d\Omega = 0$$

Where, **H**=(**f**,**g**) and in cartesian coordinate $\left(\overline{H} \cdot n\right) d\Omega$ = **f** dy – **g** dx

Finally, for subdomain ABCD the equation has the form,

$$\frac{d}{dt}\iint_{Area} w\, dArea + \oint_{ABCD} f\, dy - g\, dx = 0$$

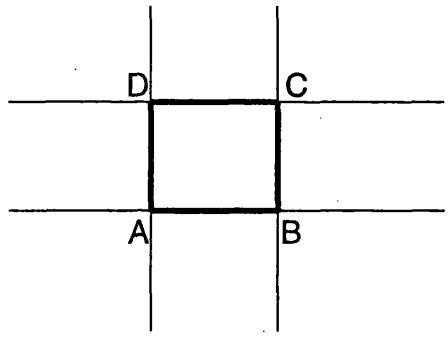

Figure A.1. Cell ABC

APPENDIX B

SCHEMATIC DIAGRAM OF A TWO DIMENSIONAL CH-TYPE GRID SHOWING INLET, EXIT, SOLID WALL AND PERIODIC BOUNDARIES

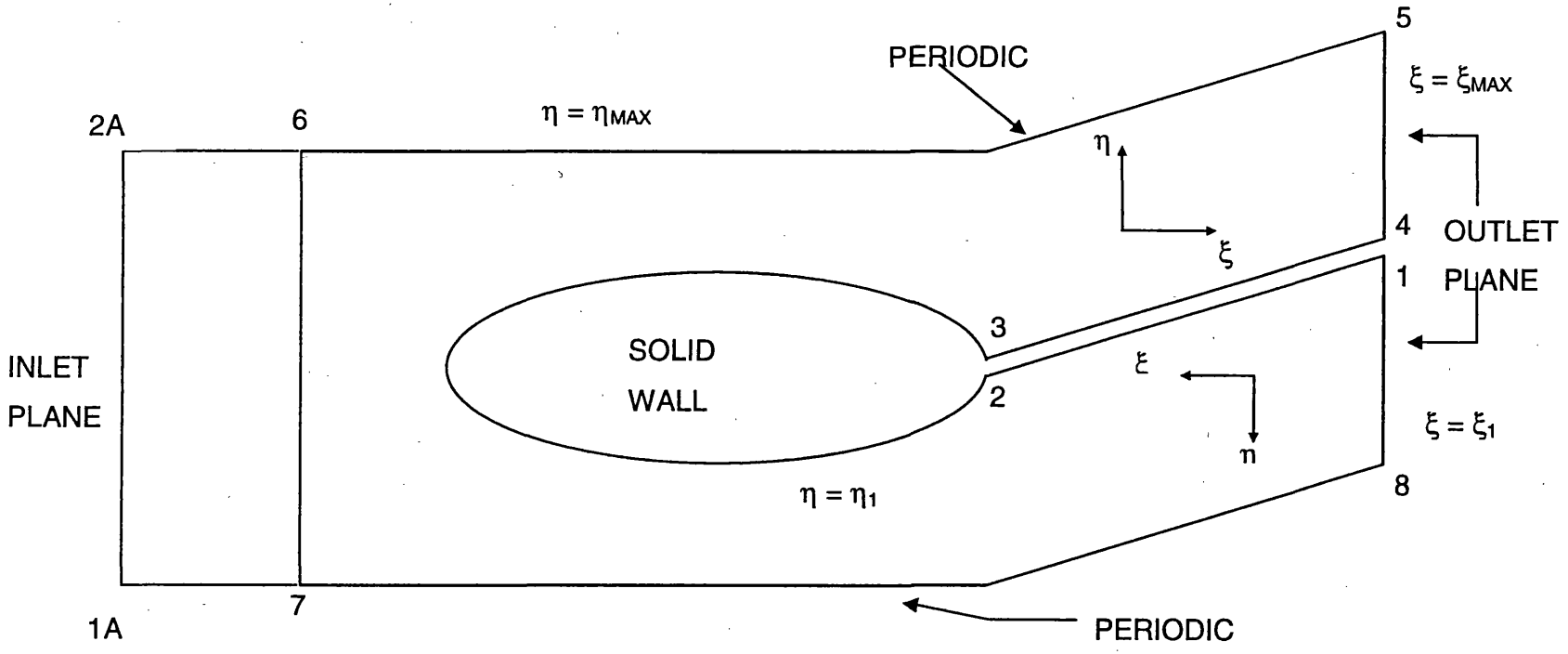

APPENDIX C

Multiblock Schematic Diagram

Figure C.1. H-Type Multiblock Grid Structure

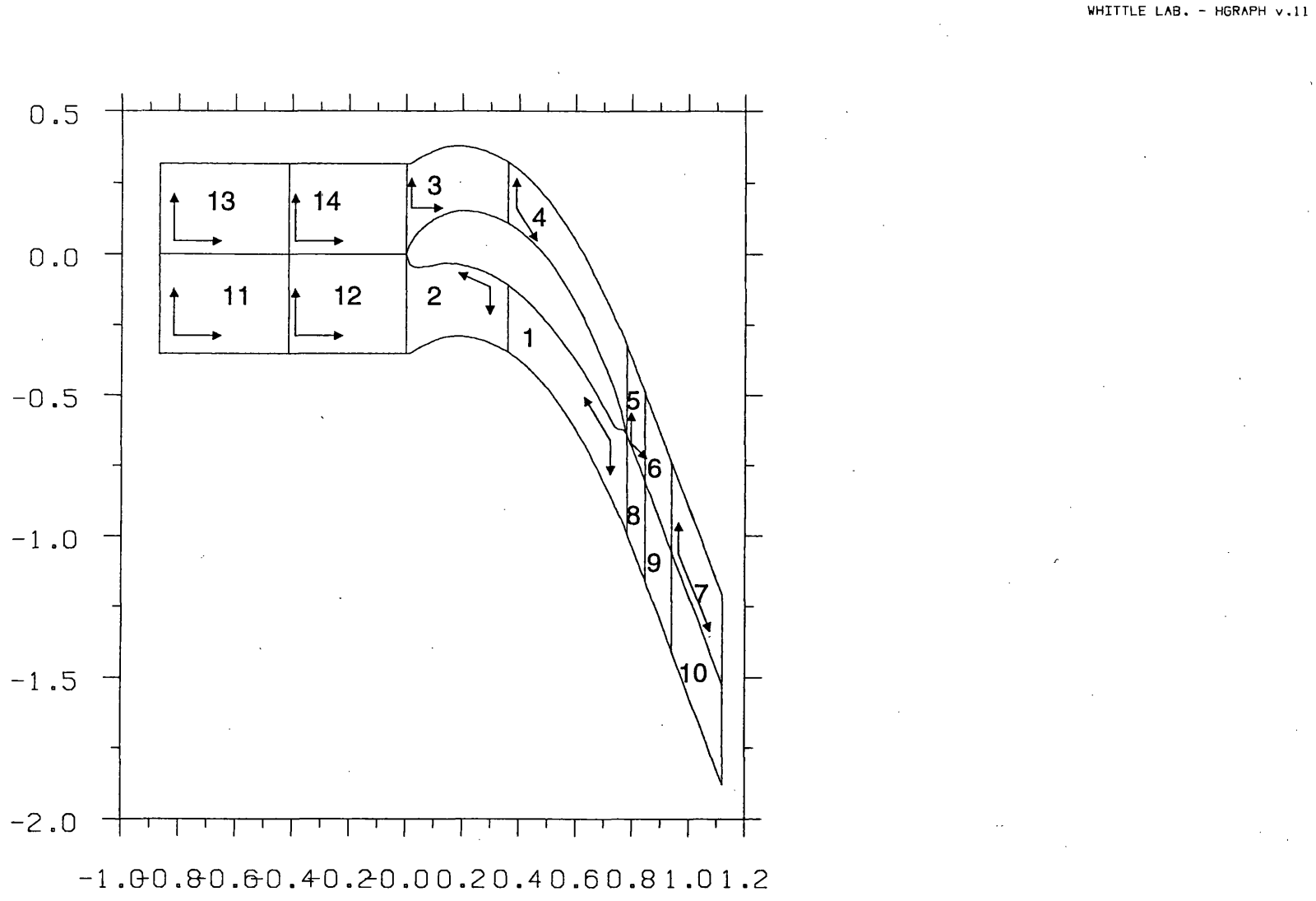

Table: C.1. Number of Grid Points of H-Type Multiblock Grid

Block	Grid Point	
1	48 x 11	528
2	48 x 11	528
3	48 x 10	480
4	48 x 10	480
5	11 x 10	110
6	11 x 10	110
7	13 x 10	130
8	11 x 11	121
9	11 x 11	121
10	13 x 11	143
11	10 x 11	110
12	26 x 11	286
13	10 x 10	100
14	26 x 10	260
Total		3507

Figure C.2. Block Structure Diagram of H-Type Multiblock Grid

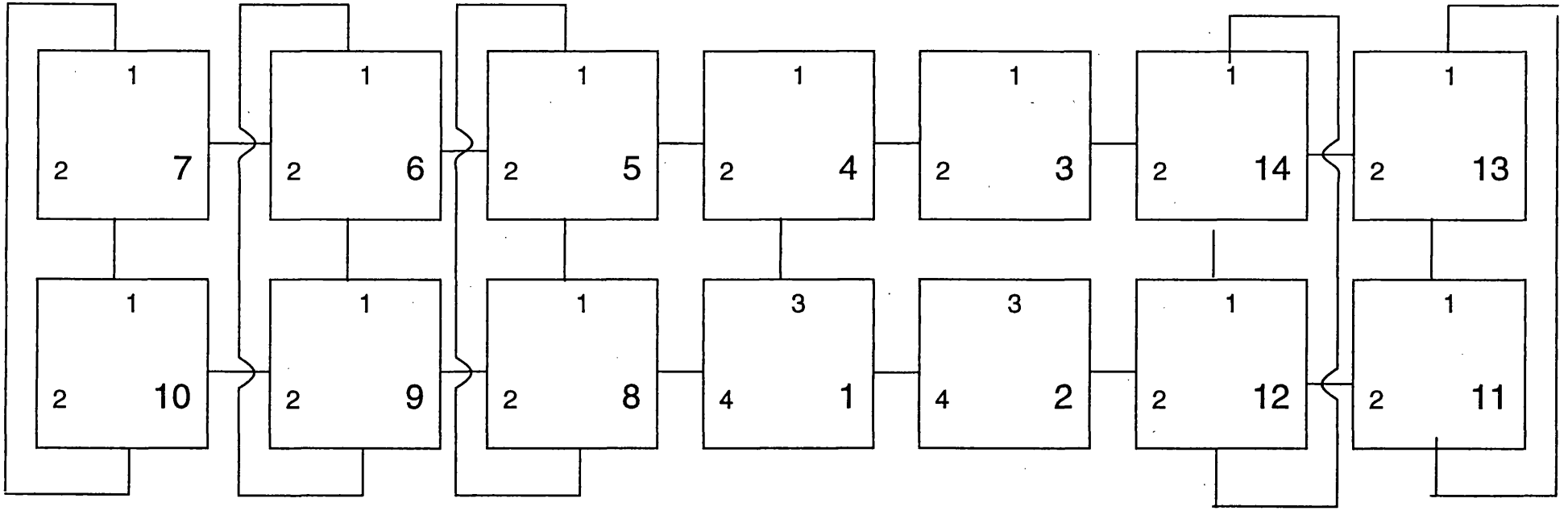

Figure C.3. CH-Type Multiblock Grid Structure

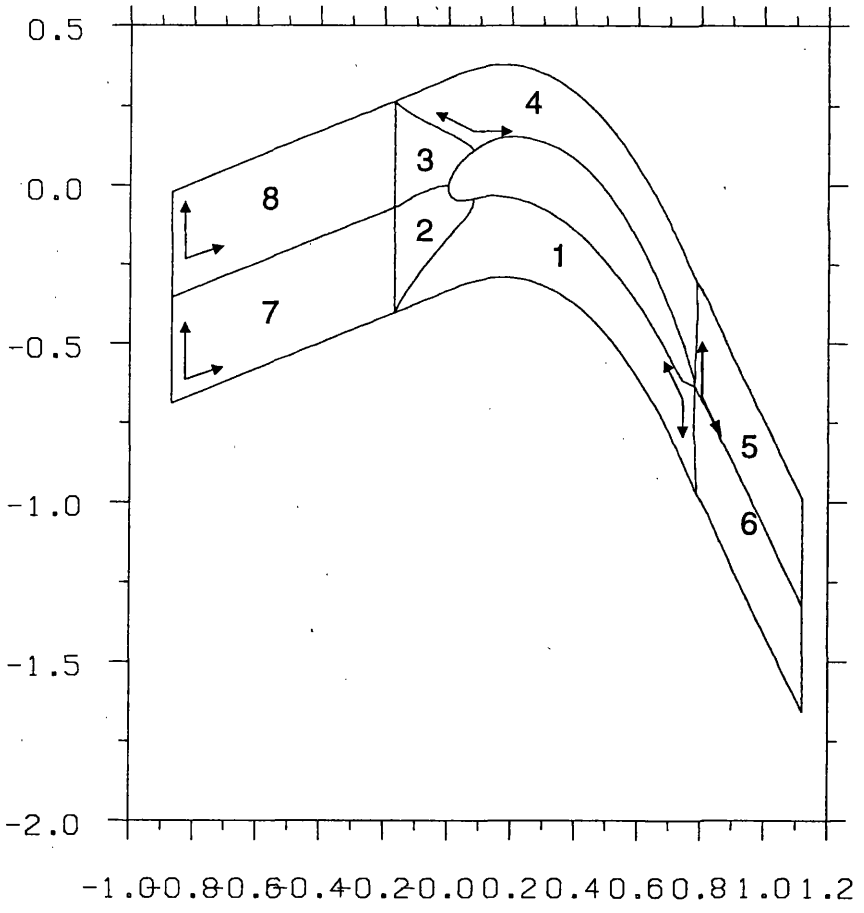

Table: C.2. Number of Grid Points of CH-Type Multiblock Grid

Block	Grid Point	
1	55 x 16	880
2	16 x 16	256
3	16 x 16	256
4	55 x 16	880
5	28 x 16	448
6	28 x 16	448
7	19 x 16	304
8	19 x 16	304
Total		3776

Figure C.4. Block Structure Diagram of CH-Type Multiblock Grid

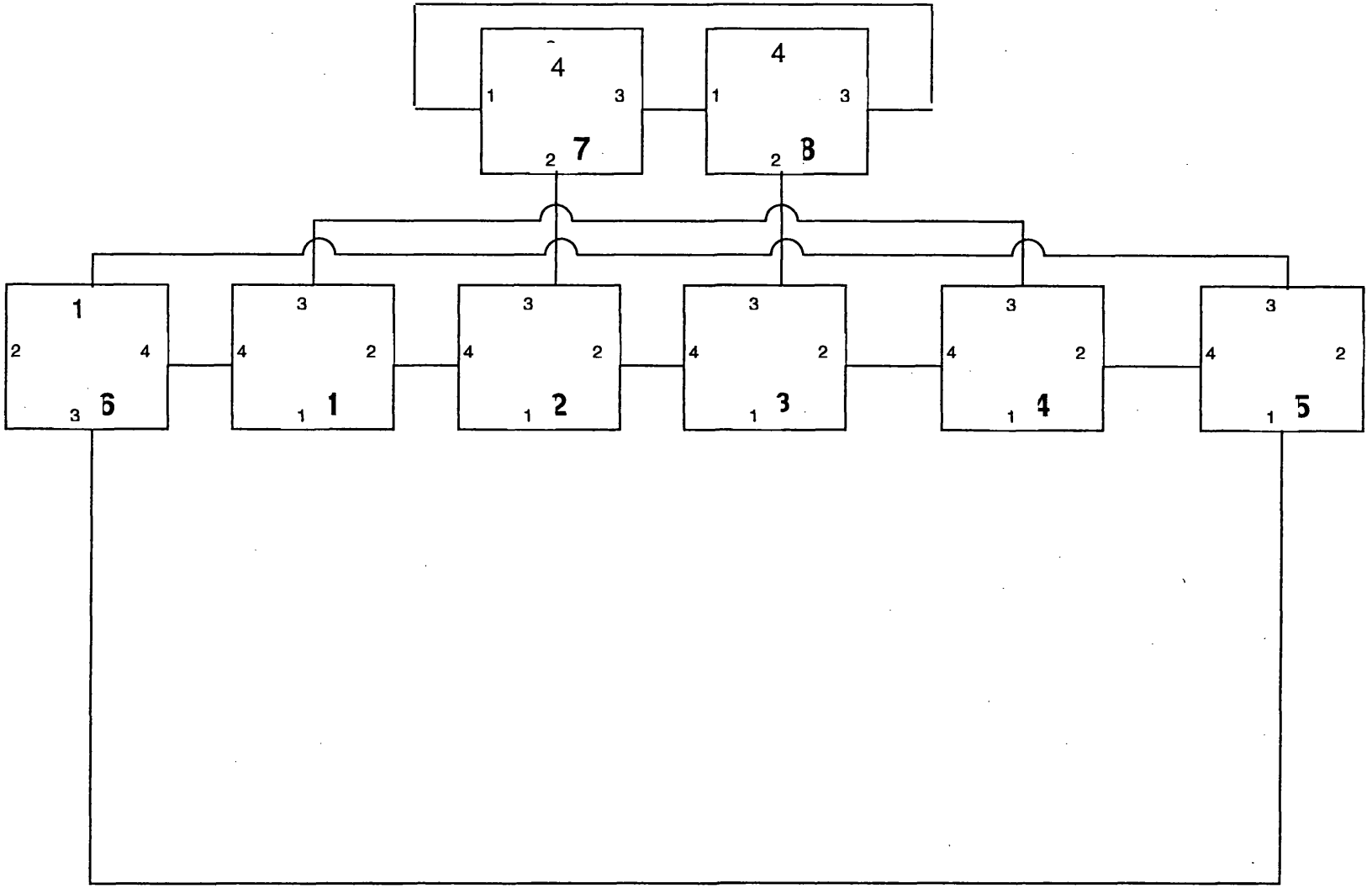

Figure C.5. OCH-Type Multiblock Grid Structure

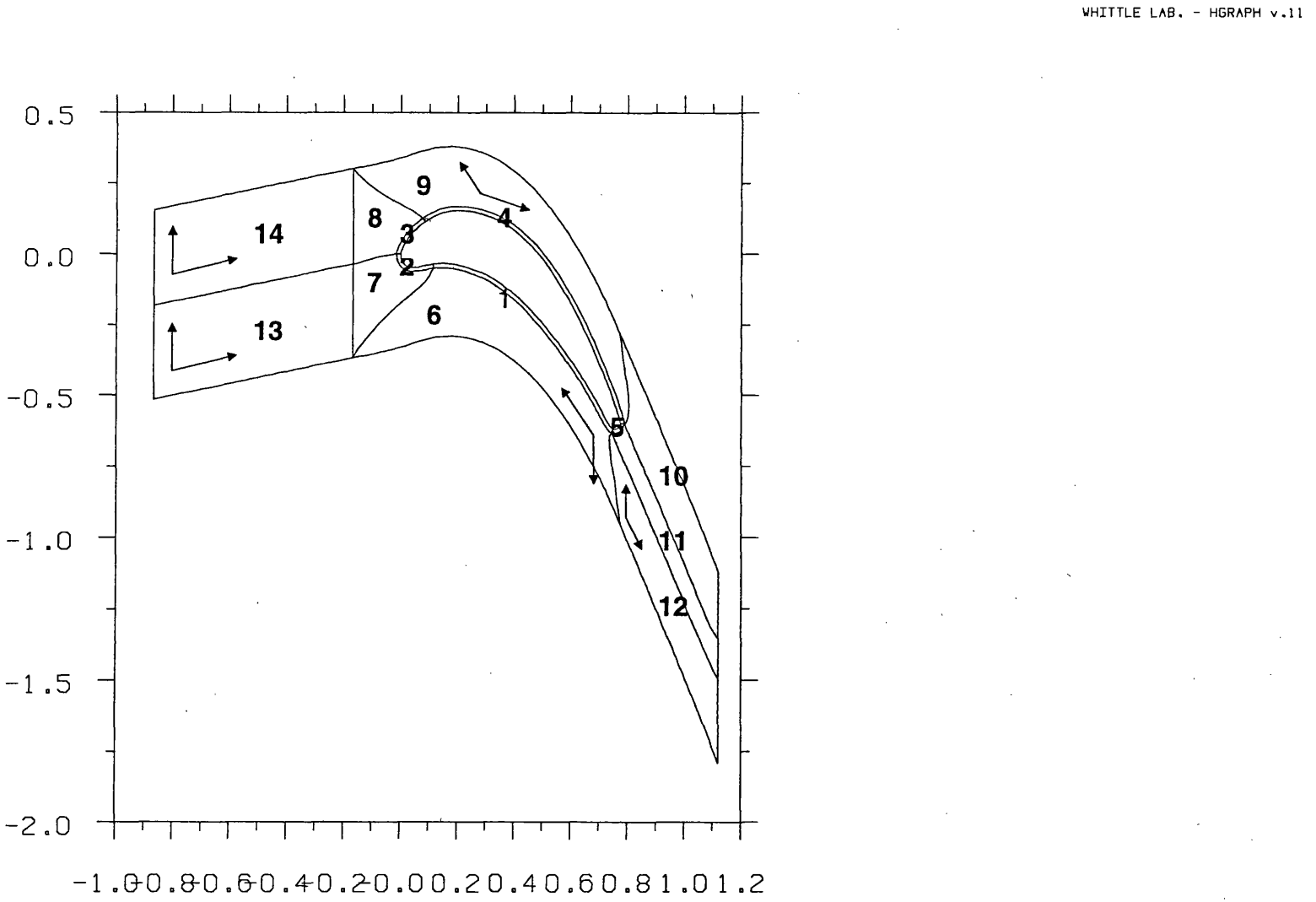

Table: C.3. Number of Grid Points of OCH-Type Multiblock Grid

Block	Grid Point	
1	56 x 3	168
2	16 x 3	48
3	16 x 3	48
4	56 x 3	168
5	7 x 3	21
6	56 x 12	672
7	16 x 12	192
8	16 x 12	192
9	56 x 12	672
10	30 x 12	360
11	30 x 7	210
12	30 x 12	360
13	18 x 16	288
14	18 x 16	288
Total		3687

Figure C.6. Block Structure Diagram of OCH-Type Multiblock Grid